Unclassified Title

R-273

INTERPLANETARY NAVIGATION SYSTEM STUDY

by

J. H. Laning, Jr.	J. M. Dahlen
R. Battin	R. J. Magee
P. Bowditch	K. Nordtvedt
M. B. Trageser	R. A. Scholten
R. L. Alonso	H. H. Seward
W. E. Toth	

April, 1960

INSTRUMENTATION LABORATORY
MASSACHUSETTS INSTITUTE OF TECHNOLOGY
CAMBRIDGE 39, MASSACHUSETTS

Approved by: *Roger B Woodbury*

Associate Director

DECLASSIFIED

ACKNOWLEDGMENT

FACILITY FORM 602

(ACCESSION NUMBER) 189

N71-75478 (THRU)

(PAGES)

none (CODE)

CR-122982
(NASA CR OR TMX OR AD NUMBER)

(CATEGORY)
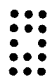
DECLASSIFIED

TABLE OF CONTENTS

Supplement (separately bound)

RN - 5337

CHAPTER 5

ADDITIONAL SUBSYSTEM STUDIES

by

Ramon L. Alonso
John M. Dahlen
Robert Magee
Harold H. Seward
Milton Trageser

6?'''''RN - **5337**

TABLE OF CONTENTS

LIST OF ILLUSTRATIONS

Page

GO, RN - 5337

CHAPTER 5

ADDITIONAL SUBSYSTEM STUDIES

Introduction

This chapter presents the results of a variety of studies on guidance and control subsystems and problems.

Problems associated with the space sextant are considered in the first three sections. A new optical and mechanical design for the space sextant is presented. This light-weight, simple, and accurate design presently exists in a state which suggests breadboarding as the next step. A study of space sextant modulation schemes is presented in the second section, and the detectability problems associated with the use of photomultipliers and silicon solar cells in the space sextant are considered in the third section. The sunfinder's stability, field characteristics, errors resulting from the close proximity of planets, and circuits are considered in the fourth section. Some of the characteristics of a particular low power counter applicable to the spacecraft clock are presented in the fifth section. The sixth section emphasizes the characteristics of the spacecraft guidance and

WRN - 5337

control computer in contrast to the computer for use in ballistic missiles. These comments relate the general discussion presented in Appendix E at the end of this report to the spacecraft application. Finally, the last section considers several planet disk scanning methods and presents some detailed error studies on one of these.

I. An Improved Space Sextant Design

This section reports the results of an effort towards refinement of the space sextant. The functions of the instrument remain the same as described in MIT/IL Report R-235, with approximately the same field of view, but with better tracking accuracies for sun, stars, and planets. The sextant has been reduced in volume and weight by combining the duties of several parts of the instrument, and has an estimated weight of 5.1 pounds. The required precision in the high-speed bearings in the area near the focal plane of each telescope has been reduced by an order of magnitude. This has been done by the substitution of a $r_0$tating wedge assembly in place of the previous focal plane modulator. As a consequence, the bearings are more compatible with the requirements for long life and operation in a near vacuum environment. Optical sensing is now done by one photomultiplier tube and a silicon light sensitive cell. A discussion of the physical details of the space sextant follows.

A. Space Sextant Function

The automatic sextant described here is a modification of the instrument described in R-235. The operation of the sextant as a part of the navigation scheme is described in Chapter 3 of this report. The observations useful for navigation are:

    1.   determining an accurate sunline;

2. measuring the angle between the sun and several stars (this angle might range from 15° to 160°);

3. measuring the diameter of a planetary disk provided it exceeds 1 milliradian in diameter; and

4. measuring the angle from the sun or a star to the center of a planetary disk.

All measurements are required to have an accuracy of 5 to 15 seconds of arc. To make these observations the sextant contains:

1. two star trackers;

2. a sun tracker; and

3. planet (disk) tracker.

The method of operation is such that all four observations can be done by two telescopes, the sun and one star tracker in one, telescope, the planet and other star tracker in the second.

B. Physical Description of the Instrument

The sextant consists of two telescopes--one mobile star/planet tracker and one body fixed sun/star tracker. Each telescope includes a 45° mirror, telephoto objective lens, field modulator, and prism train leading to a photomultiplier tube. Both telescopes use the same photomultiplier.

Two aluminized-surface steel mirrors are mounted at 45° outside the telescope objective and are optically aligned so that they deflect the lines of sight of both telescopes by 90°. A nine-inch pitch diameter precision gear is mounted concentric to the mobile telescope bearing axis. This gear and its associated train will generate bits of information corresponding to 1 bit per 8 seconds of arc of telescope rotation. Eight seconds of arc rotation uncertainty corresponds to $4 \times 10^{-5} \times 4.5 = 0.00018$ inch accuracy for the teeth of the large gear and its driver. As the

13

mobile telescope is rotated, a known angle between axes is generated accurate to within the uncertainty of the main bearings of the mobile telescope. The details of angular pickoff are described in Chapter 9 of Report R-235 under the heading Sextant Drive.

The sextant is assembled in a single block of beryllium to establish a fixed relationship between both telescope axes. Two parallel cyclinders are bored in the block, one for the fixed tracker, the other to house two sets of matched bearings. These are pre-loaded with a runout of 0.0002 inches or less. This runout, combined with bearing separation of 10 1/2 inches, results in an uncertainty of 4 seconds of arc in axis alignment. The planet-star tracker telescope rotates in these bearings at low speed-- on the order of 1/6 rpm.

C. Optical Path for the Body-Fixed Telescope

The fixed telescope is comprised of mirror M_1, objective lenses L_1 and L_2, field modulation wedges P_1 and P_2, and field lens L_3, as shown in Fig. 5-1.

L_1 has an aperture of 1.5 inches and focal length of +7 inches. L_2 has an aperture of 0.8 inches and a focal length of -5.3 inches. These two lenses form a telephoto system with a physical length of +8.5 inches and an effective focal length of 12 inches. Part M at the end of this section shows the relationship of effective focal length to physical length for a thin lens telephoto system.

A series of annular light baffles are placed in the telescope barrel between L_1 and L_2 as well as between L_2 and the hollow shaft motor. These baffles do not vignette the field of the telescope and are used to prevent out-of-field reflections from entering the focal plane aperture.

At the base end of the fixed telescope is a rotating prism pair, P_1 and P_2, of aperture 0.4 inches. P_1 has an apex angle of 2.77° and P_2 has an apex angle of 2.31°. The object of this

HOLLOW SHAFT MOTOR CONTAINING FIELD MODULATOR

SILICON CELL FOR SUN TRACKING

FIELD LENS (L₃)

TO PHOTOMULTIPLIER

FIELD LENS (L₃)

MOBILE TELESCOPE MAIN BEARING

HOLLOW SHAFT MOTOR CONTAINING FIELD MODULATOR

MOBILE TELESCOPE MAIN BEARING

LENSES (L₁)

STRAY LIGHT BAFFLES

SUN AND STAR TRACKER (FIXED TELESCOPE)

LENSES (L₂)

REF. SIGHT LINE

PLANET AND STAR TRACKER (MOBILE TELESCOPE)

MOBILE TELESCOPE DRIVE MOTOR AND GEAR TRAIN

9 IN DIAM. BULL GEAR

DIAGONAL MIRRORS (M₁)

ACQUISITION SIGHT LINE

Fig. 5-1 Space Sextant

15

assembly is to displace the cone of rays coming from the objective lens to approximately 0.048 inches off-axis at the focal plane. The prisms are mounted in a hollow shaft 2-pole phase lock synchronous motor which rotates at 75 rps. In this type of machine, 360 electrical degrees correspond to 1 revolution of the rotor; therefore, the phase of the supply voltage will imply the physical orientation of the rotor. Bearing tolerance in this motor is 3 milliradians of axial wobble, as well as approximately 0.005 inch of longitudinal or radial play.

The field lens L_3, with the aid of P_2, serves to focus the objective lens on the photomultiplier in order that the image projected onto the sensitive surface will remain stationary. Because of the large amount of light encountered in tracking the sun, a solenoid actuated light baffle closes off the light path to the photomultiplier. A silicon cell located near the photomultiplier is used for sun tracking and receives 4% of the maximum 1.4 watts of sun light through a beam-splitting prism, irrespective of baffle position.

D. Mobile Telescope

The mobile telescope is optically similar to the body-fixed sun/star tracker. Here L_1 has an aperture of 1.5 inches and a focal length of +8.6 inches. This lens is combined with L_2, of aperture 0.8 inch and a focal length of -6.45, making a telephoto system with an effective focal length of +15 inches with a star tracking field of 0.008 radians. This tracker is used for both star and planetary disk tracking.

Star tracking is done as with the fixed telescope, but disk tracking is accomplished by means of an undeviated cone of rays passing through a 0.001 inch diameter hole in the focal plane 0.068 inch off the optical center. This small aperture defines a line of sight 0.0045 radians from the optical axis with an uncertainty of ±7 seconds of arc. The details of this arrangement are shown in Fig. 5-2a.

16
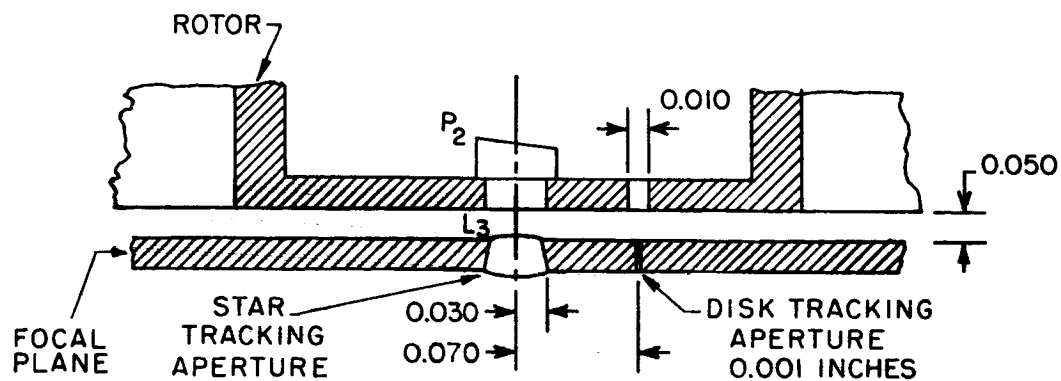
Fig. 5-2a   Planet/disc tracker details.
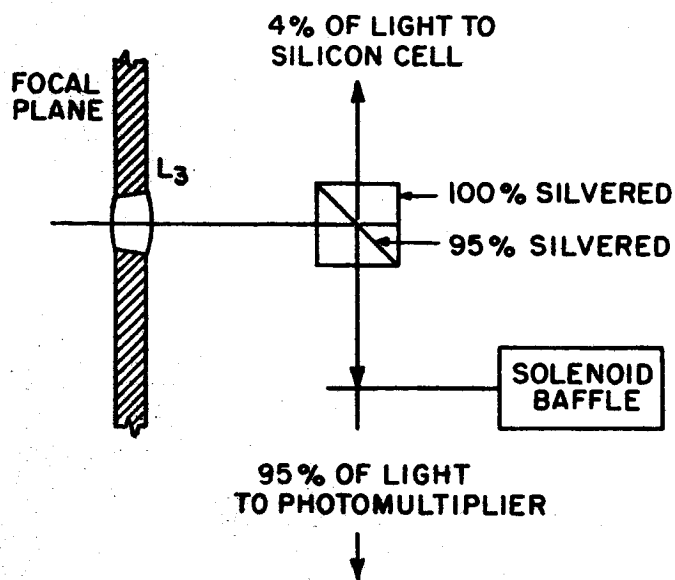
Fig. 5-2b   Beam-splitting prism.

17

The prism assembly at the base of the telescope includes a clear annular aperture around the rim of prism P_1. The 1/20 inch width of this aperture is sufficient to pass the cone of rays which converges on the 0.001 inch opening at the focal plane.

P_1 is a wedge with an apex angle of 3.46^O mounted in the center of a 0.4 inch diameter annular ring. A ring at P_2 contains a circle of 40 holes 0.010 inch in diameter, 0.010 inch apart. These provide 2000 cps modulation of the disk tracking aperture when the hollow shaft motor is revolving at 3000 rpm. Planet disk tracking procedures are described in detail in another part of this chapter.

P_2 is a prism of angle 3.22^O and corrects the angle of rays from the objective lens so that the objective lens is focused on the photomultiplier as a stationary image. Note N at the end of the section derives the value of wedge angles required to obtain the desired field and also to satisfy the stationary image condition.

E. Field Modulator Operation

The method of signal modulating is essentially the same for both telescopes in that an optical wedge is rotated in a plane approximately normal to the optical axis. This wedge deviates the cone of rays forming the image of a star or point so that it travels in a circular path at the focal plane as the wedge rotates. When the object is on-axis, the image is nutated in a locus centered on the optical axis. A circular aperture in the focal plane whose edge coincides with the path of the moving point image for on-axis stars provides means of error signal modulation. This aperture should be circular to within 0.0003 inch. A photomultiplier tube viewing the aperture from behind the focal plane will produce an output corresponding to the amount of star light received. A star on-axis produces a constant signal. A star slightly off-axis produces a signal whose phase, when compared to the phase of the wedge-driving motor, will determine the direction of motion required to align the telescope axis on the star.

Fig. 5-3 shows the graph of motor supply voltage as reference versus time compared to photomultiplier output versus time. It can be seen from the figure that the photomultiplier output is 90° out of phase with the reference voltage when the center of image-deviation is above the aperture center. The relative phases of photomultiplier output and reference voltage would be 180° and 270° for misalignment in the other two quadrants. A phase sensitive demodulator is used to detect the signal to align the star once it has been positioned in the 0.008 radian field of the tracker.

The minimum usable field and the minimum focal plane aperture of the telescope for sun tracking is fixed by the maximum expected angular diameter of the sun. Since the telescope is a combined sun and star tracker, the image may be either extended or a point. As a consequence, the center of the nutating image must lie on the edge of the focal plane aperture. As can be seen from Fig. 5-4, the radius of the extended image must always be slightly less than the diameter of the focal plane aperture to produce an error signal.

The effective field of the tracker is larger than the angle subtended by the focal plane aperture. The tracker can acquire a target once the nutating image is visible through the aperture - if only for a small portion of the nutation cycle. The tracker field can be computed as:

Effective Field Radius = 2 x Focal Plane Aperture Radius
+ Image Radius.

Thus the field of the tracker is greater for extended sources than for point sources. When tracking a maximum size image, the field is almost equal to four times the focal plane aperture diameter. Fig. 5-4(b) shows the effective maximum field.

F.   Image Astigmatism Caused by Wedge Assembly

A monochromatic ray of light passing through an optical wedge will be deviated by an angle δ depending on apex angle α of the

19

P.M.
SIGNAL

APERTURE IN
FOCAL PLANE

IMAGE AT t = 0

TIME

π

2π

MOTOR
VOLTAGE
(REF.)
SUPPLY

π

2π

TIME

P.M.
SIGNAL

APERTURE IN
FOCAL PLANE

IMAGE AT t = 0

TIME

π

2π

MOTOR
VOLTAGE
(REF.)
SUPPLY

π

2π

TIME
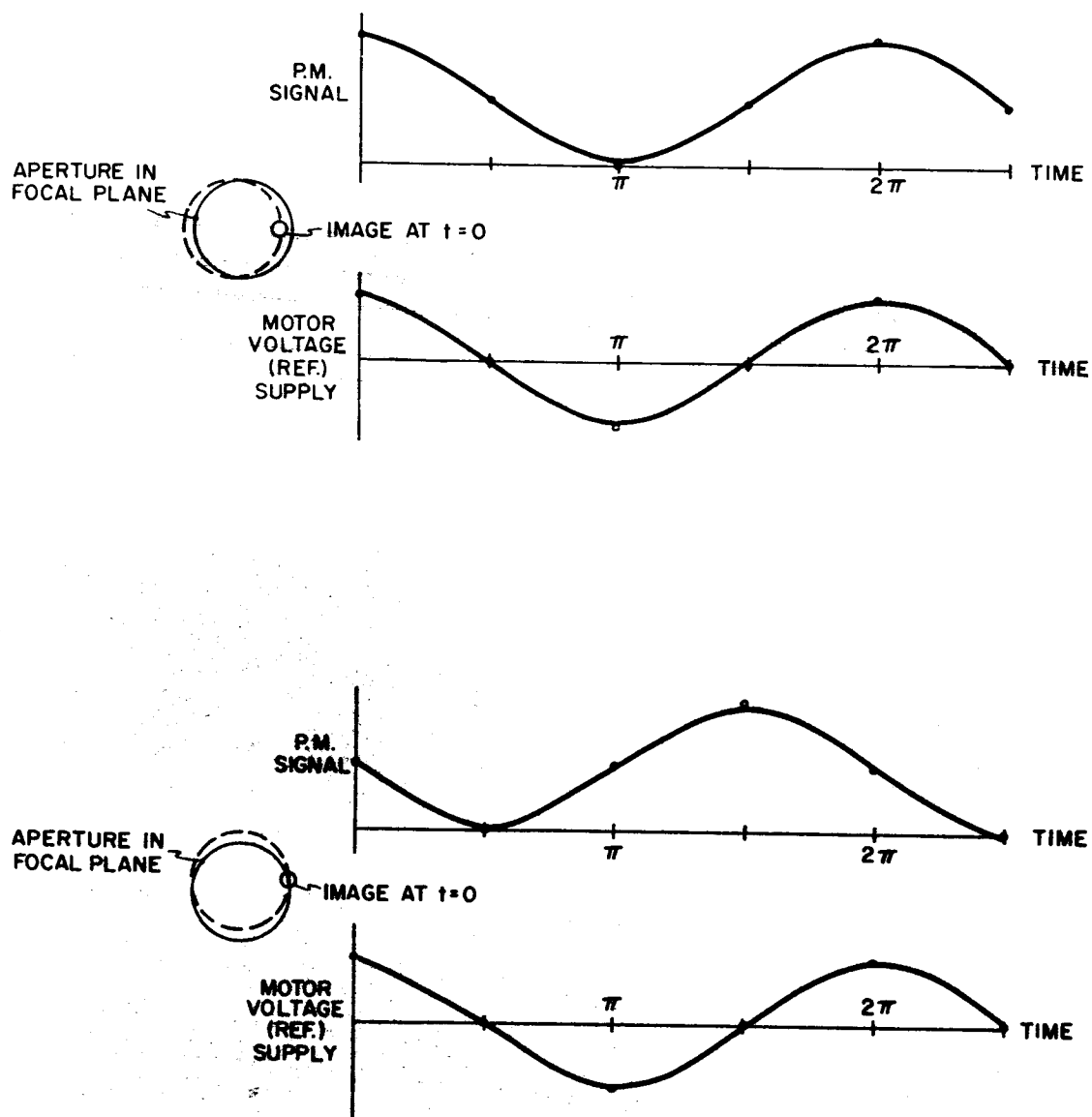
Fig. 5-3   Photomultiplier output versus reference motor supply.

(A)

MAXIMUM IMAGE SIZE

FOCAL PLANE
APERTURE
(ALSO LOCUS
OF NUTATION)

(B)
LOCUS OF ENVELOPE
OF NUTATING IMAGE

FOCAL PLANE
APERTURE

RADIUS OF
MUTATION
CIRCLE
(EQUAL TO
APERTURE
RADIUS)

IMAGE
RADIUS

RADIUS OF
EFFECTIVE FIELD
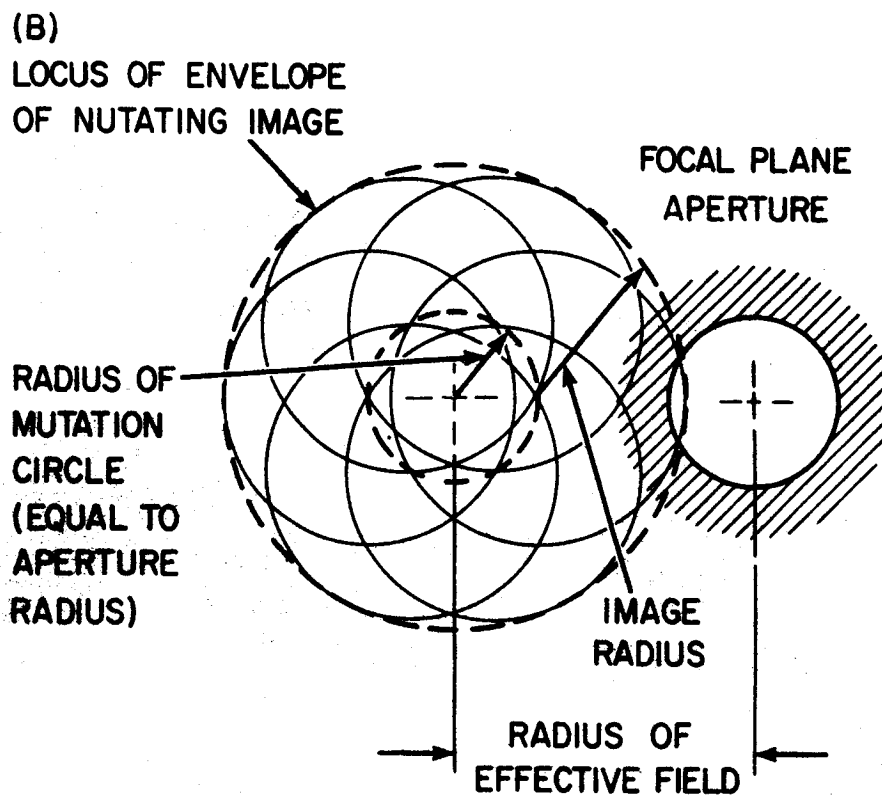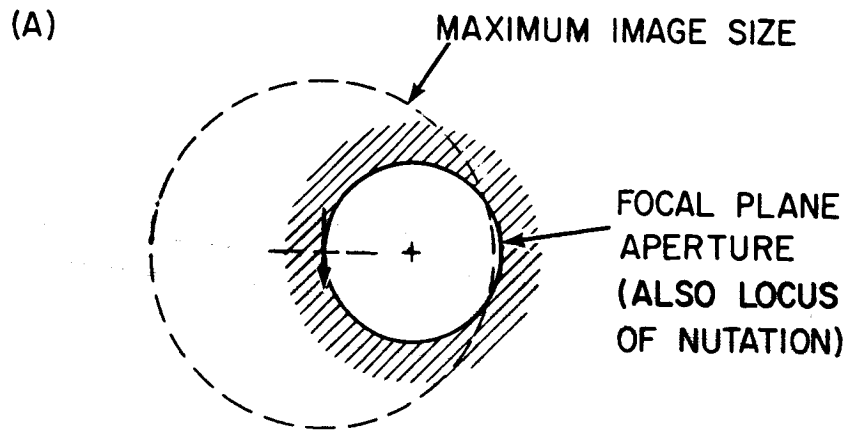
Fig. 5-4   Focal plane aperture relation to image size and
effective field radius.

WRN - 5337

wedge and the incident angle (ϕ_1) of the ray with the front face of the wedge. There is a minimum deviation angle δ_{min} when $\phi_1 = \phi_2$, where ϕ_2 is the exit angle. A graph of deviation ϕ for a ten degree wedge angle is shown on the next page. A wedge angle of approximately 4° (as in the sextant) results in less dispersion, but the general form is the same. In the fixed sun/star tracker, a cone of rays of 7.2^O apex angle is incident upon P_1. If P_1 is a thin wedge with no chromatic aberration and if the central axis of the cone of rays is incident to the wedge at the minimum deviation angle of 5.02^O, the sides of the cone are deviated slightly less than 5.040^O. The range of dispersion of the entire cone of rays is only 0.016^O. The resulting spread of the image at the focal plane is:

$$(0.016^O \text{ dispersion})(0.017 \text{ rad/deg})(2 \text{ inch distance to focus})$$

$$= 5 \times 10^{-4} \text{ inch.}$$

This is equivalent to $\dfrac{5 \times 10^{-4} \text{ inch}}{12 \text{ inches}} = 4 \times 10^{-5}$ radians or 8 sec of arc in object space.

The function of the second wedge (P_2) is primarily to correct the angle of rays going to the photomultiplier. It has little effect on the operation of the field modulating system and contributes negligibly to further image degradation, since its distance (0.050 inch) from the focal plane gives a very small lever arm for additional dispersion.

From examination of the curve of deviation δ versus angle of incidence ϕ in Fig. 5-5, it can be seen that a wobble of 0.11^O (0.002 rad) in wedge angular orientation (cocking) will give a change in deflection of approximately 0.001^O. The actual angular error of the instrument as a result of this effect is given by the product of the change of deflection times the ratio of the wedge-focus distance divided by the focal length. Thus, with 1/10 of a degree cocking of the wedge assembly and a ratio of 1/6, the
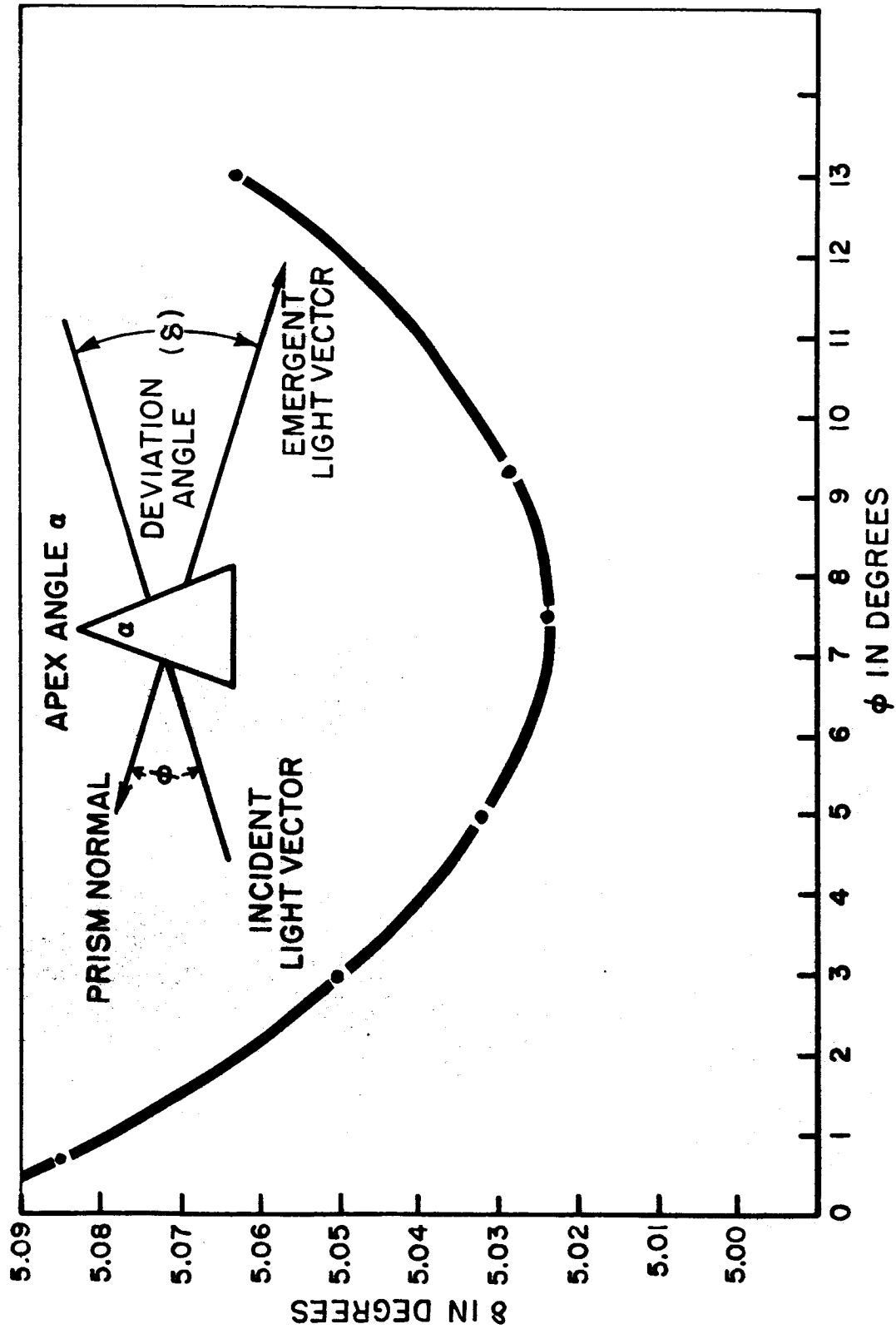
Fig. 5-5   Graph of deviation angle δ versus angle of incidence φ.

resulting error will be less than a second of arc.

G. Axial Motion of the Wedge Assembly

Axial motion of the wedge assembly of 0.004 inch will
result in an image shift in a radial direction of a little more than
0.0005 inch or about 10 seconds of arc. The inertia of the rotor
will preclude an unsymmetrical shift (i. e. , the rotor being
closest to the focal plane at time t and being farthest away at
t + 1/2 cycle later). Therefore, an axial rotor shift producing
an image shift up to the size of the image diameter (for point
source) is acceptable.

H. Allowable Image Degradation

Because of the nature of the field modulation, virtually
all image astigmatism will be in the radial direction or sym-
metrical about the radial direction. The allowable maximum
radial dispersion for the image is limited mainly by the signal
gradient (i.e. , $\frac{\text{change of error signal}}{\text{change of error angle}}$) required for accurate
sensing. Assuming the required accuracy of the tracker is 6
seconds of arc, then, as the image path center is shifted on the
focal plane by that amount, the change in modulated signal level
exclusive of noise must be above the minimum detectable level.

I. Background Noise

Other stars in the field will bias the tracker null, but on
the average only six stars of the fifteen brightest should have a
star of fifth magnitude or brighter within a radius of 0.004 radian
(i. e. , field of the sun and star tracker). A sixth magnitude star
gives 100 times less illumination than a first magnitude star;
therefore, such a bias will hardly be noticed.

J. Signal Modulation

Since the signals are received by the single photomultiplier

from both the sun/star and the star/planet trackers simultaneously, a modulation frequency difference is required to differentiate between them. The motor driving the field modulator in the star/planet tracker rotates at 3000 rpm. The modulation wave form will be approximately sinusoidal due to the finite size of the star image, and harmonic power will be mainly in the odd harmonics. Therefore, if the sun/star tracker field modulator is run at 4500 rpm, its fundamental frequency will be distinguishable from that of the star/planet tracker and there will be no interference of harmonics.

K. Heat From the Sun

At Venus the sun/star tracker will acquire 3 watts of radiant energy from the sun. Approximately 1.5 watts of this energy is dissipated in the focal plane, the rest passes through the focal plane aperture and is absorbed by the solenoid-actuated baffle.

The heat dissipated in the focal plane is conducted by beryllium walls 1/8 inch thick along the axis of the telescope barrel. This wall thickness results in a temperature gradient of 2° Centigrade from the focal plane to a point near the negative lens. The expansion from this gradient results in mechanical changes of the order of 25 millionths of an inch in the focal plane assembly. These dimensional changes could account for only 0.5 seconds of arc of thermal instability.

L. Space Sextant Environment

It is probable that operation of moving precision parts in a hard vacuum environment will pose serious problems during a long period of usage. The present design effort uses a low pressure environment for the space sextant and most other portions of the guidance package. This is to be done through the use of one of several types of vacuum seals or by means of controlled pressurant loss. A discussion of this problem and tentative

solutions is presented in Chapter 6 of this report.

One such method of vacuum seal is depicted in Fig. 5-6. This is a welded metal bellows that flexes with rotation of the mobile telescope. A window at the end of the bellows is caused to pivot simultaneously about two horizontal axes by the cam action of the telescope extension. The partially extended bellows exerts a small force on the telescope extension, but this is a constant bending **moment during normal operation; the resultant deflection,** if noticeable,could be compensated.

The second approach using the vapor of a lubricant for pressurization is illustrated in Fig. 5-1 which shows a very small radial gap exposed to the environment between the two members of the space sextant.

TABLE 5-1

WEIGHT TABLE FOR SEXTANT

Item	Weight	Volume
1. Lenses and prisms	9 oz	
2. Mirrors	4 oz	
3. PM Optical train	3 oz	
4. Electronics PM,power supply, amplifier	13 oz	
5. Hollow shaft motors & bearings (2)	8 oz	
6. Solenoids (2)	2 oz	
7. Bull gear; team and motor large bearings	13 oz	
8. Housing, barrels, etc lens mounts	29 oz	
Total	81 oz (5.06 lb)	
Bellows, window, etc.	15 oz	160 cu. inches
Total with bellows	6 lb	280 cu. inches

OPTICAL WINDOW

LINE OF SIGHT

BEARING

DIAGONAL WINDOW

BELLOWS

MOBILE TELESCOPE
OBJECTIVE LENS
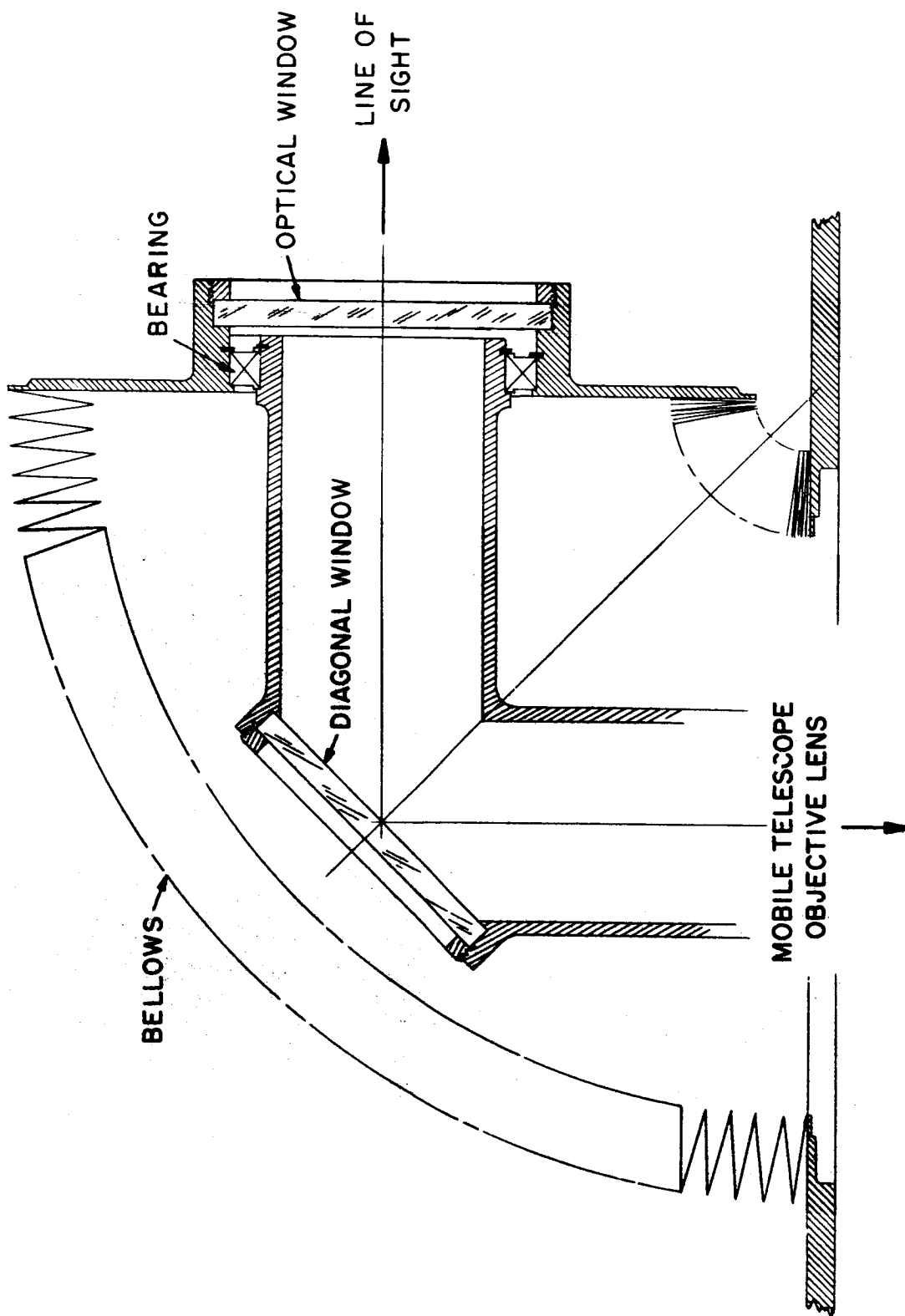
Fig. 5-6   Bellows vacuum seal for mobile star tracker.

27

M. Thin Lens Telephoto Derivation

Assuming the use of simple, thin lenses, the telephoto system can be described as follows:

For the objective lens:
$$\frac{1}{s} + \frac{1}{s'} = \frac{1}{F_1} \qquad (5\text{-}1)$$

$$s' = F_1$$

For the negative lens:
$$\frac{1}{s} + \frac{1}{s'} = \frac{1}{F_2},$$

where
$$F_1 - h = s \qquad (5\text{-}2)$$

For near axial rays
$$\frac{R_1}{F_1} = \frac{r_1}{s} \qquad (5\text{-}3)$$

and also
$$\frac{R_1}{e.f.} = \frac{r_1}{s'} \qquad (5\text{-}4)$$

Combining Eqs. (5-3) and (5-4) one obtains:

$$\frac{\dfrac{R_1}{e.f.}}{\dfrac{R_1}{F_1}} = \frac{\dfrac{r_1}{s'}}{\dfrac{r_1}{s}} .$$

This reduces to
$$e.f. = F_1 \frac{(s')}{(s)} \qquad (5\text{-}5)$$

which is independent of aperture. From this,

$$e.f. = F_1 \frac{s'}{(F_1 - h)} \qquad (5\text{-}6)$$

and since
$$s' = \frac{s F_2}{s + F_2},$$

where s here was negative due to sign convention. From Eq. (5-1) the effective focal length is found to be:

28

HERE: h = Lens separation
s = Object distance ≈ ∞
s' = Image distance
F = Focal length
e.f. = Effective focal length
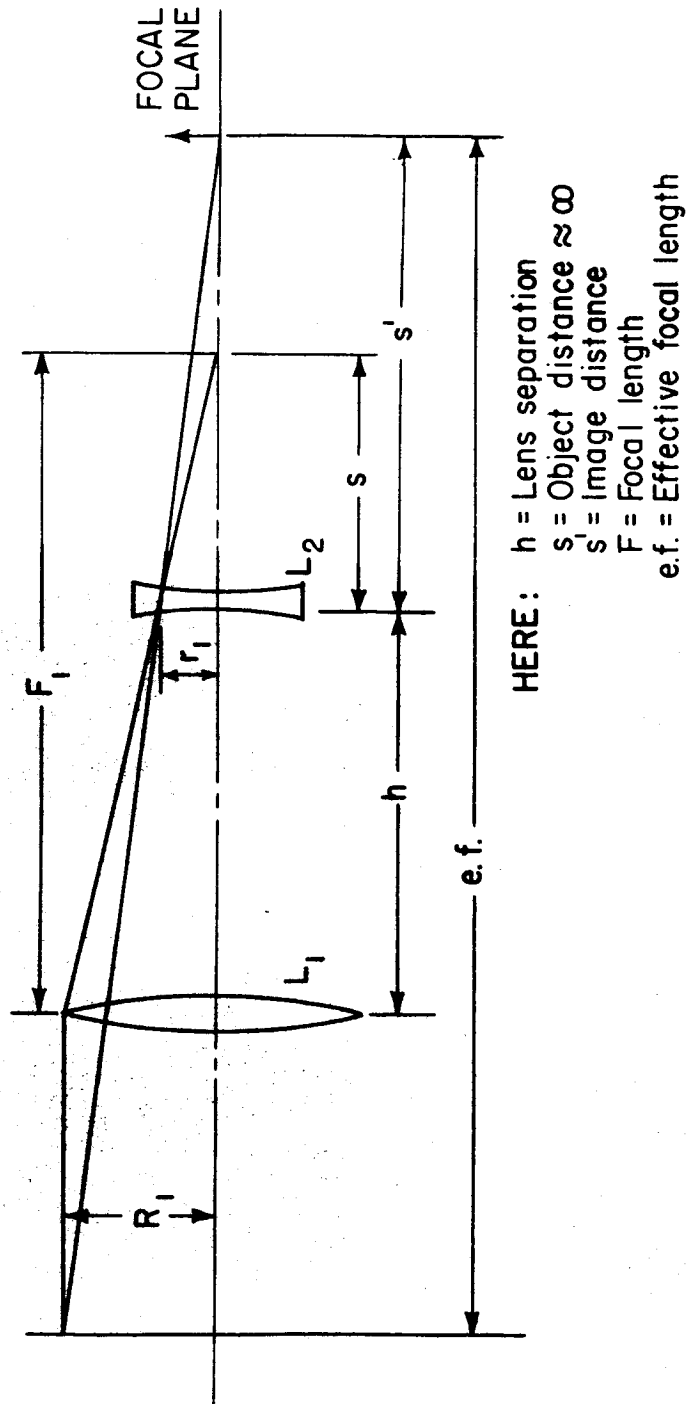
Fig. 5-7   Thin lens telephoto derivation.

29

$$e. f. = \frac{(F_1)(F_2)}{F_1 - h + F_2} \qquad (5-7)$$

From Eq. (5-7), the physical length of the system (s'+h) is computed to be:

$$\text{physical length} = \frac{e. f.}{F_1}(F_1 - h) + h$$

For the sun/star tracker, when F_1 equals 7 inches, h equals 4.87 inches, and F_2 equals -4 inches, there results a system with a physical length of approximately 8.5 inches and an e.f. of approximately 15 inches.

It might be noted that there is a certain amount of latitude in the choice of L_1, L_2, and h, various combinations of which achieve the same effective focal length. The lenses chosen for the sextant are merely a representative combination that falls within the region of practical lens design and is not necessarily the best.

N. Deviation of Field Modulator Prism Angles

To produce a stationary image at the photomultiplier, the cone of rays coming from the objective lens to the field lens 3 through the prism assembly must arrive as though the prisms were not in the path. When this condition is met lens L_3 can focus an image of the objective lens on the photomultiplier sensitive surface. Since the objective lens is fixed with respect to the photomultiplier, this image is stationary. To accomplish the above, the prism apex angles must be such that all rays emerging from the prism assembly will strike the focal plane at the same angles as rays ordinarily coming to the focal plane in the absence of the prisms.

The chief function of the prisms, namely, image displacement, must be performed. To meet both demands two prisms are required. Fig. 5-8, shows the paths of two rays striking the focal

.030 in.

S_1

S_2

P_2

P_1

FOCAL PLANE

WHERE: Δ_1 Deviation angle of P_1
Δ_2 Deviation angle of P_2
S_1 Focal plane distance of P_1
S_2 Focal plane distance of P_2

Objective lens

L_1
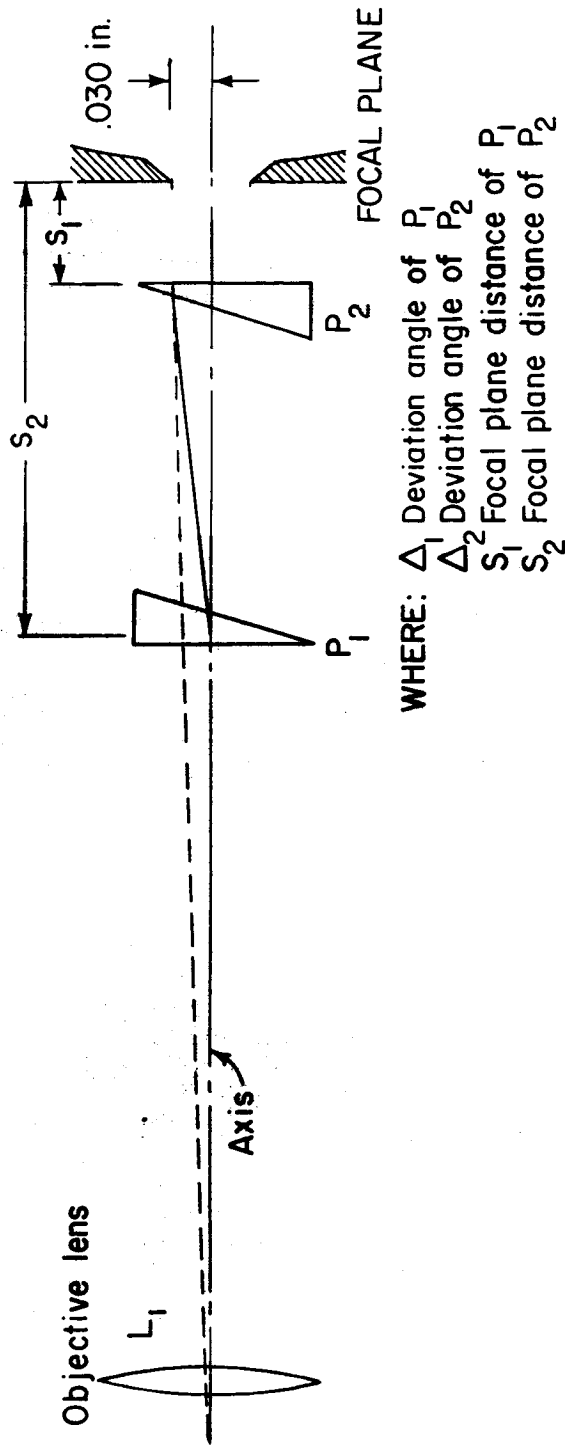
Axis

Fig. 5-8   Field modulator prism assembly optical path.

31

plane at 0.030 inches off axis. The ray passing through P_1 and P_2 will be superimposed on the ray going directly to the focal plane from L_1 when the geometry of the prism assembly is arranged as follows:

$$\Delta_1 (s_1 - s_2) + \Delta_2 (s_2) = 0.030 \text{ inches} \tag{5-8}$$

$$\Delta_1 - \Delta_2 = \frac{0.030}{\text{focal length of } L_1} \quad \text{or } 0.002 \text{ radians} \tag{5-9}$$

These two equations, when solved, determine $P_1 = 3.46^\circ$ apex angle and $P_2 = 3.22^\circ$ apex angle for the star/planet tracker. In the final case of building the instrument the calculations would be refined to include effects of prism thickness, but the foregoing indicates the required values to within approximately one percent.

II. Additional Field Modulation Studies

In addition to the field modulation method employed in the improved space sextant design presented in Section I, several other methods were studied. One of these is a mechanical method employing a rotating plate of glass in the same manner as the pair of wedges was used in Section I. It will be seen that the wedges are preferable. The remaining studies were efforts to eliminate moving parts from the field modulator while still retaining the intrinsic precision required in the instrument. The schemes presented all use polarized light modulated by electric fields, magnetic fields, and stress. None of these was found to be satisfactory.

A. Rotating Plate Modulator

The use of a rotating glass plate for field modulation was studied. A parallel plate interposed between the objective lens and the focal plane of a system will displace the image but also make the image astigmatic. Both effects are increased with increase of angle of plate normal to optical axis. To secure a

field of suitable width for sun tracking ($\frac{3}{4}°$) a ray displacement of 0.068 inches (for a 10 inch local length) will be required. This displacement can be obtained by interposing a parallel glass plate of 1/2 inch thickness with its normal at an angle of 20° with the optical axis of the telescope.

A converging beam of light incident on the plate will be displaced by varying amounts depending on the angle ϕ of the incident ray by the proportion:

$$\text{displacement} = t \sin \phi \left(1 - \frac{n \cos \phi}{n' \cos \phi'}\right)$$

n = index of refraction of air

n' = index of refraction of plate

Because of the variation in ϕ, the emerging beam becomes astigmatic and the projected rays no longer intersect at a point but now converge to a circle of least confusion--or area of best focus. An enlarged graph (see Fig. 5-10) using the dimensions of the above example gives a two dimensional picture of the vertical dispersion of the image. A three dimensional graph would show that there actually are two best foci, one for the least vertical dispersion and the other for the least lateral dispersion. Both distortion effects are comparable in size to the example shown.

On the basis of present study, the solid plate appears to be less effective than the wedge pair mainly because of wider dispersion due to greater incident angle. However, since a hollow shaft motor is employed, a more rigid rotor might be constructed using a plate. Both types--wedge and plate--should be made to compare overall advantages of each as a field modulator.

B. Polarized Light Shutters

Along with the study that was done towards the reduction of precision required in rotating parts, efforts were made to

33
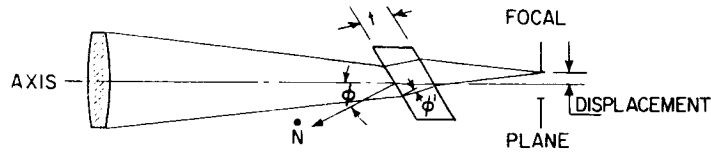
Fig. 5-9   Rotating plate modulator.
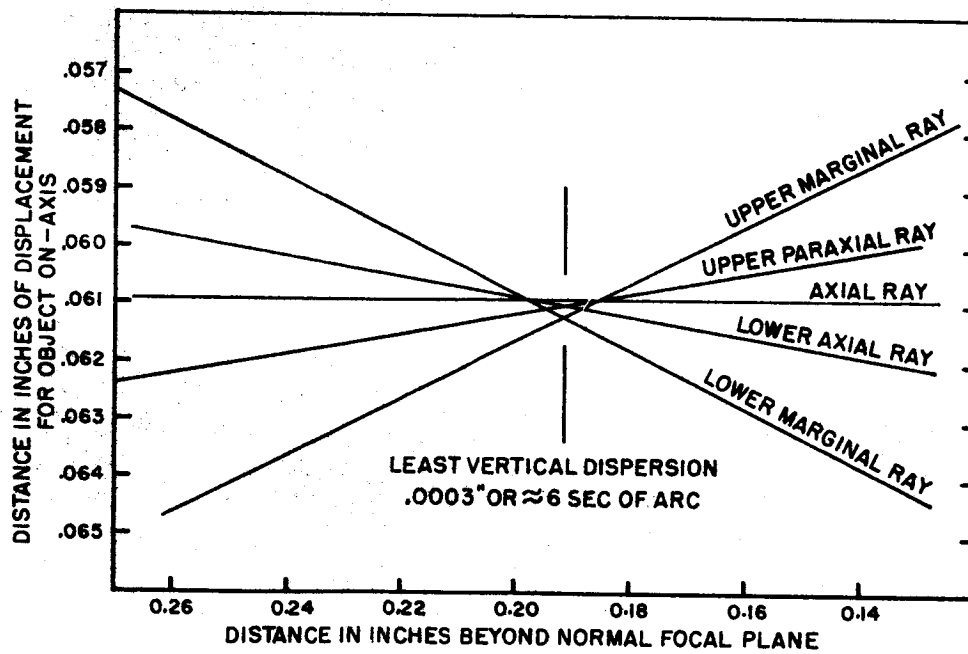
Fig. 5-10   Ray trace through thick plate

34

remove rotating items from the sextant entirely. Several schemes presented themselves, but for one reason or another were not practical for the present sextant. A brief outline of each method follows.

Polarized light shutters may use the Kerr cell, the Faraday cell, or the stress cell. * In general, all of these are methods of accurately resolving the field of the tracker into quadrants and modulating the incoming signal in order that the quadrant of the field from which the signal is obtained can be detected by the photomultiplier and associated circuitry. This is done by transmission modulating the field quadrant on a time basis and compares the phase of this modulated signal to a reference signal (e.g. if the phase difference between the reference and observed signals is zero degrees then the star signal is in the first quadrant). A phase difference of 90° between the observed signal and reference signal would put the target in the second quadrant, etc. The means of modulation in all cases is polarized light where the incoming signal light is linearily polarized and whose polarization is altered by the polarized light shutter. An immediate disadvantage of those schemes is the reduction of signal by a factor of slightly more than 2. The associated weight and power consumption of the polarized light shutters as well as the difficulty in obtaining an accurate division of quadrants further limits the effectiveness of this type of system.

1. **Kerr Cell**

Nitrobenzene, water and other materials, when under the influence of a strong electrostatic field become doubly refracting.

The change of optical path length of the extraordinary

---

*References for information on polarized light shutters and photoelasticity are Fundamentals of Optics by Jenkins and White, Chapter 29, for the former and Principles of Optics by Hardy and Perrin, Chapter 29, for the latter.

ray is found to be

$$\Delta = \frac{LE^2\lambda}{d^2} j ,$$

where:

Δ	=	optical path difference in cm.
L	=	path length in cm,
E	=	electric field in esu (1 esu = 300v),
d	=	plate separation in cm,
j	=	Kerr constant, (nitrobenzene $j = 2.2 \times 10^{-5}$)
λ	=	wavelength of light in medium in cm.

Behind the Kerr cell at the focal plane is a 4-quadrant plate made up of four precisely fitting plates as shown. All quadrant wave plates are oriented with their axes as shown in Fig. 5-11. As the field is applied, the Kerr cell acts as a variable wave plate. Light passing through a particular quadrant is polarized according to the sum of the retardation of that quadrant plate plus the effective value of the retardation of the Kerr cell at the time of transmission.

In Table 5-2 a table of values of transmission is presented for various quadrants with respect to different field strengths.

TABLE 5-2

TRANSMISSION VALUES

Kerr Cell	Transmission			
	Quad 1	Quad 2	Quad 3	Quad 4
0	1	c	0	c
$\frac{\lambda}{4}$	c	1	c	0
$\frac{\lambda}{2}$	0	c	1	c
$\frac{3}{4}\lambda$	c	0	c	1

36

QUADRANT PLATE
(EXTRAORDINARY AXES
AT 45° TO POLARIZER)

(QUAD 2) $\frac{\lambda}{4}$ PLATE — $\frac{\lambda}{2}$ PLATE (QUAD 1)

(QUAD 3) λ PLATE — $\frac{3}{4}\lambda$ PLATE (QUAD 4)

POLARIZER

OBJECTIVE LENS

KERR CELL

QUADRANT PLATE
(AT FOCAL PLANE)

ANALYSER
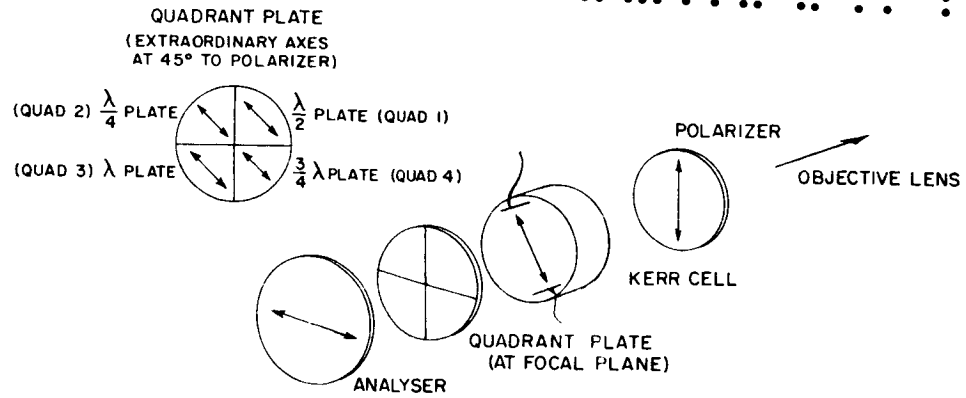
Fig. 5-11   Kerr cell quadrant analyzer.

No. 1 P.M.

FARADAY CELL

PRISM

No. 2 P.M.

FARADAY CELL

CALCITE CRYSTAL

OBJECTIVE LENS
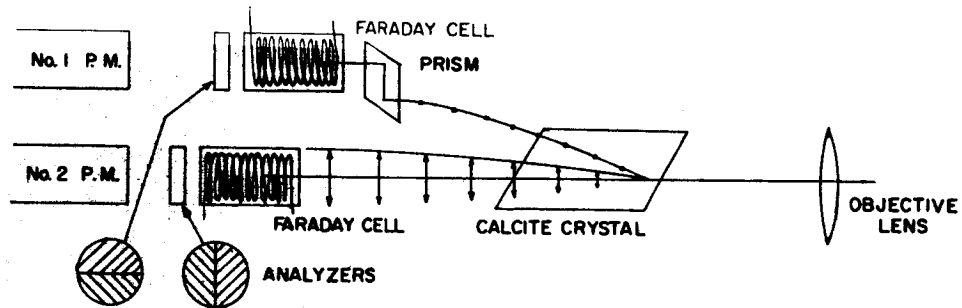
ANALYZERS

Fig. 5-12   Faraday cell quadrant analyzer.

FORCE

$\frac{\lambda}{4}$ $\frac{\lambda}{2}$

λ $\frac{3}{4}\lambda$

QUADRANT PLATE
(AT FOCAL PLANE)

POLARIZER

OBJECTIVE LENS

STRESS CELL

ANALYSER
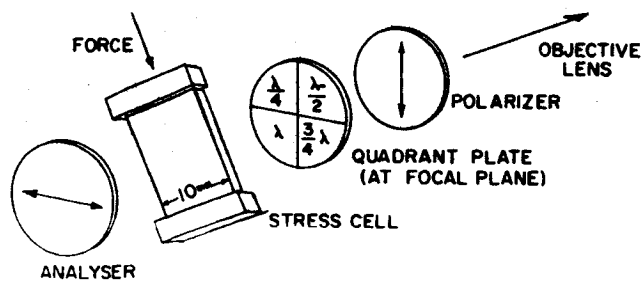
Fig. 5-13   Stress cell quadrant analyzer.

37

where   1   =   maximum transmission,

c   =   circularly polarized light
(transmission $\approx \frac{1}{2}$ max),

0   =   zero transmission.

As the field strength is increased, maximum transmission is sequenced through all four quadrants. A Kerr cell retardation of $\frac{3}{4}\lambda$ will require a maximum positive (or negative) voltage of 24.8 kv. A 4-quadrant modulator might be set up as 4 separate Kerr cells operating in sequence from one power supply, switched electrically from cell to cell. In this way maximum voltage is reduced to 14.3 kv.

2. Faraday Cell

Water, glass, carbon disulfide and other materials became optically active when subjected to a strong magnetic field. As plane polarized light is sent through the material in a direction parallel to the applied field, the plane of vibration is rotated through an angle θ, to the proportion:

$$\theta = VHL,$$

where θ =   the angle of rotation in minutes,

V   =   Verdet constant, rotation/unit path/unit field strength,

L   =   path length in cm.

A quadrant analyzing device might be set up as in Fig. 5 -12. As a strong magnetic field is applied to both Faraday cells in turn, the quadrant in which the signal appears can be isolated. Analyzer No. 1 determines right or left, while analyzer No. 2 determines up or down. A comparison of photomultiplier output with field supply will indicate the proper quadrant. Maximum signal will be obtained by rotating the plane of polarization in the Faraday cell by $\pm$ 45°. In this way, light is completely transmitted by one-

38

half of the analyzer and completely block in the other half.
To obtain a rotation of polarizing plane of 45°:

$$\theta = 60 \times 45 \qquad\qquad L = 5 \text{ cm}$$

$$= 2700 \text{ minutes of arc} \qquad V = 0.042 \text{ for } CS_2$$

$$H = \frac{\theta}{VL}$$

$$H = 12,900 \text{ oersted.}$$

3. Stress Cell

Glass, celluloid, transparent bakelite and many other plastics become doubly refracting (bi-refringent) when subjected to mechanical stress. The active axis is in the direction of the stress.

The retardation in path length of the extraordinary ray in respect to the ordinary ray in millimeters per millimeter thickness of material, when a uniform stress of 1 gram/mm^2 is applied, is given by the constant C. Typical values for this constant are:

$$\text{bakelite,} \qquad C = 60 \times 10^{-8}$$

$$\text{glass,} \qquad C = 2.5 \times 10^{-8}$$

A quadrant type of modulator might be set up as in Fig. 5-13. The quadrant analyzer would be constructed similarly to the Kerr cell example with quarter sections comprised of λ, $(1/4)\lambda$, $(1/2)\lambda$ and $(3/4)\lambda$ plates. The retardation of path for a 1 cm^2 cell of 1 mm thickness is computed from:

$$\text{Retardation (mm)} = \frac{\text{Const} \times \text{Force (gm)}}{A \text{ (cross-section in mm}^2\text{)}} \text{,}$$

or, for $(3/4)\lambda$ retardation, the force required is:

$$6,270 \text{ grams} = 13.8 \text{ lbs.}$$

where

$$\lambda = 5 \times 10^{-4} \text{ mm.}$$

III. Space Sextant Detector Noise Studies

In evolving the improved space sextant design presented in Section I, various detectors were considered for the functions of sun tracking, star tracking, and disc scanning. The selection resulted from studies of noise, sensitivity, and other characteristics of the various detectors considered. This section presents some of the noise characteristics of photomultipliers and silicon photovoltaic cells applied to sun and star tracking.

A. Noise Measurements on a Silicon Photovoltaic Cell Transistor-Amplifier for Star Tracking

Representative noise measurements were made on some silicon solar cells in combination with a suitably designed transistor amplifier in an effort to eliminate the need for photomultiplier tubes. The results indicate that these detectors will not give satisfactory performance with an objective of reasonable aperture.

1. The Measurement of the Cell-Amplifier Noise

The experimental apparatus for the measurement of the noise equivalent power of the cell-amplifier combination is shown in Fig. 5-14. The light source was a tungsten lamp which was chopped at 90 cps. The chopped illumination at a distance of 4.5 inches from the small source was measured using a calibrated solar cell. The rms value of the fundamental component of the calibrated cell output current was equal to that which would result from 472×10^{-6} watt-cm^2 of illumination having the same spectral characteristics as sunlight.

The illumination at the solar cell undergoing the test was provided by the reflection of the source in a small polished sphere. This enabled the attenuation of the measured illumination by a factor which could be readily calculated. In this experiment the attenuation was calculated to be 5.38×10^{-6}.

90 CPS SQUARE-WAVE CHOPPER

TUNGSTEN FILAMENT 23" FROM SPHERE

INT. RECTIFIER SOLAR REFERENCE CELL (AT 4.5")

TO 736-A

32 Ω

OUTPUT

TO GENERAL RADIO 736-A WAVE ANALYZER
$\Delta f = 5$ CYC, S/N READS 15.8

PREAMP + −

LIGHT SHIELD **58C HOFFMAN SILICON SOLAR CELL − 8 mm² 23" FROM SPHERE**

ALUMINUM COATED GLASS SPHERE (RADIUS = 1.4 CM)
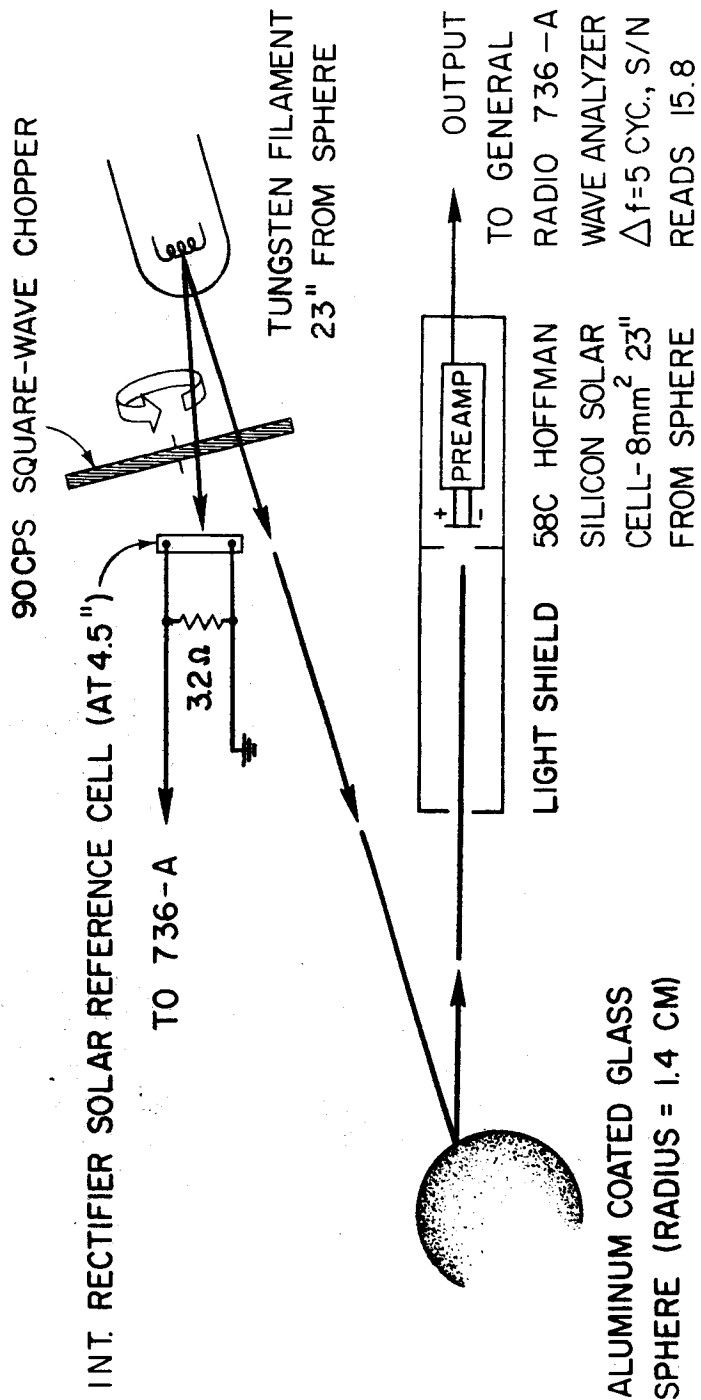
Fig. 5-14 Experimental apparatus for noise measurement.

41

The test cell signal was the input to a transistor amplifier (circuit shown in Fig. 5-15). A wave-analyzer having a bandwidth of 5 cps was used to monitor the amplifier output signals of several millivolts. A signal-to-noise ratio of 15.8 was obtained by comparing the wave-analyzer output with the test cell illuminated to its output with the test cell unilluminated. The test cell used had an area of 0.08 cm^2 and was Hoffman Type 58c.

The noise equivalent power (NEP) input of the test cell and amplifier can be computed.

$$NEP = (472 \times 10^{-6} \text{ watt-cm}^{-2})(5.38 \times 10^{-6} \text{ attenuation})(0.08 \text{ cm}^2)$$

$$(\frac{1}{15.8} \text{ noise-to-signal})$$

$$= 1.28 \times 10^{-11} \text{ watts-rms silicon cell equivalent of solar energy.}$$

A speculation on the nature of the noise is of interest. First, the noise equivalent input current to the amplifier can be deduced by assuming linearity of the test cell. The responsivity, R, of the 58c test cell was measured by placing it 4.5 inches from the source. The output of the cell at this location was 6.3×10^{-6} amp-rms, giving a responsivity of:

$$R = \frac{6.3 \times 10^{-6} \text{ amp-rms}}{(4.72 \times 10^{-6} \text{ watts-cm}^{-2})(0.08 \text{ cm}^2)} = 0.167 \text{ amp-rms-watt}^{-1}.$$

Thus, the noise equivalent current input to the amplifier during low level illumination must have been $(0.167 \text{ amp-watt}^{-1})$ $(1.28 \times 10^{-11} \text{ watt-rms NEP}) = 2.13 \times 10^{-12}$ amp-rms.

Since the amplifier input of the circuit shown in Fig. 5-15 looks at the parallel-connected 42K bias resistor and the 100K resistance of the test cell, it would be expected that the noise current into the amplifier includes thermally excited Johnson noise from a 29K ohm resistor. The noise current from this resistor at room temperature is calculated to be:

Fig. 5-15   Amplifier for silicon cell output.
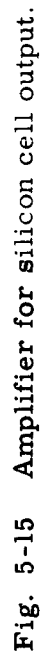
$$(i_{rms})^2 = \frac{(1.6 \times 10^{-20} \text{ watt-sec})(5 \text{ cps})}{(29 \times 10^3 \text{ ohms})} = 2.76 \times 10^{-24},$$

$$i_{rms} = 1.65 \times 10^{-12} \text{ amps.}$$

No noticeable change in noise level occurred when the cell was replaced with a resistor of equal impedance. Thus, the noise from the cell appears to be entirely of the Johnson type. The remaining noise may be assumed to originate in the amplifier which therefore has a noise figure of

$$NF = \frac{2.13}{1.65} = 1.7 = 2.3 \text{ db.}$$

For comparison, it is interesting to deduce the approximate **normalized detectivity (D*) of the test silicon cell. The experiment suggests that the noise equivalent current from it alone would be that of a 100K resistance, or:**

$$i_{rms} = \frac{(1.6 \times 10^{-20} \text{ watt-sec})(5 \text{ cps})}{105 \text{ ohms}} = 80 \times 10^{-26} \text{ amp}^2 = 0.9 \times 10^{-12} \text{ amps.}$$

This would give a noise equivalent power for the cell alone of:

$$NEP = \frac{0.9 \times 10^{-12} \text{ amp-rms}}{0.167 \text{ amp-rms-watt}^{-1}} = 5.4 \times 10^{-12} \text{ watt-rms.}$$

Thus, the normalized detectivity would be:

$$D* = \frac{(A \Delta f)^{1/2}}{NEP} = \frac{[(0.08 \text{ cm}^2)(5 \text{ cps})]^{1/2}}{5.4 \times 10^{-12} \text{ watts}} = 1.17 \times 10^{11} \text{ cm-sec}^{1/2} - \text{watt}^{-1}.$$

Since D* is independent of cell area and signal bandwidth within the bandpass of the semiconductor photodetectors, this parameter is used to compare types of semiconductors regardless

of area or bandwidth D^* for the best PbS cells[†] is less than half that deduced from this experiment on a 58 c silicon cell.

The minimum noise levels realized in this experiment leave little opportunity for further noise reduction in the cell-amplifier combination. Cooling the cell reduces the Johnson noise from it, but the amplifier noise prevents any significant reduction in the overall noise level. Increasing the impedance of the cell would **make it possible to transformer-match the cell to the amplifier.** This increases the input current with a subsequent improvement of the ratio of the signal to the Johnson noise current. However, the use of a transformer introduces additional weight and pickup problems particularly at low frequencies. Increasing the chopping frequency may lessen the effect of amplifier noise but increases the problems in the chopper mechanism. This increased chopper **speed was attempted in the present experiment but the motor was too noisy at the higher speeds to permit conclusions.**

The most likely improvement results from the use of a cell having a better response, but with roughly the same impedance of 60 K to 120 K ohms. The response of the calibrated cell was about 1.65 times that of the 58 c. The conductance per unit area of the reference cell was about 0.6 that of the 58c. Since D^* increases with the response, and since the Johnson noise equivalent current varies with the square root of the conductance, D^* would be expected to improve by a factor of at least

$$1.65/\sqrt{0.6} = 2.15$$

if selected cells are used. These expected results have been demonstrated by later experiments the details of which are not presented here.

[†] Jones, R. C., Phenomenological Description of the Response and Detecting Ability of Radiation Detectors, Proc. I. R. E., Vol. 47, No.9 p. 1502, 1959.

2. Application of the Cell-Amplifier Combination to Star Tracking

The signal-to-noise ratio for star tracking using the cell-amplifier combination under study will be calculated. The sixth brightest star gives an illumination of 0.25×10^{-10} lumens/cm^2. This illumination is equivalent to 2.5×10^{-12} watt-cm^2 of solar radiation assuming that the spectrum of the star and the sun are equivalent.

Suppose that the illumination from this star is collected with a lens having an aperture of d. Then $(2.5 \times 10^{-12})(\frac{\pi}{4})$ d^2 watts would fall on the test cell under consideration. If this light were chopped as indicated previously, the modulated signal would have an rms value of $1.25 \times 10^{-12} \frac{\pi}{4}$ d^2 watts.

The signal-to-noise ratio using a 10 cps bandwidth is given by:

$$\frac{S}{N} = \frac{1.25 \times 10^{-12} \frac{\pi}{4} d^2 \text{ watt-rms}}{(1.28 \times 10^{11} \text{ watt-rms})(\sqrt{2})} = 0.054 \, d^2 \, ,$$

if d is expressed in centimeters.

The values of S/N for several values of d are:

d (inches)	S/N
1.5	0.8
3.0	3.1
4.0	5.6
5.0	8.7

If the factor-of-two improvement resulting from the use of selected cells is considered, the above values would be doubled. It is seen that the four-inch aperture has satisfactory signal-to-noise ratio but is not of satisfactory size.

B. Star Tracker Photomultiplier Noise Calculations

The predominant source of noise in the photomultiplier use for star tracking arises from the shot effect in the very small cathode currents. Typically, currents of 0.3×10^{-12} amperes leak from the cathode of an unilluminated photomultiplier tube at room temperature. Noise generated in the amplifying stages of the tube and in the transistor amplifier following are negligible in comparison with cathode current shot noise. The rms noise current i_N, in bandwidth f, resulting from the random emission of single electrons in a current of average value I, can be calculated by the formula for shot noise:

$$i_N = \sqrt{2\ qIf}\ ,$$

where q is the charge on the electron. Using f = 10 cps, $I = 0.3 \times 10^{-12}$ amperes and $q = 1.6 \times 10^{-19}$ coulombs yields:

$$i_N = \sqrt{(2)(1.6 \times 10^{-19})(0.3 \times 10^{-12})(10)} = 10^{-15} \text{ amperes-rms.}$$

This current must be compared with the rms current resulting from the modulated star light to be detected in order to obtain the signal-to-noise ratio. Using the sixth brightest star as in the previous calculations on noise from silicon detectors, and using the 1.5 inch collecting aperture in the space sextant design presented earlier, it is seen that the starlight available for the photomultiplier is $(2.5 \times 10^{-10} \text{ lumens-cm}^2)(2.54 \text{ cm-in}^{-1})^2 \cdot (1.5 \text{ in})^2 \left(\frac{\pi}{4}\right) = 3 \times 10^{-9}$ lumens. Cathode current sensitivities are usually greater than 33×10^{-6} amps-lumens^{-1}. Thus the starlight causes cathode currents of more than 10^{-13} amperes.

Since the dark current is not stable, the light from the star must be modulated so that its detection will be possible. The modulation described in Section I of this chapter is roughly of a square wave type. Using this scheme and ignoring the average value of the cathode current, there is a modulated cathode

current of 0.5×10^{-13} amperes rms which can be detected. It can be seen that the starlight-caused cathode current divided by the shot noise current gives a signal-to-noise ratio of $\frac{50 \times 10^{-15}}{10^{-15}} = 50$ with a 10 cps bandwidth. This is a good signal-to-noise ratio, and it should give reliable detection.

With the optics presented in Section I, it can be expected that the image of the star will be somewhat more extended than the theoretical 4 seconds of arc resolution of the 1.5-inch aperture. Assume that, because of aberrations in the optics, the image is evenly smeared over a circle 20 seconds of arc in diameter. There would then be a signal-to-noise ratio of 6 in the indication of a 2-second of arc displacement of the center of the star's image. This is the order of magnitude of the noise expected in the detection of the misalignment of the telescope.

With the space sextant presented in Section I, it is occasionally necessary to simultaneously track the brightest star and to scan the least bright planetary disk using the single photomultiplier. The light from the brightest star will increase the cathode current from its dark value of 0.3×10^{-12} amperes to approximately 2.7×10^{-12} amperes. This will result in an increase by a factor of three in the shot noise current. The disk scanning signal for the moon is only 10^{-8} lumens peak which gives a cathode current of 10^{-13} amperes-rms. Disk scanning requires a signal having a bandwidth of nearly 1,000 cps. The approximate calculation gives:

$$i_N = \sqrt{(2)(1.6 \times 10^{-19})(2.7 \times 10^{-12})(1000)} = 3 \times 10^{-14} \text{ amperes-rms.}$$

Thus it is seen that a signal-to-noise ratio of slightly more than 3 is encountered in scanning the moon while tracking the brightest star.

The reverse case of simultaneously tracking the sixth brightest star while scanning the brightest disk is also of interest.

The disk scanning aperture can gather 3×10^{-7} lumens from Venus. This light gives a 10^{-11} ampere cathode current which subsequently increases the noise for star tracking by a factor of 5. These conditions give a signal-to-noise ratio of 10 for star tracking. This is still acceptable.

Scattered sunlight could be a very important noise factor in the space sextant. It is apparent from the above calculation of noise that, while disk scanning Venus, an equal quantity of scattered sunlight would be tolerable. However, 5×10^{-7} lumens would represent the upper limit for allowable scattered light. Approximately 100 lumens of sunlight enter the baffled lens hoods of the telescope when tracking a star which is 15° away from the sun. Only one part in 2×10^{8} of this light can be permitted to reach the photomultiplier. Further, this light must be modulated by less than 1% in order not to provide false indication of a star. It is apparent that the design against scattered sunlight is the major noise problem in the space sextant.

C. Sun Tracker Shot-Noise Calculation

A silicon solar cell is used as the detector for sun tracking in the space sextant of Section I of this chapter. The main problem in sun tracking is quite different from that in star tracking since in the former there is a strong modulated signal in the presence of a very large steady signal. The shot noise current resulting from the large steady signal in the cell is the primary interference in the detection of the modulated signal.

In Fig. 5-16 the scanning aperture on the sun's on-axis image is represented by the solid circle. The sun's image has a radius of 8 milliradians as it would at a distance of slightly more than one-half an astronomical unit which represents the worst noise situation to be encountered. As the wedge modulator rotates, the scanning aperture is rotated on the axis of the telescope and a constant amount of the sun's light is seen by the

SUN OFF NULL 25 x 10^{-6} RADIANS

SUN IMAGE AT NULL OF SUN TRACKER

$$\frac{\text{PEAK SIGNAL}}{\text{BACKGROUND SIGNAL}} \approx \frac{25 \times 10^{-6} \times 4 \times 10^{-3}}{\pi (4 \times 10^{-3})^2} = .002$$

$> r_s/2 = 4 \times 10^{-3}$ rad

SCANNING APERTURE

25 x 10^{-6} rad

$r_s = 8 \times 10^{-3}$ rad

SUN IMAGE ROTATION
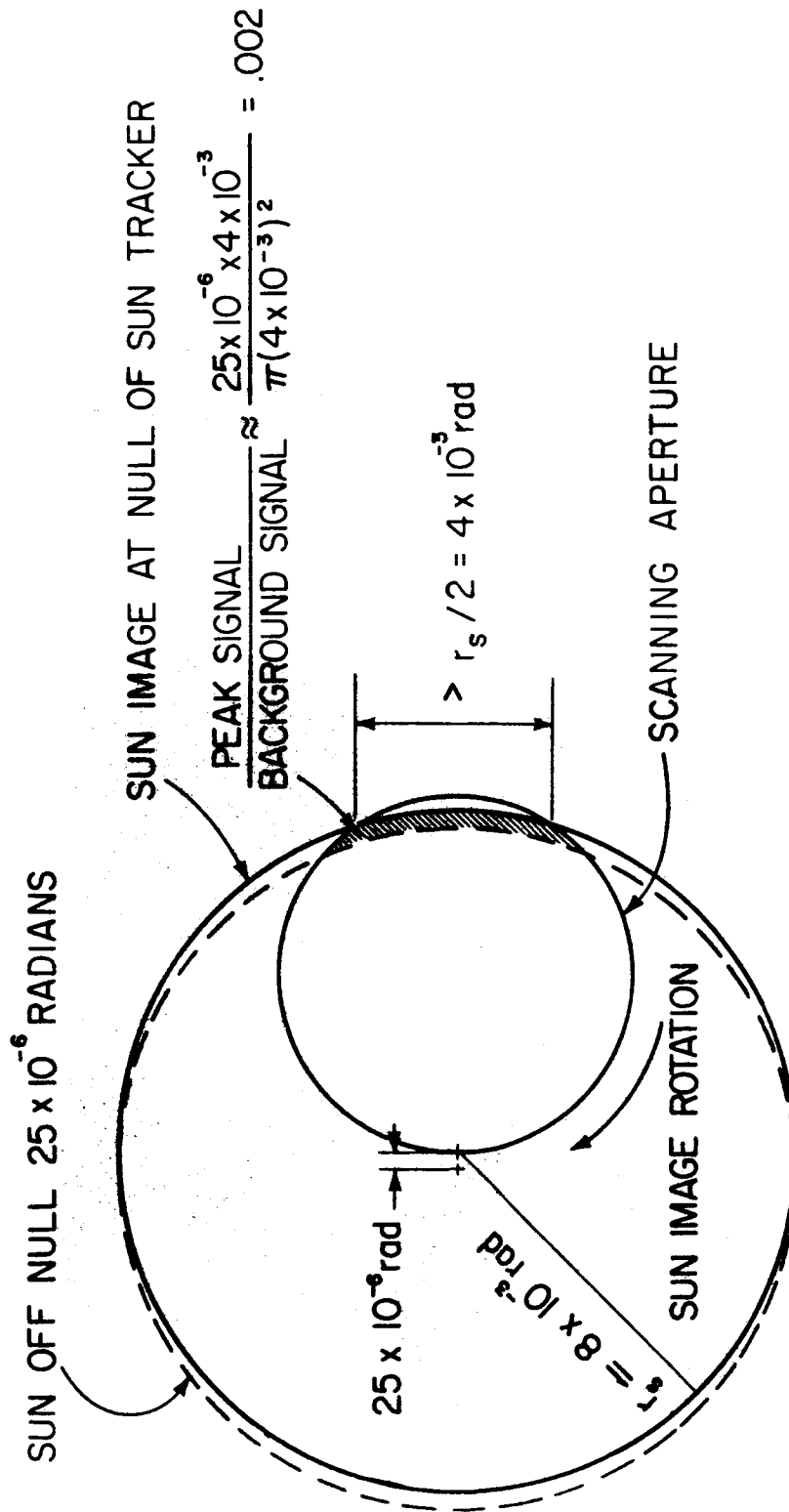
Fig. 5-16   Sun scanning geometry at distance of one-half astronomical unit.

detector. This steady light signal has a power load of approximately one-quarter of the 6 watts gathered by the lens at this distance.

The dotted circle represents the sun's image off-axis by five seconds of arc $(25 \times 10^{-6}$ rad). The shaded area in the figure represents the center to peak amplitude of the modulated light. It can be seen from the geometry that the modulation is approximately 0.2% of the steady light.

In the space sextant, 4% of the light which passes through the scanning aperture of the sun/star tracker is focused on a silicon solar cell using a beam-splitting prism.

For this distance from the sun, the steady and the modulated light incident on the cell are then 60 and 0.12 milliwatts, respectively. These light signals cause currents of 15 and 0.03 milliamperes, respectively.

Now the rms value for the shot noise current can be calculated by the following formula:

$$I_{N_{rms}} = \sqrt{2qIf}.$$

Taking q to be 1.6×10^{-19} coulombs, I to be 0.015 amperes, and f to be 10 cps yields a value for $I_{N_{rms}}$ of 2.2×10^{-10} amperes. A signal-to-noise ratio of 10^5 is obtained by comparing the 0.02 milliampere rms with this noise.

The above signal-to-noise ratio is decidedly adequate. For greater distances from the sun the signal-to-noise ratio increases further.

IV. Sunfinder Investigations

Further investigation of the sunfinder described in Chapter 9 of R-235 has generated additional information on sunfinder repeatability, field of view, blind zones, and dead-zone

operation. The possible errors caused by illumination from nearby planets was also considered and several methods of sun-orienting the vehicle were considered. The method chosen uses two sunfinders at opposite ends of the vehicle, and allows orientation to be done directly without any search pattern.

A. Repeatability Measurements

The procedure chosen for measuring sunfinder drift consisted of making relative drift measurements between four single-axis sunfinders rigidly mounted on a common base with their null planes approximately parallel as in Fig. 5-17. A fifth sunfinder is mounted with its null plane perpendicular to the other four and is used to establish the plane of the sun's path.

In operation of the test, the sunfinders are directed toward the sun and the base structure is rotated about the sunline until the fifth sunfinder registers null current steadily with time. The null planes of the other four sunfinders are positioned just ahead of the sun's path. As the sun passes normally through the null plane of each sunfinder, the time is recorded by a stop watch. Since it is most improbable that all of the sunfinders would drift at the same rate and in the same direction, any relative drift between them would indicate the absolute drift rate of the device.

It is possible to measure relative null angles with an accuracy of better than 3 seconds of arc using a stop watch and to measure the sun's motion of 15 seconds of arc per second of time across the four null planes.

Measurements on two successive days indicated less than 30 seconds of arc drift between the sunfinders. However, the meter output showed up to 30 arc-seconds of random fluctuations which are assumed to be due to some combination of atmospheric effects, high winds, and operating difficulties associated with the extreme cold of clear winter days. More complete measurements are planned during warmer weather.

SUNFINDER PRISM

NULL METERS
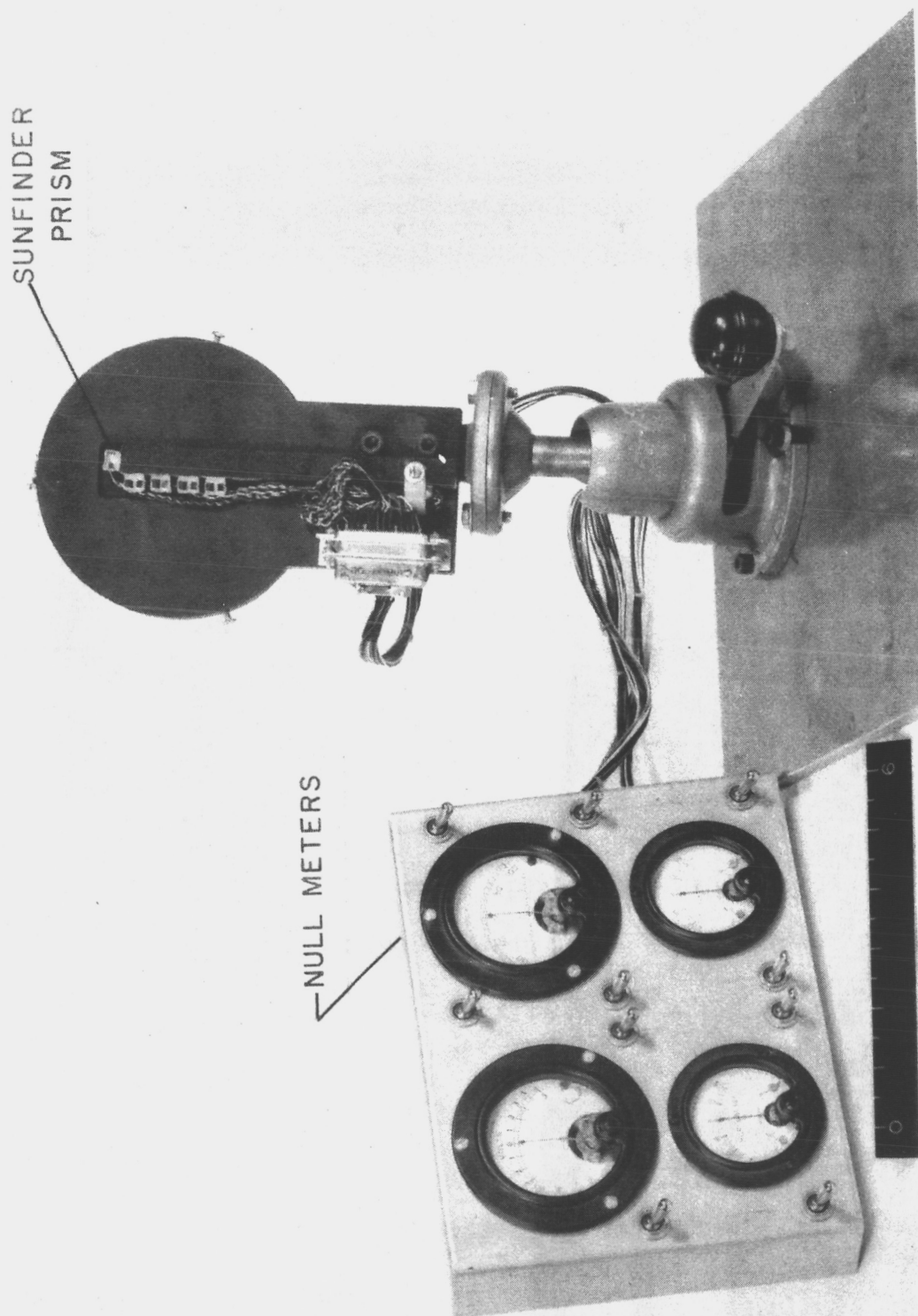
Fig. 5-17 Experimental set-up for sunfinder repeatability measurements.

53

B. Field Characteristics

The characteristics of a sunfinder pair were plotted using a tungsten lamp as an artifical sun. The results are shown in Fig. 5-18. It is evident that a blind zone exists towards the sides of the null plane. However, a common blind zone for both of the orthogonal sunfinders cannot occur anywhere less than 85° from the sunline. Hence, even if one unit gives no signal within this $\pm 85^\circ$ range, the other unit will provide a signal indicating the direction of its null plane. The use of this signal will soon bring the former unit out of its blind zone.

When the sun is greater than 85° from the null of the units, it was previously assumed that some search routine would guarantee acquisition of the sun. Several solutions to this problem were considered, but the simplest uses a second set of sunfinders mounted on the opposite face of the spacecraft and pointing in the opposite direction from the first set. The basic prism structure can be altered slightly to increase the maximum field to over 95°. This arrangement will provide a complete 360° field of view with no common blind zone. Hence, no search pattern is necessary.

The revised prism structure is shown in Fig. 5-19. It can be seen that ray b, 80° from null, illuminates the right hand silicon cell after refracting through the long side of the prism. However, as the null angle of ray b is increased to 90°, this illumination drops to zero. The increased null angle increases the illumination from ray c by an amount sufficient to keep the output indication at the proper strength and polarity. This is also true for rays d and e. In fact, it has been demonstrated that sufficient signal is received up through null angles of $\pm 180^\circ$.

Because of the shadow of the spacecraft, however, two sunfinders on opposite ends of the spacecraft are used. The arrangement for one axis is shown in Fig. 5-20. The right hand cells of the two prisms are connected in parallel aiding as are the left hand pair. The sums from the two pairs are differenced to
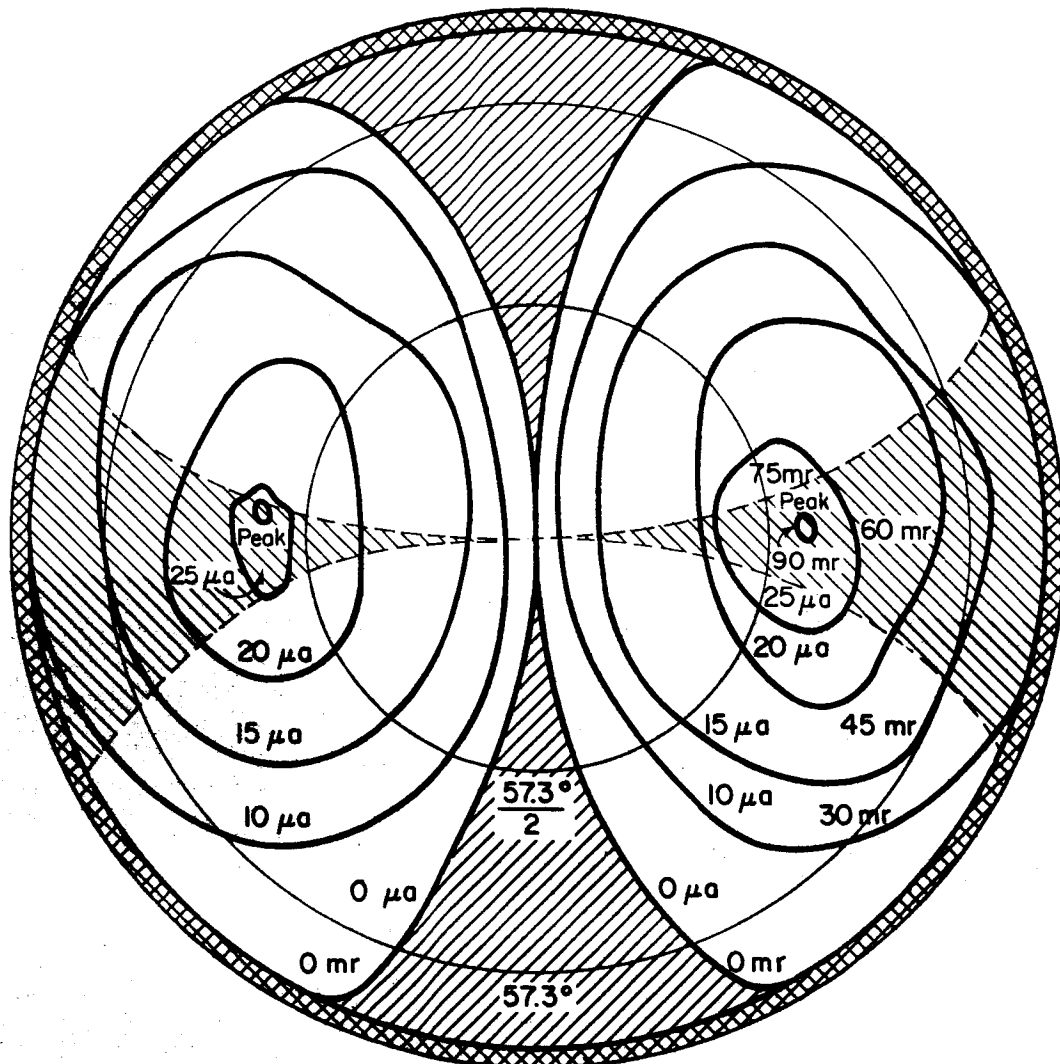
NULL SENSITIVITY:
3 mr /μa (< 10 mr from null)

TEST LAMP ILLUMINATION=
.5 x 10^{-3} wt /cm^2

DEAD ZONE
(ONE PRISM)

DEAD ZONE FOR A SEC-
OND PRISM AT 90°

COMMON DEAD ZONE FOR
BOTH PRISMS

Fig. 5-18   Sunfinder field characteristics.

SUN RAY AT NULL

RAYS AT 80°

CRITICAL ANGLE
FOR 1.0 MICRON ≈ 42°

−.001" SPACE

RAY AT
135°

SOLAR CELL OUTPUT:
13 μ AMPS/ MILLIRADIAN
(NEAR EARTH WITH SUN
± 15 MR FROM NULL)

ACTUAL SIZE
OF PRISM
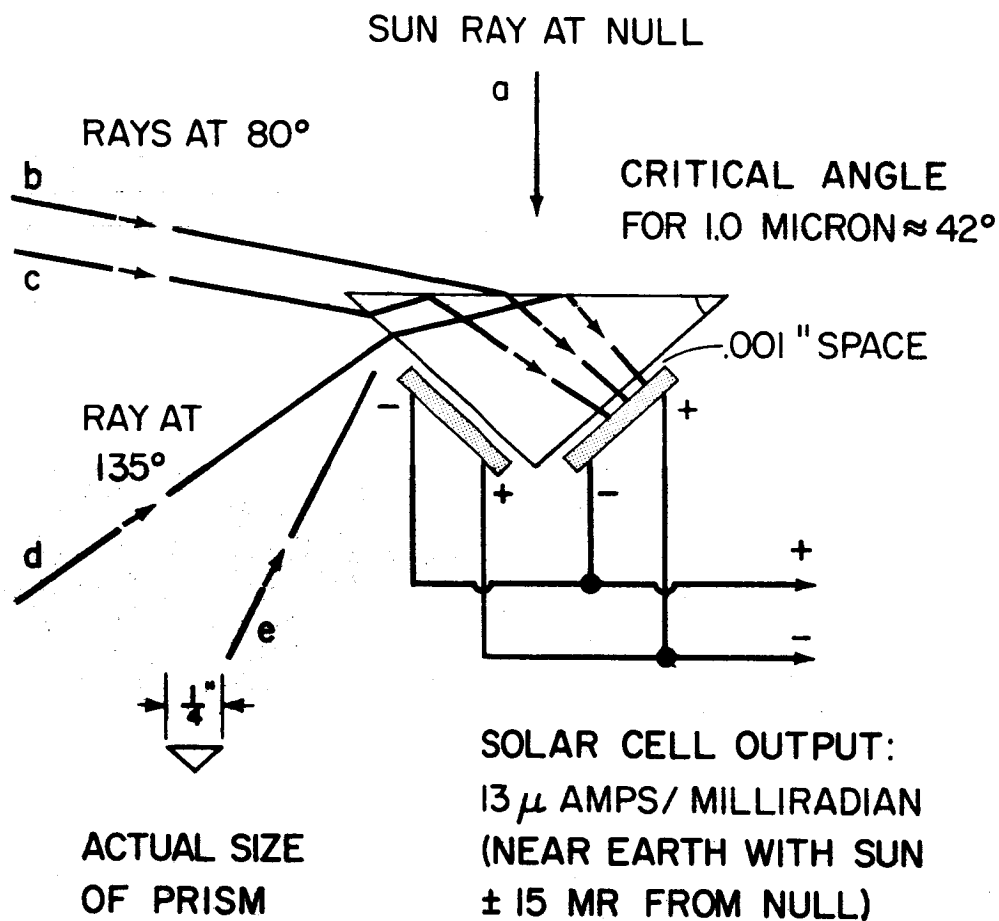
Fig. 5-19   Prism structure for extending field beyond ± 90°.

200° FIELD

SUNFINDER

VEHICLE

200° FIELD
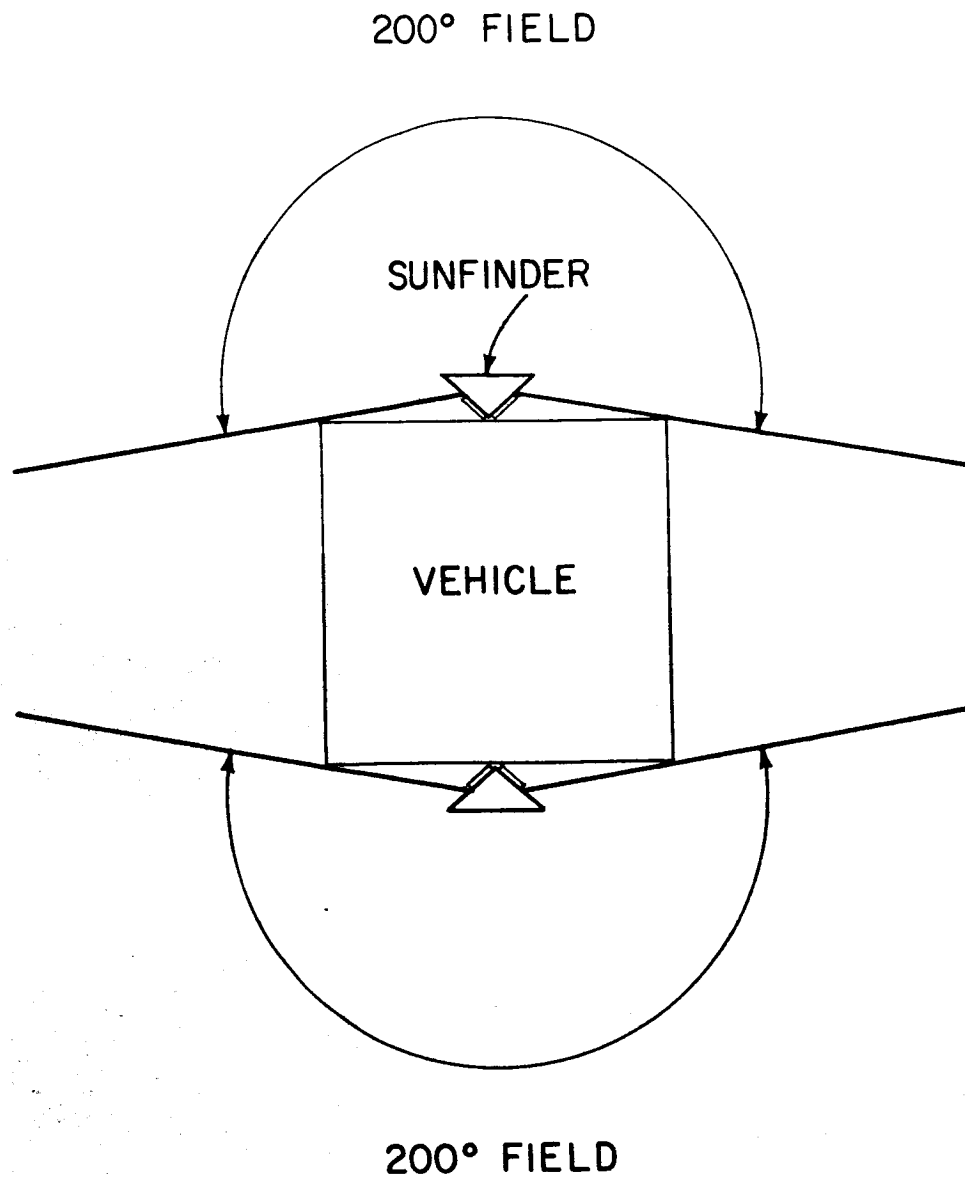
Fig. 5-20   Sunfinder system providing complete spheroid field of view.

give one signal indicating whether the sun is to the left or right of the null plane.

In some instances, spacecraft parts, such as the protuberance of the space sextant, may block the sun from a particular prism. However, as long as one prism of the pair for the other axis is not in such a shadow or in its inherent blind zone, no difficulties are encountered. An arrangement depicting this property is shown in Fig. 5-21.

C. Effect of Nearby Planets or Satellites

The effects of planet or satellite radiation on the sunfinder may be computed with the characteristics plotted in Fig. 5-18. The isolines shown are labeled with both the current output due to the test lamp used and the equivalent angle of this current referred to the measured gain about null (3 milliradians per microamp).

By way of example, if the sun was at null and a planet appeared at the peak response point (90 mr), the null position would shift toward the planet by the angle

$$\theta_p = 0.09 \frac{E_p}{E_s} \text{ radians,}$$

where θ_p is the angular error caused by the planet and E_p and E_s are the illumination from the planet and sun, respectively. Hence, if the planet illuminated the vehicle with approximately 1% of the sun's illumination, the null would shift by

$$\theta_p = 0.09 \times 0.01 = 9 \text{ milliradians}$$

Since this amount is within the 10 mr linear range about null, the result is valid. A more general expression for this error may also be derived. For simplicity, the planet will be assumed to be a disc of the same albedo, diameter, and located at the same distance as the planet. Further, it is assumed that

58

60W WRN - 5337

PROTRUDING OBJECT

SUNFINDERS

VEHICLE

SIDE VIEW

PROTRUDING OBJECT

SUNFINDERS

PROTRUDING OBJECT

END VIEW
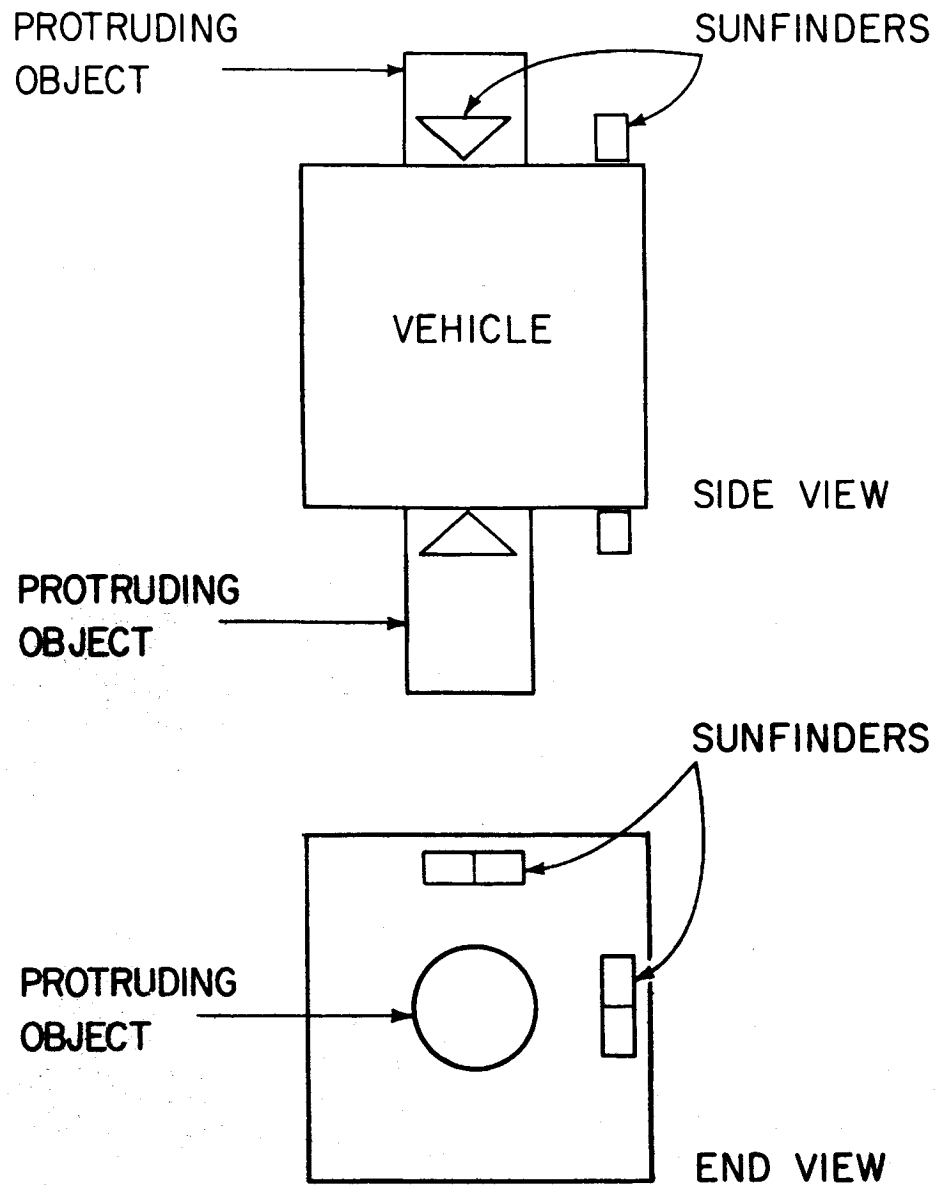
Fig. 5-21   Sunfinder placement to avoid simultaneous blind zones
on both axes.

59

both the sun and the sunfinder view the disc from a direction normal to the surface. Although these assumptions are geometrically impossible, the planet illumination computed therefore is conservatively high. The previous expression for θ_p may thus be stated as

$$\theta_p = 0.09 \frac{E_p}{E_s}$$

$$= 0.09 \frac{B_p}{B_s} \left[\frac{d_p}{d_s}\right]^2 ,$$

where B_p, B_s are the brightness values and d_p, d_s are the angular diameters of the planet and sun respectively as seen from the vehicle. Now substitute the expression for albedo of the planet, A_p,

$$A_p = \frac{B_p}{B_s} \left[\frac{R_s}{r_s}\right]^2 ,$$

where r_s is the radius of the sun and R_s is the distance between the sun and the planet, the result is

$$\theta_p = 0.09 A_p \left[\frac{r_s}{R_s d_s}\right]^2 d_p^2 .$$

The effect of the planet on the sunfinder is only significant when the vehicle is very close to the planet. Therefore, using small angle approximations, the quantity in the bracket is always equal to $\frac{1}{2}$. Substituting this value results in:

$$\theta_p = 0.0225 A_p d_p^2 .$$

Applying this to the particular instance when the planet Venus subtends an angle of 0.5 radian gives an error of

$$\theta_p = 0.0225 (0.6)(0.5)^2 = 3.4 \text{ milliradians.}$$

RN - 5337

This result is within the linear range about null ($< \pm 10$ mr) and is therefore valid. Since Earth and Mars have lesser albedoes of 0.3 and 0.15, respectively, the same θ_p is obtained for Earth subtending 0.7 radians and Mars subtending 1.0 radians.

Although these results are based on the measured characteristics of a sunfinder not having the extended field of Fig. 5-19, the characteristics around null and the peak response area are identical. Hence, negligible difference will occur with the extended-range design.

Another possible consideration of planet effects arises when for some reason, the sun is not at null but at an angle which gives the lowest response possible. If the planet is in a position of high response, it is possible that the planet signal could be large enough to oppose the sun signals such as to create a new erroneous null position. If this condition occurred in one sunfinder, it could not simultaneously occur in the second sunfinder of Fig. 5-18. The use of the correct signals from the second would soon move the vehicle so that a false null became impossible in the first.

D. Dead Zone Mode

The dead zone as described in R-235 was obtained by using two pairs of sunfinder prisms at slightly different angles. Since that time a simpler system was designed and incorporated into the sunfinder demonstrator shown in Fig. 5-22.

This system uses a pair of solar cells to create a bias current for use with the two sunfinder coordinates. The resulting dead-zone angle is independent of the distance to the sun.

E. Sunfinder Circuit

The circuit for the sunfinder is shown in Fig. 5-23. The two parallel-connected pairs of silicon cells are applied in a grounded-base connection to each of two series-connected transistors, T_1 and T_2. This produces only unity current gain but

SUNPOINTER
PRISMS
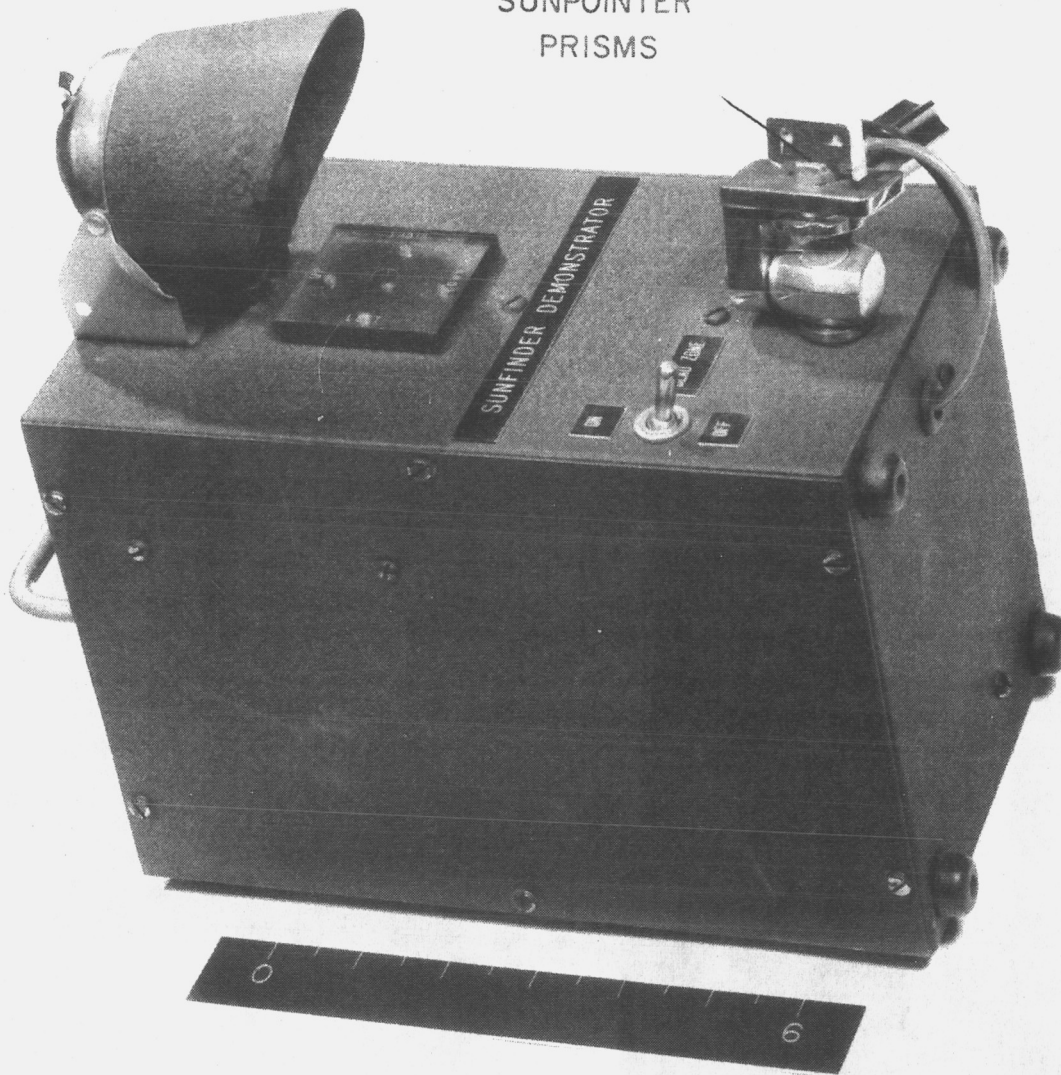
Fig. 5-22 Sunfinder demonstrator.
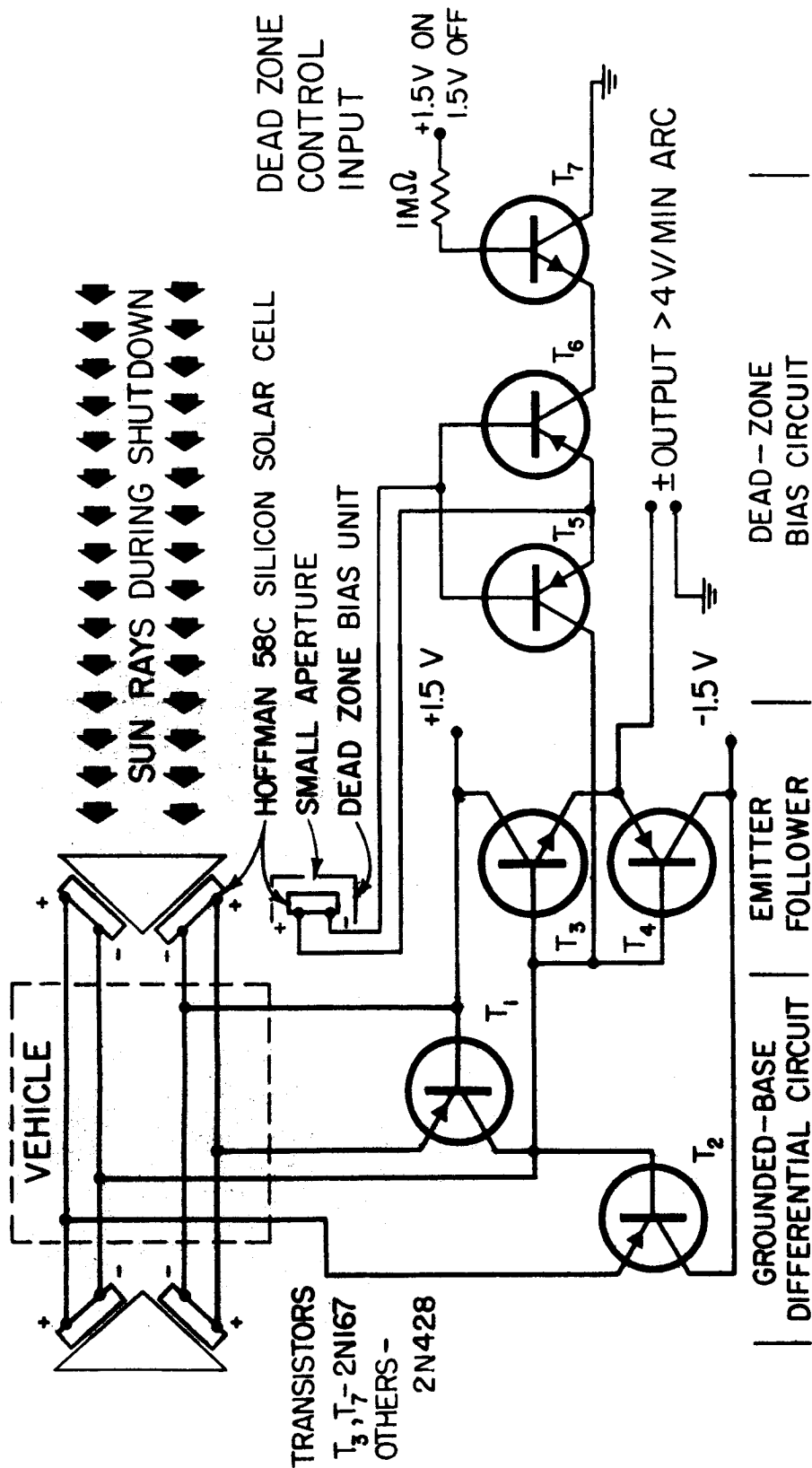
Fig. 5-23   Sunfinder circuit (one axis).

50WWRN - 5337

gives a voltage gain in excess of several hundred.

The following pair of transistors, T_3 and T_4 , form a pnp-npn emitter follower with unity voltage-gain but considerable current-gain in order to lower the impedance level of the output signal. A second follower may be used to further reduce the impedance, if necessary.

The dead-zone bias circuit consists of three transistors. The bilateral transistor, T_7 , acts as a switch to connect or isolate the dead-zone feature, which is controlled by the computer.

The other pair of transistors, T_5 and T_6 , is connected as shown to the bias solar cell. With the dead-zone operating, these two transistors short the input of the emitter follower with a few ohms impedance, preventing an output voltage of either polarity. When the differential signal from the prism cells exceeds the current of the bias cell, this same transistor pair becomes a high impedance of several megohms, and allows the output voltage to increase sharply.

As the sun illumination changes due to changing sun distance, the sunfinder sensitivity and the bias cell signal change by the same proportion. A dead-zone of constant angular width regardless of sun distance is thereby maintained. The design of the circuit also allows unimpaired operation throughout wide variations of either or both of the supply voltages (e. g. , in the range 0. 5 to 2. 0 volts on either supply).

The power dissipation for the circuit is about 3 milliwatts, which could be reduced to 30 microwatts if the first-stage supply voltage was applied only during sampling by the computer.

The sunfinder used for orienting the sun tracker would use the same circuit without the dead-zone circuit or the extra parallel-connected sunfinder.

V. Low-Power Clock

A clock-counter of 9 flip-flops was constructed in an attempt to attain a low power dissipation during dormant operation of the vehicle. The flip-flop used was a modified version of one used at M. I. T. Lincoln Laboratory.[*] The modified circuit is shown in Fig. 5-24.

The minimum-power necessary for bi-stable operation occurs when an "on" transistor is always in saturation while conducting the current flowing through the "off" transistor and the conducting bias resistor R_B. That is,

$$I_c \geq I_c' + E/R_B \, ,$$

where I_c and I_c' are the unsaturated currents that the "on" and "off" transistors could supply and E is the supply voltage.

Substituting the following transistor relations:

$$I_c = \beta \, (I_B + I_{co}) \, , \quad I_B = E/R_B$$

$$I_c' = \beta' \, (I_B' + I_{co}') \, , \quad I_B' = 0/R_B$$

into the above equation

$$I_{co} \geq I_c' + E/R_B \, ,$$

$$\beta \, (I_B + I_{co}) \geq \beta' \, (I_B' + I_{co}') + E/R_B \, ,$$

$$\beta \, (E/R_B + I_{co}) \geq \beta' \, I_{co}' + E/R_B \, .$$

Making the conservative assumption that $I_{co} = 0$,

$$\beta \, E/R_B \geq \beta' \, I_{co}' + E/R_B \, , \quad E/R_B \geq \frac{\beta' \, I_{co}'}{\beta - 1} \, .$$

---

[*]R. H. Baker, Maximum Efficiency Transistor Switching Circuits, TR-110, M. I. T. Lincoln Laboratory, March 1956.

FLIP-FLOPS MOUNTED ON PRINTED CKT BOARDS
3 PER BOARD

POWER DISSIPATION PER BOARD
Ve = 3 VOLTS — 4.2 MW
Ve = 1.5 VOLTS — 1.05 MW

TOTAL DISSIPATION FOR 3 BOARDS
1 BOARD @ 3 VOLTS — 4.2 MW
2 BOARDS @ 1.5 VOLTS — 2.1 MW
6.3 MW

NPN = 2N169A
PNP = 2N413
Ve = 3 + 1.5 VOLTS

NPN   NPN   PNP   PNP

OUT

+Ve

INPUT

100μFD R_b 27K R_b 27K 100μFD
R_b 27K R_b 27K
$.01\mu$FD
470μFD
IN116   IN116
5K   5K   5K

120 Kc — 2^0 — 2^1 — 2^2 — 2^3 — 2^4 — 2^5 — 2^6 — 2^7 — 2^8

3 VOLTS 4.2 MW   1.5 VOLTS 1.05MW   1.5 VOLTS 1.05 MW
6.3MW
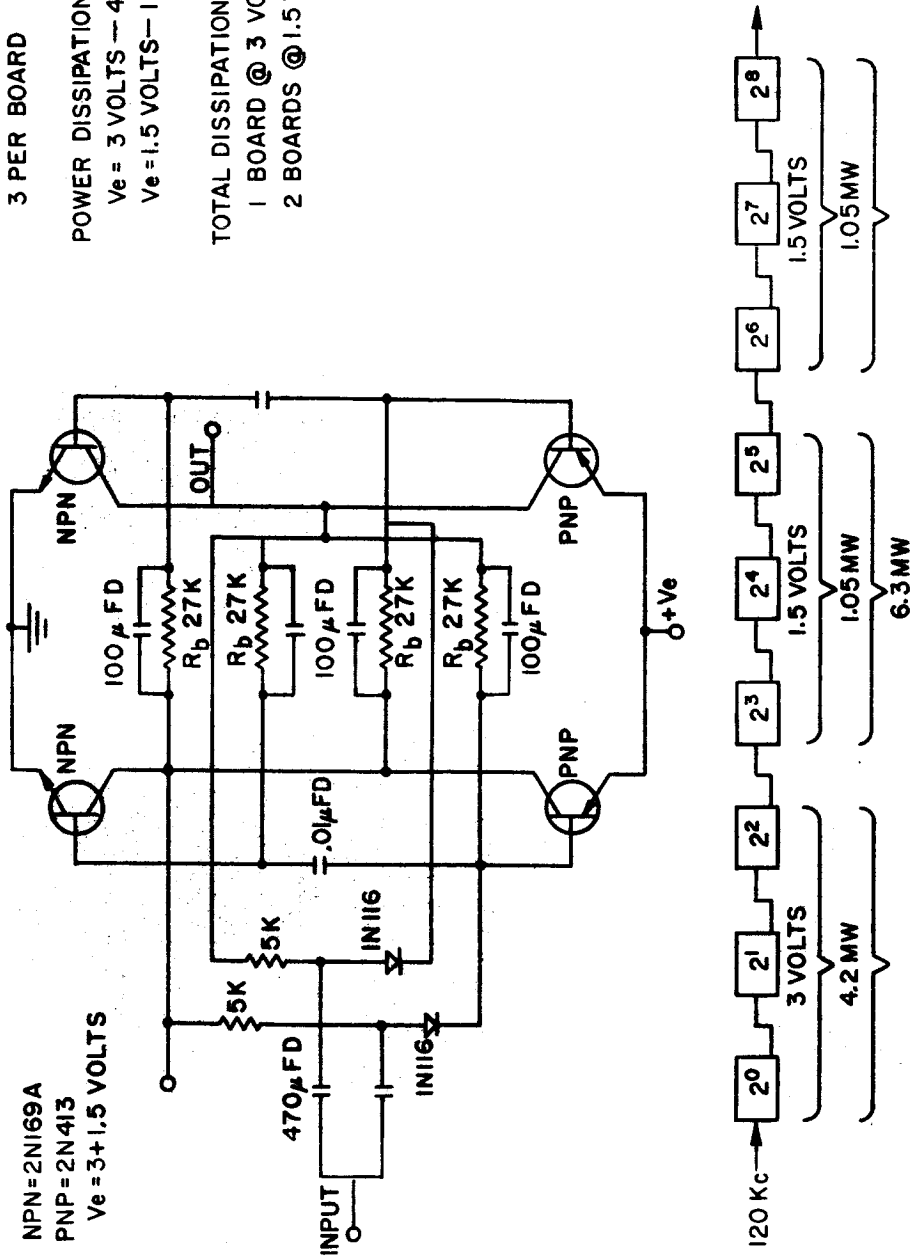
Fig. 5-24   Low power flip-flop counter.

Hence for 25°C operation this condition for germanium transistors is approximately

$$E/R_B \geq \frac{60 \times 1.5\,\mu amp}{19 - 1} \text{ or } 5\,\mu amp.$$

The circuit shown gives E/R_B a value of about 50 micro-amps which gives a conservative safety factor of ten. To test this estimate, the counter was operated with 120 kc input pulses of amplitude equal to the supply voltage as shown in Fig. 5-24. The temperature was raised slowly until the increased $I_{co}{}'$, which approximately doubles every 10°C rise, caused the counter to either stop or free-run. The voltage was then raised until E/R_B reached a high enough value to restore the operating condition. The various plots of Fig. 5-25 were made using the flip-flops in different positions in the counter.

At about 55°C (a 30°C rise) it is seen that the estimated safety factor of 10 is nearly down to unity. This is to be expected, since the 30°C rise would have produced about 8 to 10 times the leakage current, $I_{co}{}'$. The total dissipation for a 12-stage clock counter is approximately 7 milliwatts (significantly less than assumed in R-235).

VI. <u>Computer</u>

The Computer Appendix at the end of this report presents work which is the continuation of that presented in Chapter 10, Vol. III, R-235, "A Recoverable Interplanetary Space Probe". The Appendix does not deal with a finished computer design suitable for a space navigation unit, but with a collection of useful computer techniques loosely unified by reference to a "representative" computer. Because of Navy-Air Force sponsorship of the work presented in the Appendix, the "representative" computer is representative of a missile application for the proposed techniques. In these brief pages the specifications for a space computer will
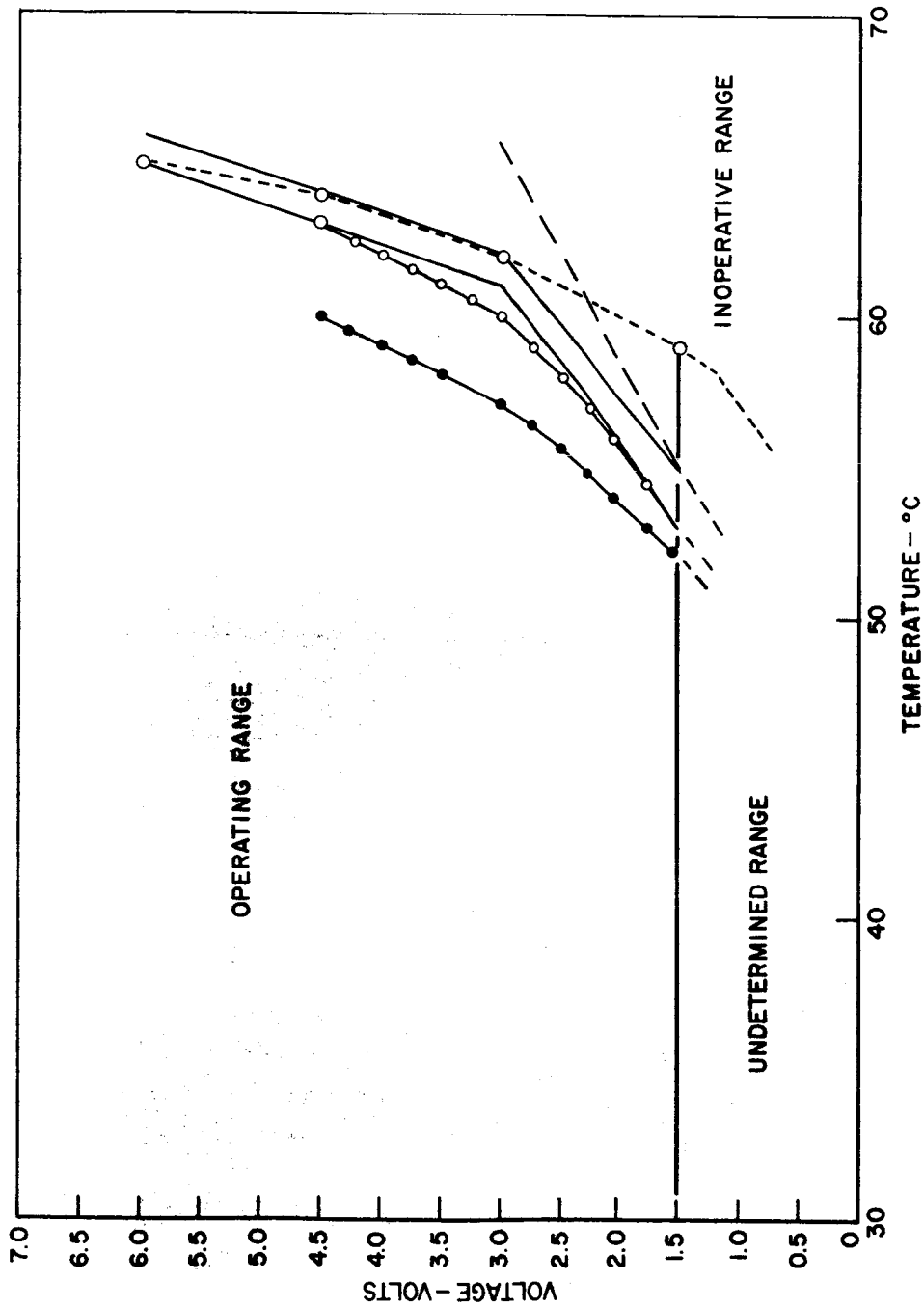
Fig. 5-25 Temperature characteristics for low power counter.

be discussed, and comparisons with the missile counterpart made wherever applicable.

A. Organization

1. Speed Requirements

It must be capable of variable speeds in order to take advantage of variable power consumption capability. Top speed requirements are forseen as less than those required for a missile version, which can be used to simplify organization and reduce equipment.

2. Word Length

At present, it is estimated that about 18 bits are sufficient for the space computer word length, versus 24 bits for the missile computer. Power consumption as well as quantity of equipment and likelihood of failure increase with word length; therefore the shortest possible word length is a worthwhile goal of design. Word length also affects other things, as is discussed below.

3. Memory Requirements

Fixed storage requirements are presently estimated at 4000 words, which is the same number used in the representative missile computer. The required erasable storage is of the order of 200 registers in the space case, versus 128 registers in the missile case. This increase represents an increase in the erasable memory core-diode count of about 650, from 2950 cores and diodes for the missile case to 3600 cores and diodes for the space case. The clear and write transistor count also increases from 256 to 400.

4. Order Code

The shorter word length of 18 bits allows only 5 bits for the order code, versus 11 bits in the missile case. This is enough for 32 different instructions. Additional instructions may be synthesized as subroutines. A simpler and slower order code is

acceptable in the space case because of its less stringent speed requirements, and may result in substantial savings in the number of transistors used in the Sequence Generator and the Control Pulse amplifiers.

5. Central Registers

Again, lower speed requirements than those of the missile case can be used to reduce the number of Central Registers, and perhaps eliminate or reduce the length of some of the more complex registers, such as the Z register or the Parity register. These reductions, together with the reductions due to a simpler order code and word length, can save on the order of 100 to 150 transistors in the area of Central Registers and Control Pulse amplifiers.

6. Input - Output

The details of input and output systems are of course different for the space and missile computers. The space guidance capsule has 32 input leads which carry pulses which must be counted. These leads can be connected to 3 counter registers through a switching network with the result that the computer controls which three quantities are being counted.

Other inputs are of the kind described in the Appendix as State inputs, i.e., the present state of a switch can be determined by a sampling pulse, and the information stored in a core. The input from the Disc Scanning mechanism is one such input. Present planning allows for 20 wires for information originating within the guidance capsule, and 20 more wires for information originating in the balance of the space craft. Normally, each state input requires two wires.

The kinds of circuits required for outputs fall into two categories, Rate outputs (corresponding to Counter inputs) and State outputs (corresponding to State inputs). There are seven rates required at present: four 250 cps pulse rates, 90° out of

phase with each other; a 400 cps rate; and 50 cps and 75 cps rates for the sextant motors. The Rate Generators described in the Appendix can be used to generate these rates. The State outputs required are 32 on-off gates, for controlling the connection of Counter input leads to Counter registers, in addition, there is provision for 20 on-off gates for things pertaining to the navigation capsule, and 20 more for controlling devices within the rest of the space craft. Each on-off gate consists of a latch type of transistor, and a normal transistor.

B. Circuitry

There are some differences in the circuit requirements of the space and missile computers. Low power consumption is much more important in the former than in the latter. The missile computer still has the basic features which make power consumed proportional to speed, but no further attention has been paid to the low power consumption feature. Specifically, the question of leakage currents through transistors must be investigated. There usually are ways in which the combined leakage of many units in parallel can be reduced to the leakage of a single unit, e. g. , by putting a transistor in series with all the parallel ones, but these schemes have not yet been worked out in detail. Another related problem is that of development of suitable latch type devices. These can be synthesized out of two or three transistors and several resistors, or they can be obtained as single solid state units. These have appeared on the market only recently, and may not be dependable at this time.

C. Construction

Although may of the packaging techniques developed for a missile computer will be directly applicable to a space version, the overall physical configuration of the two computers is apt to be very different. In the guidance capsule, the computer must fit into an eccentric doughnut, and this space allotment is sure to

influence the physical layout of the computer's submits and sub-assemblies. The space and weight assigned to the computer (0.3 ft, 20 lb) is based on estimates made for the missile computer and does not make allowance for difficulties in matching the assigned shape.

D. Programming

There must be special subroutines, and possibly equipment, developed for detection and correction of error. What should be done if an error is detected is very different in the missile case than in the space capsule case, because the latter allows for long computing times and the former does not. By and large, if an error is detected in the missile computer at the end of a long computation, it may be too late to do anything about it. This is not the case in a space computer.

VII. Preliminary Analysis of Disc Scanning Errors

A. Introduction

A preliminary look at the errors involved in planetary disc scanning has been performed in order to detect possible weaknesses in the scheme proposed in R-235, Appendix I. Sun and star tracking errors, on the other hand, are more easily estimated, and appear to be clearly within the ten seconds of arc assumed in the navigation studies.

To quickly review the R-235 disc scanning scheme, the following description is offered in conjunction with Fig. 5-26. The angle from the sun to the planet's center, β_o, and the apparent diameter of the planet, 2S, are computed from data measured during two sweeps about the sun-line. The mobile tracker's disc scanning line of sight is swept across the planet for two sextant drive angles, α_1 and α_2. The rotations about the sun-line, n_1 and n_2, required to completely traverse the planet are measured by the x gyro.

VIEW OF SCANNING
ARCS SEEN FROM
SPACECRAFT
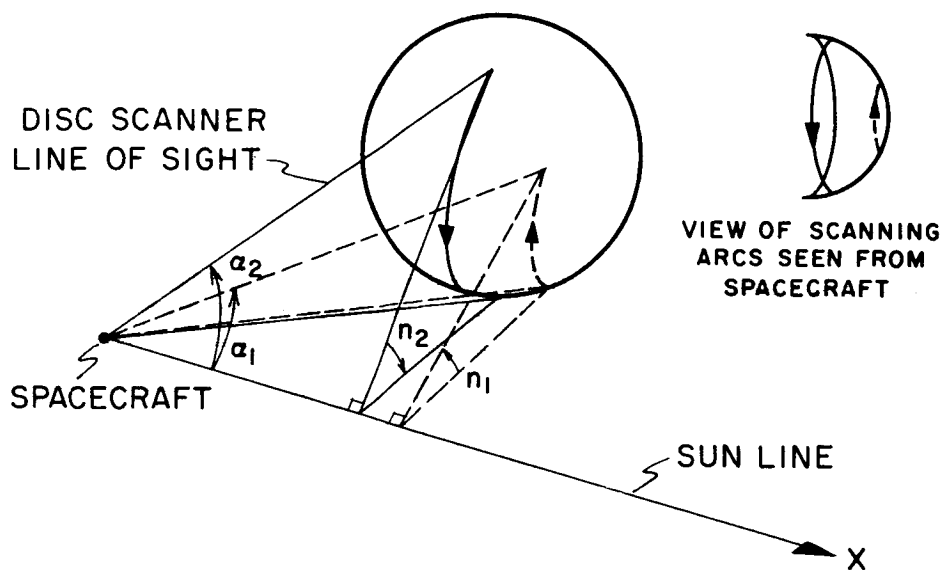
Fig. 5-26a Disc scanning procedure, planet to sun

VIEW OF SCANNING
ARCS SEEN FROM
SPACECRAFT
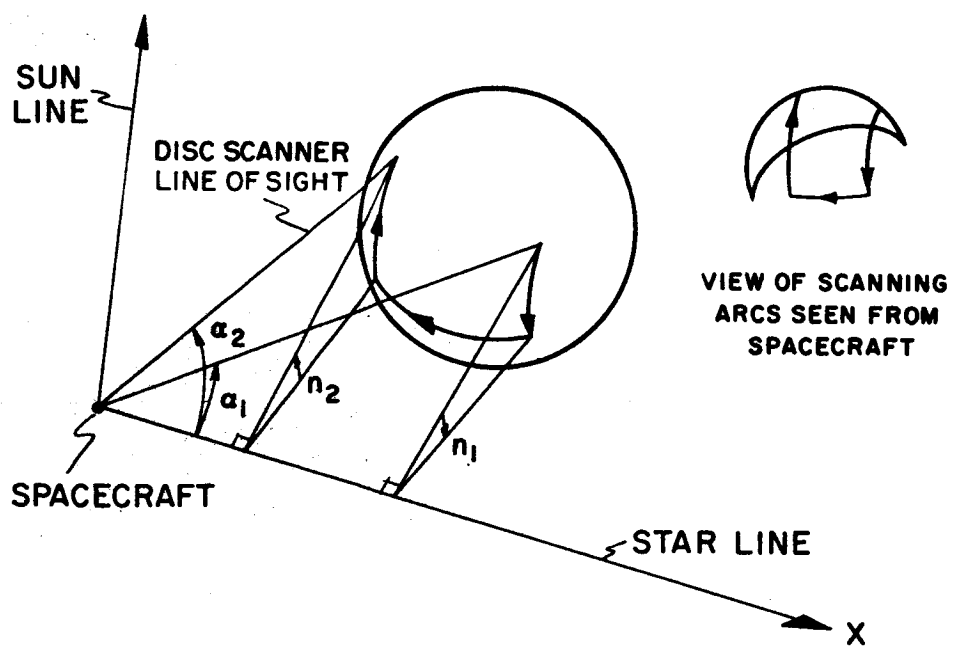
Fig. 5-26b Disc scanning procedure, planet to star

The angle from a star to the planet's center, α_0, is computed from the x gyro-measured arc swept across the planet while rotating the spacecraft about the star-line. In this case the mobile tracker is set at α_1, for the first sweep down past the illuminated edge of the planet, and then at α_2 for the return sweep up past the edge again. The angle of rotation used for this computation is $n = n_2 - n_1$, the difference between the two rotations.

For more detailed information about disc scanning and space sextant design, the reader is referred to Appendix I, R-235 and Section I of this chapter. R-235 assumed that the scanning area would be measured by counting flywheel revolutions. In the CIGS, however, we use the x gyro for this purpose in order to obtain more accuracy. Flywheel counting would limit accuracy to 1/2% because of the uncertainty in spacecraft moment of inertia and the disturbing effects of sloshing propellant and rotating equipment in the mother spacecraft.

B. Alternative Methods

Other methods of measuring angles from the sun or stars to a "large" object such as a close planet or moon are being continually investigated. Such alternative methods may be used in order to simplify procedures or improve accuracy. The brief analysis given later in this section has indicated the possible need for an alternative method of measuring α_0 and β_0. That is, it appears that gyro errors may not permit the attainment of the desired 10 seconds of arc accuracy.

Another method which is not critically dependent upon gyro performance is illustrated in Fig. 5-27. In this scheme the planet or moon involved would be "grazed" by the disc scanner line of sight during sweeps about the sun line and/or one or more star-lines. The sextant drive angles required to just graze the edge of the body are useful navigational angles and may be used
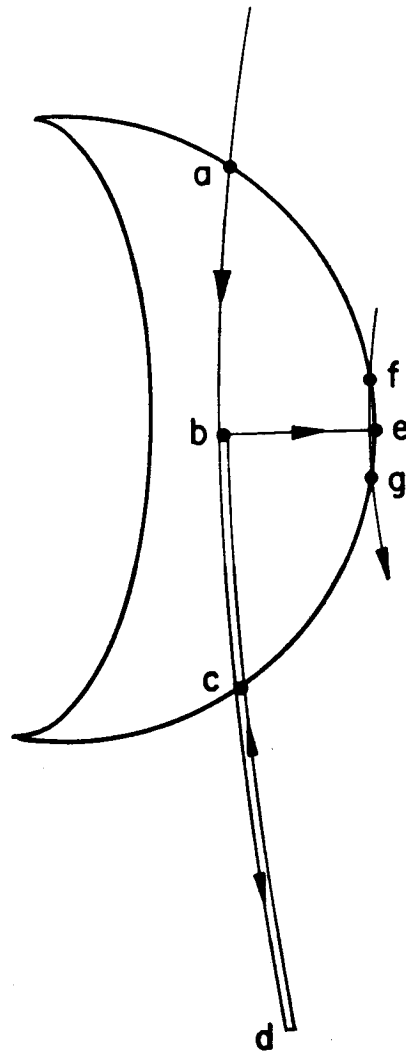
**VIEW OF SCANNING ARCS AS
SEEN FROM THE SPACECRAFT**

Fig. 5-27   An alternative method of measuring angles to "large" bodies.

60WWRN - 5337

with other angles to determine a fix.

To understand this it is only necessary to note that the angle from a celestial body to the edge of a planet differs from the angle to its center by exactly the apparent radius, S. Since S depends solely upon the distance from the planet, it is clear that the mathematical process for computing a fix can readily be formulated to use either angles to planetary centers or to planetary edges, or both.

In order to find the sextant drive angle which is just sufficient to cause the line of sight to graze the planet, the following procedure would be followed: The sextant drive is set and the spacecraft slewed about the sun (or star) line so that the scanning line of sight traces an arc across the body. This arc will not graze the edge of the body but will pass across it, as shown in Fig. 5-27 where it is labeled arc $\overset{\frown}{a\ b\ c}\ d$. When point c is detected by the loss of the modulated photomultiplier signal, the spacecraft is stopped (at point d) and rotated back to return the line of sight to point b. The arc $\overset{\frown}{ac}$ was measured by the x gyro which now monitors the return arc to make $\overset{\frown}{cb} = 1/2\ \overset{\frown}{ac}$. When point b is found in the above manner, the spacecraft is held fixed in space while the sextant drive angle is reduced. When the line of sight reaches point e, the modulated photomultiplier signal is lost indicating that the edge of the planet has been found. The sextant drive angle is now increased by one or two bits, in order to retrieve the lost signal, and then read into the computer. A trial sweep about the sun (or star) line is now performed to check the results. This trial sweep traces the arc $\overset{\frown}{fg}$ which is very close to the edge of the disc. The x gyro will measure $\overset{\frown}{fg}$, which will be required to be less than some specified few bits in order to test that the sextant drive angle is sufficiently close to the actual angle to the planet's edge. It is clear how one or more trials may be required, and carried out, in order to achieve a sextant drive angle which results in the test being passed. It is felt that this method will result in navigational angle errors close

63   RN - 5337

to 10 seconds of arc.

C. Summary

Fig. 5-28 illustrates the results of the analysis made of errors in the R-235 scheme of disc scanning. It is evident that expected errors in β_0 , S and α_0 (plotted as standard deviations $\sigma (\beta_0)$, $\sigma (S)$ and $\sigma (\alpha_0)$ are of the order anticipated, 10 - 30 seconds of arc, only at large distances from the planet. For this region of small apparent diameters, the error is attributable mostly to sextant drive errors and the quantization error associated with the gyro pulse count, both of which errors have comparable effects. In the region of high apparent diameters, the errors increase sharply due to gyro scale factor and drift errors. It is seen that a calibration of the gyro, described later, significantly delays the onset of the error growth. It should be noted that the large errors inherent in close-up scanning do not necessarily degrade navigation accuracy. Particularly in the case of apparent angular radius determinations, the resulting percentage error in computed distance from the planet (assuming perfect knowledge of planetary radius) is sharply reduced when close to the planets. This result is also plotted in Fig. 5-28.

It should be pointed out that the results shown are derived from only a few representative cases without attempting to optimize sighting parameters for minimum errors. For example it appears fairly certain that small improvements over the errors shown can be had merely by intelligently selecting sextant drive angles.

D. Method of Analysis

Reference to R-235, Appendix I will show the formulas for planetary angular diameter (2S), angular separation of the planet and star (α_0) and angular separation of the planet and the sun (β_0) are given in the form:

PER CENT ERROR IN ESTIMATE OF DISTANCE FROM PLANET CENTER

STANDARD DEVIATION OF NAVIGATION ANGLE-SECONDS OF ARC

NO CALIBRATION

$100 \frac{\sigma(d)}{d}$

WITH CALIBRATION

NO CALIBRATION

WITH CALIBRATION

$\sigma(\alpha_0)$

$\sigma(\beta_d)$

$\sigma(S)$
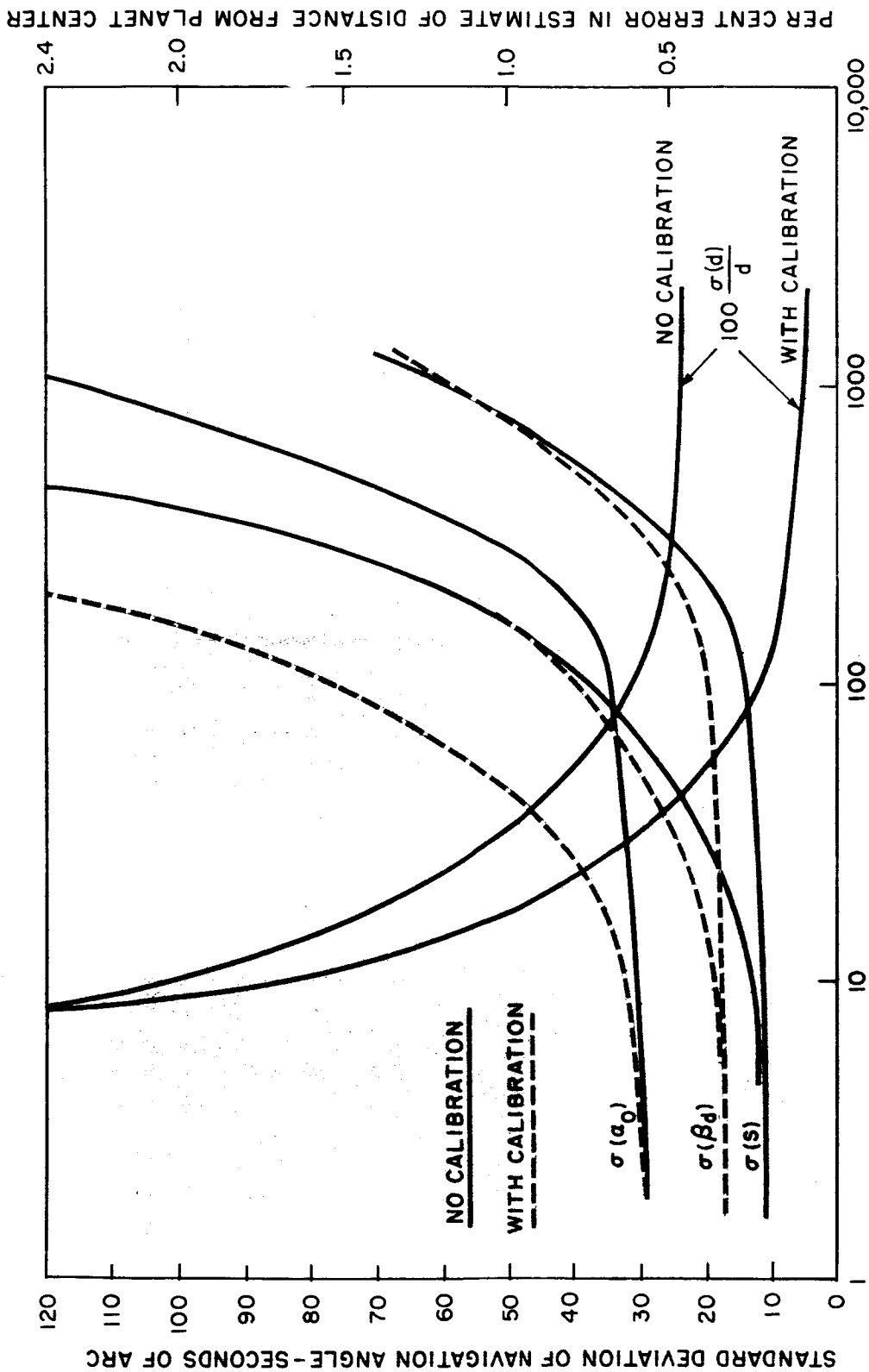
Fig. 5-28   Planetary angular radius, $S \sim$ minutes of arc.

$$S = S(\alpha_1, \alpha_2, n_1, n_2)$$

$$\beta_o = \beta_o(\alpha_1, \alpha_2, n_1, n_2)$$

$$\alpha_o = \alpha_o(\alpha_1, \alpha_2, S, n)$$

Referring to Fig. 5-26 we see that α_1 and α_2 are the angles set by the sextant drive between the disk scanning line of sight and the sun (or star) line for the first and second sweeps, respectively. The angles n_1 and n_2 (and $n = n_2 - n_1$ in the planet-to-star case) have already been explained. By taking the partial derivatives,

$$\frac{\partial S}{\partial \alpha_1}, \frac{\partial S}{\partial \alpha_2}, \cdots, \frac{\partial \beta_o}{\partial \alpha_1}, \cdots, \frac{\partial \alpha_o}{\partial \alpha_1}, \cdots, \frac{\partial \alpha_o}{\partial n}$$

one can estimate the effect of the measurement errors, $\Delta\alpha_1 \ldots \Delta n$ on the desired navigational angles. General expressions for these derivatives were determined and then reduced to numbers for several representative cases. It was found that each derivative varied only slightly between cases. Table 5-3 shows the cases considered and Table 5-4 shows the average value of the partial derivatives (termed error coefficients). These cases are representative and are taken from the Mars around trip trajectory Number 1034 described in more detail in R-235 Vol. II.

In the planet-to-sun cases, the sextant drive angles, α_1 and α_2, were selected so as to have the first sweep pass close to the edge of the planet and have the second sweep scan nearly the full planetary diameter. In the planet-to-star case the sweeps were chosen to pass equal distances on either side of the planet's center. This procedure is believed to be conservative for the purpose of this error analysis since the sextant drive angles can be selected differently so as to minimize the total expected errors.

The following sections discuss the estimations of measurement errors.

TABLE 5-3

Disc Scanning Parameters for Representative Cases

Planet Scanned / Parameter	Earth (on departure)	Mars (during approach)	Mars (while passing at minimum altitude)
Approx. distance from planet center while scanning $\sim$ miles	110,000	910,000	6,800 (altitude = 4690 miles)
Approx. planet angular radius: S	$2°2'$	$8'$	$18°17'$
Approx. angle from planet to sun: β_o	$123°59'$	$39°11'$	$74°5'$
Sextant settings for determination of β_o, S: α_1/α_2	$122°/124°$	$38°52'/38°59'$	$56°/72°$
Gyro-measured rotations leading to β_o, S: n_1/n_2	$1°/4°54'$	$6'/26'$	$6°/38°$
Angle from planet to star: α_o	$91°$	—	—
Sextant settings for determination of α_o: α_1/α_2	$90°/92°$	—	—
Gyro-measured net rotation leading to α_o: n	0	—	—

$\dfrac{\partial \beta_o}{\partial \alpha_1} = 1.07$	$\dfrac{\partial S}{\partial \alpha_1} = 0.12$	$\dfrac{\partial \alpha_o}{\partial \alpha_1} = 0.50$
$\dfrac{\partial \beta_o}{\partial \alpha_2} = -0.07$	$\dfrac{\partial S}{\partial \alpha_2} = -0.08$	$\dfrac{\partial \alpha_o}{\partial \alpha_2} = 0.50$
$\dfrac{\partial \beta_o}{\partial n_1} = -0.08$	$\dfrac{\partial S}{\partial n_1} = -0.06$	$\dfrac{\partial \alpha_o}{\partial n} = 0.87$
$\dfrac{\partial \beta_o}{\partial n_2} = 0.44$	$\dfrac{\partial S}{\partial n_2} = 0.46$	$\dfrac{\partial \alpha_o}{\partial S} = -0.0006$

TABLE 5-4

Average Disc Scanning Error Coefficients

E. <u>Sextant Drive Angle Errors</u>

The angles α_1 and α_2 should ideally represent the angles from the sun (or star) line to the scanning line of sight on the first and second sweeps, respectively. An error in either of these angles has three possible contributions:

a. A disparity between the true sun (or star) line and the fixed sun/star tracker housing which is assumed to be the sun (or star) line.

b. An error in locating the mobile tracker relative to the fixed sun/star tracker.

c. An uncertainty in the angle between the mobile tracker housing and the scanning line of sight.

The first error has an rms value of 6 seconds of arc due primarily to the tracking oscillation. The second error should be in the neighborhood of 11 seconds due to 10 seconds sextant drive error and 4 seconds bearing run-out wobble. It is expected that uncertainties in the relative positions of the two housings (caused by distortions and other effects) will be negligible after calibration. The final error will arise primarily from the distortion of the mobile tracker assembly after calibration and should be no more than two seconds of arc. One therefore should expect the rms errors to be approximately:

$$\sigma(\alpha_1) = \sigma(\alpha_2) = 13 \text{ seconds of arc.}$$

F. **Scanning Arc Measurement Errors**

Errors in the measured scanning arcs n_1, n_2, and n arise from two sources.

a. Uncertainties in the times at which the planet is first touched and finally left by the scanning line-of-sight.

b. Gyro measurement errors.

The first error, which may be termed the "planetary edge pickup error", is caused by several factors:

a. There is a negligible quantization error, about 0.4 seconds of arc, due to the rotating shutter which causes the planet's image to flicker at 2000 cps.

b. Arrival of the planetary image at the disc scanning aperture and similarly its departure, cannot be detected exactly in time. This uncertainty, for any given image brightness, depends upon our ability to predict the time delay required to detect the 2000 cps modulation in the background photomultiplier noise. It is difficult to generalize this problem, particularly since non-linear detection techniques are involved. Furthermore, a good deal of analytical and **experimental effort is usually required to develop a suitable circuit. However, from past experience, it appears not unreasonable to expect delay time uncertainties less than 2 milliseconds. Variations in image brightness further complicate the problem because the sextant is required to scan several planets and the moon. The resulting** contribution to planetary edge pickup error should be about 10 seconds of arc.

c. **The remaining error contribution would arise from roughness in the edge of the planetary image due to topographical and atmospheric nonhomogeneities.**

It is therefore apparent that rms planetary edge pickup errors will probably be no more than 10 seconds except possibly for image roughness effects.

Gyro measurement errors however, will be of primary importance and may be estimated as follows:

a. Quantization error: Because vehicle angular motion is measured by counting gyro input pulses, each of which corresponds to a small unit of rotation (28.8 seconds),

the quantization error in measuring any change of vehicle orientation has an rms value of 23.5 seconds.

b. Gyro drift: Gyro drift is expected to be less than 3 degrees/hour or 3 seconds of arc/second.   Since, in the planet-to-sun case, the sweep rate is intended to be 1 degree/second, the drift error should be of the order of n/1200.   In the planet-to-star case, the drift error must be estimated on the basis of a calculated time to complete the scan because vehicle angular rate will be variable and significant time is required to change the sextant drive angle midway through the scanning procedure.   If excessively long times are required in this case, it may be advisable to count flywheel turns rather than use the gyros.   Typical numbers are considered below.

c. **Gyro Scale Factor: The linear relationship between pulse count and vehicle rotation is critically dependent upon the stability of the constant dc torquing current source.   A long-term stability of 1/2 percent is certainly reasonable. An order of magnitude accuracy improvement can be obtained over short periods provided a calibration run is made prior to the scanning procedure.   This could be done by performing a 360 degree rotation about the x-axis so as to clock two successive crossings of the sun line by the z-axis sun finders.   Thus we can expect scale factor errors of n/200 or n/2000 depending upon whether or not a calibration is performed.   It will be apparent upon examination of the numbers below that a calibration is valuable except when scanning very distant planets.**

The following Table 5-5 illustrates the gyro errors for the three representative cases used earlier and described in Table 5-3.

Planet Scanned / Parameters	Earth (on departure)	Mars (during approach)	Mars (while passing at minimum altitude)
Approximate planet angular radius, S	$2^\circ2'$	$8'$	$18^\circ17'$
n_1/n_2	$1^\circ/4^\circ54'$	$6'/26'$	$6^\circ/38^\circ$
Quantization error, $\sigma(n_1) = \sigma(n_2)$	$23.5''$	$23.5''$	$23.5''$
Gyro drift error, $\sigma(n_1)/\sigma(n_2)$	$3.0''/15''$	$0.3''/1.3''$	$18''/110''$
Scale factor error NO CALIBRATION. $\sigma(n_1)/\sigma(n_2)$	$18''/88''$	$1.8''/7.8''$	$108''/684''$
Scale factor error WITH CALIBRATION, $\sigma(n_1)/\sigma(n_2)$	$1.8''/8.8''$	$0.2''/0.8''$	$10.8''/68.4''$
Total gyro error NO CALIBRATION, $\sigma(n_1)/\sigma(n_2)$	$30''/92''$	$24''/25''$	$110''/690''$
Total gyro error WITH CALIBRATION $\sigma(n_1)/\sigma(n_2)$	$24''/29''$	$24''/24''$	$32''/140''$

TABLE 5-5

Gyro Errors for Three Representative Scanning Cases

G. Navigation Sighting Angle Errors

The above results have been consolidated to estimate $\sigma(S)$, $\sigma(\beta_O)$, and $\sigma(\alpha_O)$ for the representative cases. The only significant variables which can be identified as determinants of the expected error are the apparent planetary diameter and the use or neglect of gyro scale factor calibration. The results have therefore been plotted in Fig. 5-28.

CHAPTER 6

ENVIRONMENTAL PROBLEMS
TESTS, FACILITIES, AND PROGRAM

by

William E. Toth

60WWRN - 5337

TABLE OF CONTENTS

LIST OF ILLUSTRATIONS

CHAPTER 6

ENVIRONMENTAL PROBLEMS, TESTS, FACILITIES, AND PROGRAM

Introduction

The significant lack of reliable data makes it difficult to evaluate the environmental problem. Fortunately, this situation is being rectified. Various laboratories throughout the world are conducting tests which will show behavior of materials and gadgetry operating in a wide variety of environments. Space vehicles (U.S. and Russian) are supplying a great deal of information about space environment. Astronomers, physicists, and engineers are originating theories and testing them with bits of experimental data. Thus, the state-of-the-art is being advanced, but with some confusion due to conflicting data. The purpose of this chapter is to collect the available information regarding salient features of the environment and its problems.

In chronological order, a space probe will encounter environments classified under the headings:

1. Booster phase
2. Earth upper atmosphere and near space
3. Interplanetary space
4. Planetary environment

The sections to follow will elaborate on these items.

I. The Environments

A. Booster Environment

Booster operation imposes severe conditions of shock, vibration, acceleration, and noise upon the payload. The exact nature of this environment will depend upon final configuration of the booster, the payload, mounting, etc. Even then, the environment must be measured during actual operation before it is known. We can, however, discuss typical conditions peculiar to the Booster environment.

1. Vibration

Vibration measurements are available for several missiles currently being flown. Examples are the Atlas, Titan, Jupiter, and Thor. The data allow one to make an educated guess at order-of magnitudes to be expected in an advanced launching vehicle, for example, the Centaur. Convair[1] has made an estimate of vibrations expected in a Centaur guidance compartment. Table 6-1 is a summary of this estimate. The estimate seems reasonable in view of vibration data available for several missiles. Atlas data are shown in Fig. 6-1. Peaks appear at about 540 cps and 1080 cps, with an rms value of 5g and 3.5g, respectively, seen through a 100 cps bandpass. Titan data are shown in Fig. 6-2. Peaks in this spectrum appear at about 650 cps and 850 cps, with rms values of about 1g, seen through a 100 cps bandpass. Also shown for the Titan is a plot of composite vibration (rms value seen through a 2100 cps bandpass) as a function of time. Note the typical high peak at lift-off, having a value of 2.4g. Figure 6-3 shows composite vibration data for the Thor. Here vibration is low, even at lift-off. The Jupiter[6] exhibits low vibration in its instrument compartment. The rms value is 1.5g in the 700 → 900 cps band at lift-off. These data will be helpful in establishing vibration test criteria.

2. Shock

Shocks originate principally in handling and transportation

TABLE 6-1

ESTIMATED VIBRATION FOR CENTAUR
GUIDANCE EQUIPMENT

Time from Launch (min)	Component of Vibration	
	Three Dimensional	Transverse
T = 0 → 2 (Atlas Booster)	$0.02g^2$/cps random 3g @ 500 cps sinusoidal	0.5g @ 2.5 cps sinusoidal
T = 2 → 5 Atlas sustainer	$0.02g^2$/cps random 3g @ 500 cps sinusoidal	0.01g @ 1.5 cps sinusoidal
T = 5 → 10 Centaur $H_2 - O_2$	$0.005g^2$/cps random 0.8g @ 500 cps sinusoidal	0.05g @ 2 cps sinusoidal
Coast	0.2g @ 60 cps sinusoidal 0.01g @ 100 → 2000 cps sinusoidal	

NOTE:

From Convair preliminary Specification 55-0400 (Ref. 1) SECRET.

Fig. 6-1   ATLAS random frequency spectral density of vibration.

NOTES:

(1) MEASUREMENT AT GUIDANCE PACKAGE TRUSS SUPPORT

(2) REFERENCE (4)

COMPOSITE VIBRATION
VS TIME
(0~2100 CPS BANDWIDTH)

TIME-SECONDS

LIFT OFF

RMS AMPLITUDE "g"

SPECTRAL DENSITY
VS. FREQUENCY
(LIFT OFF)

FREQUENCY-10^2 CPS

SPECTRAL DENSITY (10^{-3} g^2/CPS)
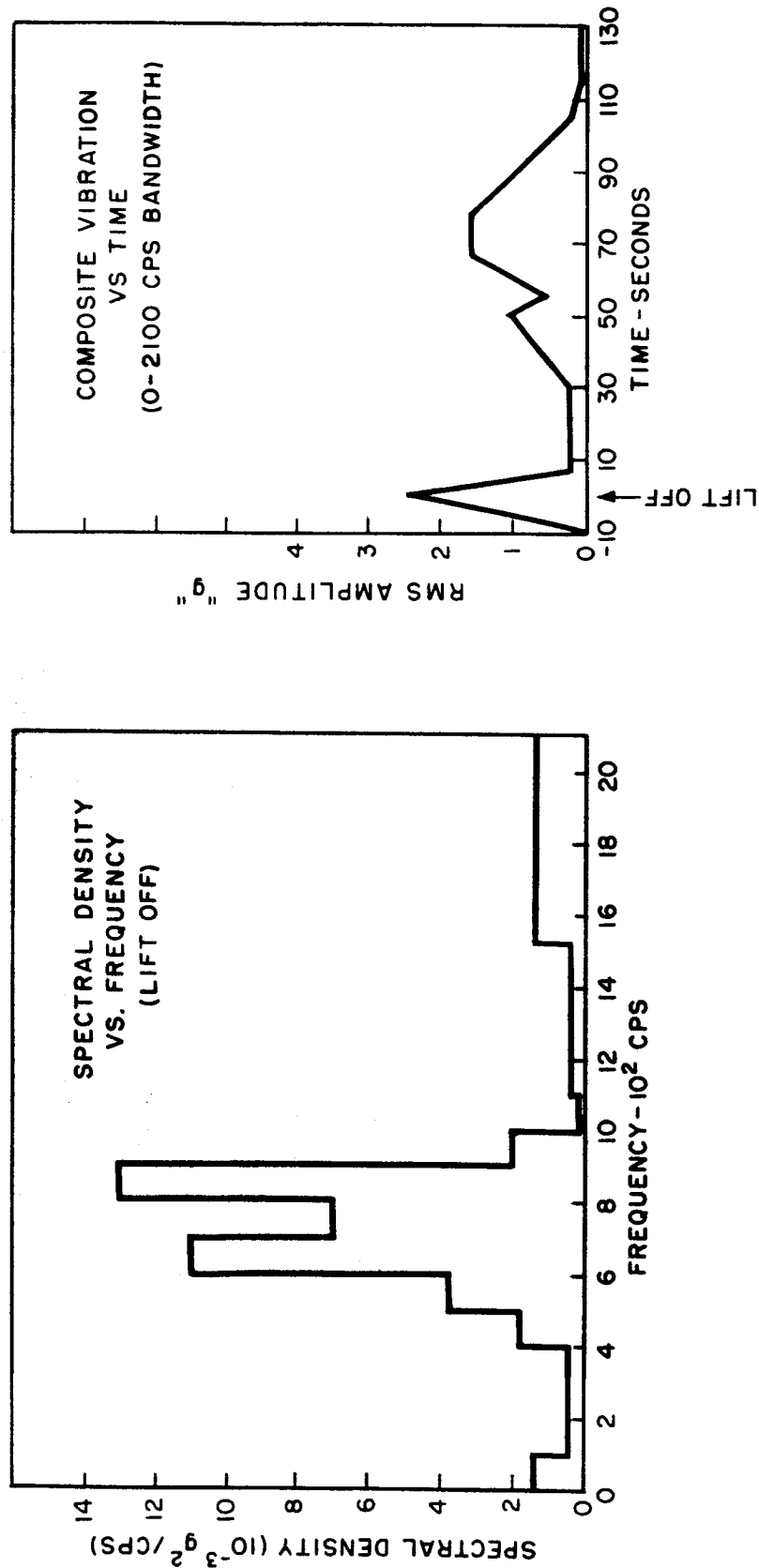
Fig. 6-2   TITAN vibration spectrum.

NOTES:

(1) MEASUREMENT AT GUIDANCE COMPARTMENT

(2) REFERENCE (5)

(3) BANDWIDTH 0-2100 CPS

(4) RANDOM ENERGY CONCENTRATED PRINCIPALLY BETWEEN 200 → 800 CPS

RMS AMPLITUDE - g

1.5   1.0   0.5   0

TIME - SECONDS

0   40   80   120   160   200

LIFT OFF
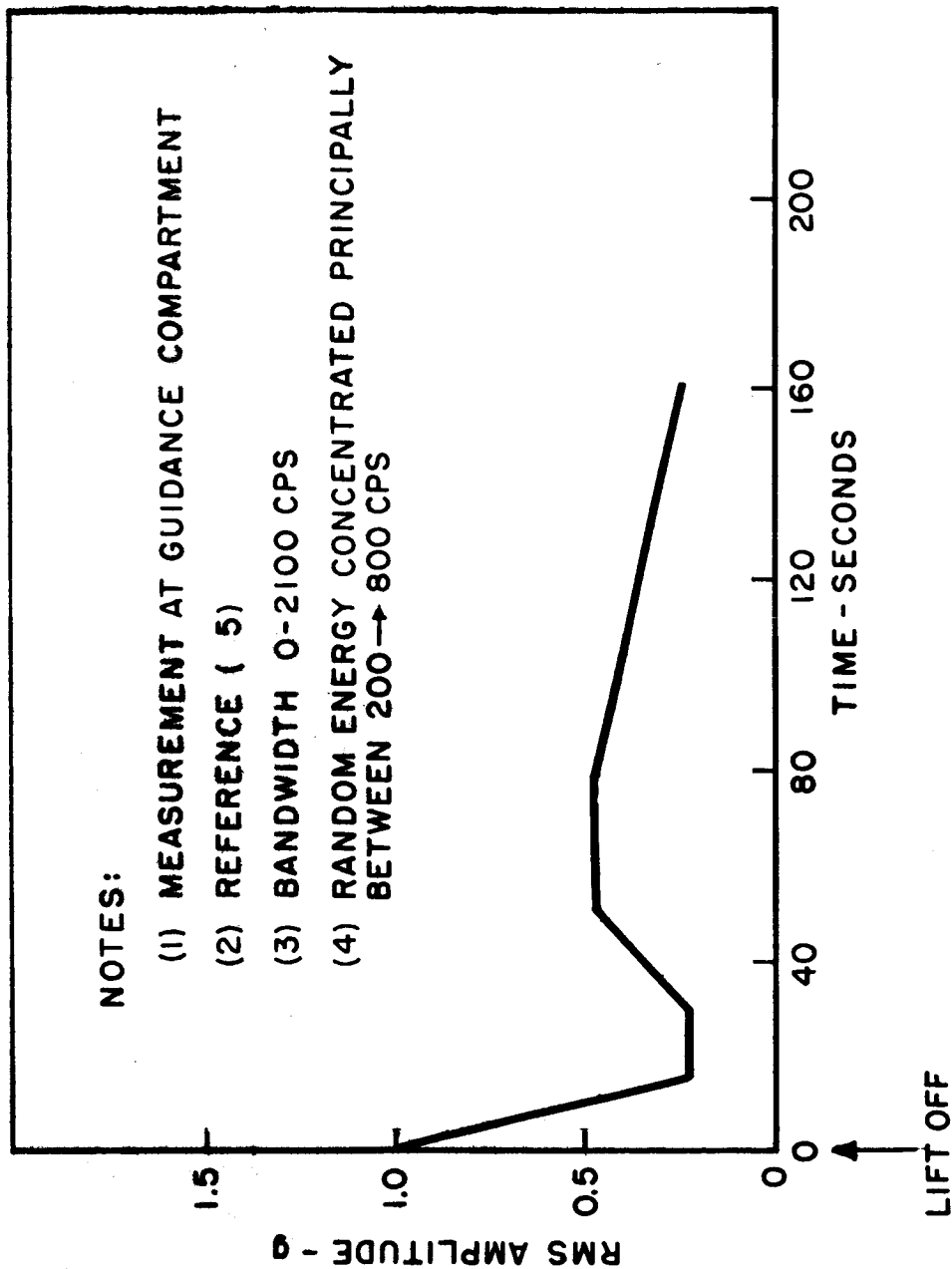
Fig. 6-3   THOR composite vibration versus time.

60WWRN - 5337

of equipment, and from propulsion unit ignition, rough burning, and cutoff. The type of shock experienced in handling and transportation is normally velocity shock, producing an impulse of short duration (10 millisec.) with amplitudes below 30 g.

The propulsion unit causes shock by rapid changes in acceleration,i. e , simple shock pulses. Simple shock pulses are commonly specified in terms of a sawtooth, half sine, or a square acceleration pulse. The peak values, at locations distant from the thrust point, are of the order of 15 g.

3. Acceleration

Steady acceleration profiles (for missiles) generally fall below 10 g. The maximum acceleration specified in Ref 1 for a Centaur vehicle is approximately 7 g. Re-entry accelerations are not considered.

4. Noise (Acoustic)

The level of noise produced by a rocket engine varies with missile velocity and position on the missile. Maximum values occur at time of launch, and, for the guidance equipment location, could reach values in excess of 130 db (Ref. .0002 microbar). The frequency range may extend to 10,000 cps. Ref 1 specifies an acoustic sound pressure level of 145 db for a frequency range of 100 → 7000 cps.

5. Temperature, Pressure and Humidity

During pre-launch and launch phase, limits of the temperature environment are expected to be 40° and $150^{\circ}F$[1]. Relative humidity may reach 100%, including condensation due to temperature change. Atmospheric pressure will vary in about 2 minutes from 760 mm Hg at sea level to 1 mm at 30 miles.

B. Earth's Upper Atmosphere and Near Space Environment

1. Atmospheric Pressure

The density of the earth's atmosphere reaches a negligible value beyond about 600 km. Satellite data[8] indicate a density of approximately 10^{-15} gm/cm^3 at this altitude. If the molecular scale temperature is 2000°K, the pressure is 6×10^{-9} gm/cm^2. The lowest pressure in space is suspected to range between 10^{-12} and 10^{-16} gm/cm^2.

2. Van Allen Radiation

Two concentric equatorial belts of radiation, named after Dr. James Van Allen, have been detected by space probes. The belts are concentric about the geomagnetic axis, and consist of particles trapped in the earth's magnetic field.

The inner belt begins at an altitude of about 1300 miles and extends to 3000 miles. It is approximately 4000 miles wide (north to south).

This zone seems unaffected by solar activity. About 30% of the radiation penetrates 4 gm/cm^2 of lead shield[10]. Van Allen and Frank[10] propose the following tentative composition of the trapped radiation at the heart of the inner zone.

    a. Electrons of energy greater than 20 Kev maximum unidirectional intensity $\approx 2 \times 10^9$/cm^2 sec steradian.

    b. Electrons of energy greater than 600 Kev maximum unidirectional intensity $\approx 1 \times 10^7$/cm^2 sec steradian.

    c. Protons of energy greater than 40 Mev omnidirectional intensity $\approx 2 \times 10^4$/cm^2 sec.

The extent of the outer belt seems to vary with solar activity. Pioneer III (December 6, 1958) and Pioneer IV (March 3, 1959) experienced considerably different radiation fields. The

difference is thought to be the result of high solar activity commencing February 25, 1959.

Pioneer IV data indicated a belt beginning at altitude 8000 miles, extending to approximately 52,000 miles, and about 20,000 miles wide north to south. Pioneer III data indicated a field extending to only 30,000 miles, with only 1/3 the number of trapped particles shown by the March 3 data.

Measurements made by Pioneer IV[10] indicate that the omnidirectional flux of electrons of energy greater than 200 Kev did not exceed $1 \times 10^8/cm^2 sec$; of electrons of energy greater than 2.5 Mev, $1 \times 10^6/cm^2 sec$; and of protons of energy greater than 60 Mev, $1 \times 10^2/cm^2 sec$.

C. Interplanetary Space Environment

1. Vacuum

A magnitude cannot be assigned to the vacuum, since it has never been measured. It is suspected, however, that if we were able to measure its density-equivalent pressure, it would have a value of the order of 10^{-16} mm Hg.

2. Meteoritic Material

We know that space contains solid material of varying size and composition, traveling at high velocity. Recent observation techniques (radio, radar, photography) have yielded basic knowledge about those particles which enter the earth's atmosphere. Watson[17] and others point out that most meteors seem to be of cometary origin, following elliptical orbits similar to comets with inclination less than $35°$ to the ecliptic. Heliocentric velocity of the meteors at 1 A. U. is approximately 42 km/sec. Orbits of high inclination ($\geq 50°$ to ecliptic) are uniformly distributed in direction. Orbits of low inclination ($\leq 50°$ to ecliptic) are direct, about 1 in 50 being retrograde[16].

The earth encounters meteor streams (showers) and sporadic meteors. Meteor showers are experienced when the earth passes through a point in space occupied by the orbit of a stream. This occurs at specific times each year. Watson lists nearly a dozen annual showers, many having orbits indentified with comets.

Though less spectacular, sporadic meteors account for most of the particles encountered by the earth. The number of visible sporadic meteors entering the earth's atmosphere follow the relationship[16]:

$$\log_{10} N = N_o + M \log_{10} r,$$

where

N = number with magnitude equal to or brighter than M.

r = ratio of increase in number between magnitude M and M + 1.

Recent data[16] place N between 75×10^6 and 200×10^6 particles of magnitude $M \leq +5$ encountered by the earth in 24 hours; and r between 2 and 4.1.

On the basis of the assumptions listed below, Whipple calculates a distribution of sporadic meteors.

1. A meteor of visual magnitude of zero has a mass of 25 gm.
2. Meteoritic mass decreases by the factor r for each unit increase of magnitude M.
3. Meteoritic particles have a density of 0.05 gm/cm^3 (similar to a light foam-plastic).
4. For the earth, $N = 200 \times 10^6$ particles of magnitude $M \leq +5$ in 24 hours.
5. r = 2.5

102

TABLE 6-2

WHIPPLE'S ESTIMATE OF METEOROIDS IN SPACE (From Ref. 13)

Meteor Visual Magnitude	Mass (gm)	Radius (10^{-4} cm)	Assumed Velocity (km/sec)	Kinetic Energy (ergs)	Penetration of Aluminum (cm)	Number* Striking Surface (m^{-2} day^{-1})
5	0.25	10,600	28	1×10^{12}	4.59	3.92×10^{-7}
7	3.96×10^{-2}	5,740	28	1.58×10^{11}	2.48	2.85×10^{-6}
9	6.28×10^{-3}	3,110	26	2.17×10^{10}	1.28	1.8×10^{-5}
11	9.95×10^{-4}	1,680	24	2.93×10^{9}	0.656	11.3×10^{-5}
13	1.58×10^{-4}	910	22	3.89×10^{8}	0.335	7.15×10^{-4}
15	2.5×10^{-5}	492	20	5.1×10^{7}	0.170	4.52×10^{-3}
17	3.96×10^{-6}	266	18	6.55×10^{6}	0.086	2.85×10^{-2}
19	6.28×10^{-7}	144	16	8.2×10^{5}	0.0430	1.8×10^{-1}
21	9.95×10^{-8}	78	15	1.14×10^{5}	0.0223	1.13
23	1.58×10^{-8}	39.8	15	1.81×10^{4}	0.0121	7.15
25	2.5×10^{-9}	15.8	15	2.87×10^{3}	0.0065	4.52×10
27	3.96×10^{-10}	6.3	15	4.55×10^{2}	0.0035	2.85×10^{2}
29	6.28×10^{-11}	2.51	15	7.21×10	0.0019	1.8×10^{3}
31	9.95×10^{-12}	1.0	15	1.14×10	0.0010	11.3×10^{3}

*Number includes all particles of greater mass, and applies to a surface traveling at earth's distance from the sun, not influenced by the earth.

The data, abstracted from Ref 13, is shown in Table 6-2. Note the extrapolation of data into the meteoric dust range. It is interesting to compare Whipple's data with that of Beard[12], who studies meteoric dust using observations of solar corona and brightness of the night sky. Beard also concludes that the dust is concentrated in the ecliptic plane, and estimates a flux of approximately 10^{-6} particles/cm^2/sec near the earth for particles of radius larger than 4 microns. This is an excellent agreement with Whipple, and with the measurements made by Explorer satellites[15].

Recent Russian data[14], reproduced in Table 6-3, indicate dust densities in agreement with those of Whipple.

TABLE 6-3
RUSSIAN MICROMETEORITE DATA

Means of Exploration	Date	Mean Approx mass (gm) if $v = 40$ km/sec	Flux of micro-meteors m^2 sec^{-1}
Third Sputnik	5/15/57	2×10^{-8}	5 to 10
	5/16-17/57	2×10^{-8}	5×10^{-3}
	5/19-26/57		$< 10^{-4}$
First cosmic rocket		10^{-9}	$< 2 \times 10^{-4}$
Second cosmic		10^{-8}	$\approx 2 \times 10^{-4}$

It should be noted that data of this type are derived from a very small sample and may be quite difficult to interpret. The data for (5/15) illustrate this. The large flux may be attributed to such things as electronic difficulty, error due to small sample, or chance encounter of a meteor stream.

3. Cosmic Radiation

The nature and damage potential of cosmic radiation has

GOWWRN - 5337

been discussed by Kraushaar[18]. Kraushaar, however, used Pioneer III data in evaluating the cosmic ray hazard. Observations by Pioneer IV provided improved information as to total primary cosmic ray intensity in the general astronomical vicinity of the earth during early March, 1959[10]. These observations indicate an interplanetary value for the omnidirectional cosmic ray intensity of

$$J_o = 1.8 \pm 0.3 \text{ per cm}^2 - \text{sec.}$$

This value is one-half that measured by Pioneer III. It is believed that Pioneer III was not entirely free of the geomagnetic field, and that the above value is more reliable for deep space.

4. Solar Radiation

Most of the energy radiated by the sun is electromagnetic radiation. Wave-lengths range from 3×10^{-8} cm to 5×10^{-4} cm. The spectrum includes x-rays, ultraviolet, visible and infrared radiations. The spectral distribution, outside the earth's atmosphere, is shown in Fig. 6-4.

The total energy received at the earth's mean distance from the sun is 1.946 cal-cm^{-2} min^{-1} [19]. This number, called the Solar Constant, varies by about $\pm 1.5\%$ due to solar activity. The energy is shared approximately as follows: 8% UV, 47% visible, 45% IR.

The solar spectrum between $3A^{\circ}$ and $2000\ A^{\circ}$ includes solar x-rays and the intense emission of hydrogen in the Lyman - alpha line at $1215.7\ A^{\circ}$. Rocket measurements indicate the total flux due to x-rays between $3\ A^{\circ}$ and $1000\ A^{\circ}$ is about 1 erg-cm^{-2} -sec^{-1}, with peak intensity at about $50\ A^{\circ}$ [20]. Lyman-alpha intensity varies from 0.1 to 6 erg - cm^{-2}-sec^{-1} with solar activity.

SOURCE: SMITHSONIAN PHYSICAL
TABLES—W.E. FORSYTHE
9th EDITION 1954

NOTES:

1. TOTAL AREA FOR $0 < \mu < 5.0$ IS
   1330 RELATIVE UNIT MICRONS

2. CURVE TAKES FOLLOWING
   VALUES BEYOND $\mu = 1.5$

μ	I
1.5	260
2.0	105
3.0	26
4.0	9
5.0	4

3. SOLAR CONSTANT = 1.946
   CAL–CM^{-2} MIN^{-1}

VISIBLE RANGE

ENERGY (E) = 0.925
CAL–CM^{-2} MIN^{-1}

INFRA RED
E = 0.870 CAL–CM^{-2} MIN^{-1}

ULTRA VIOLET
E = 0.151

WAVELENGTH—MICRONS (μ)

I – RELATIVE INTENSITY UNITS
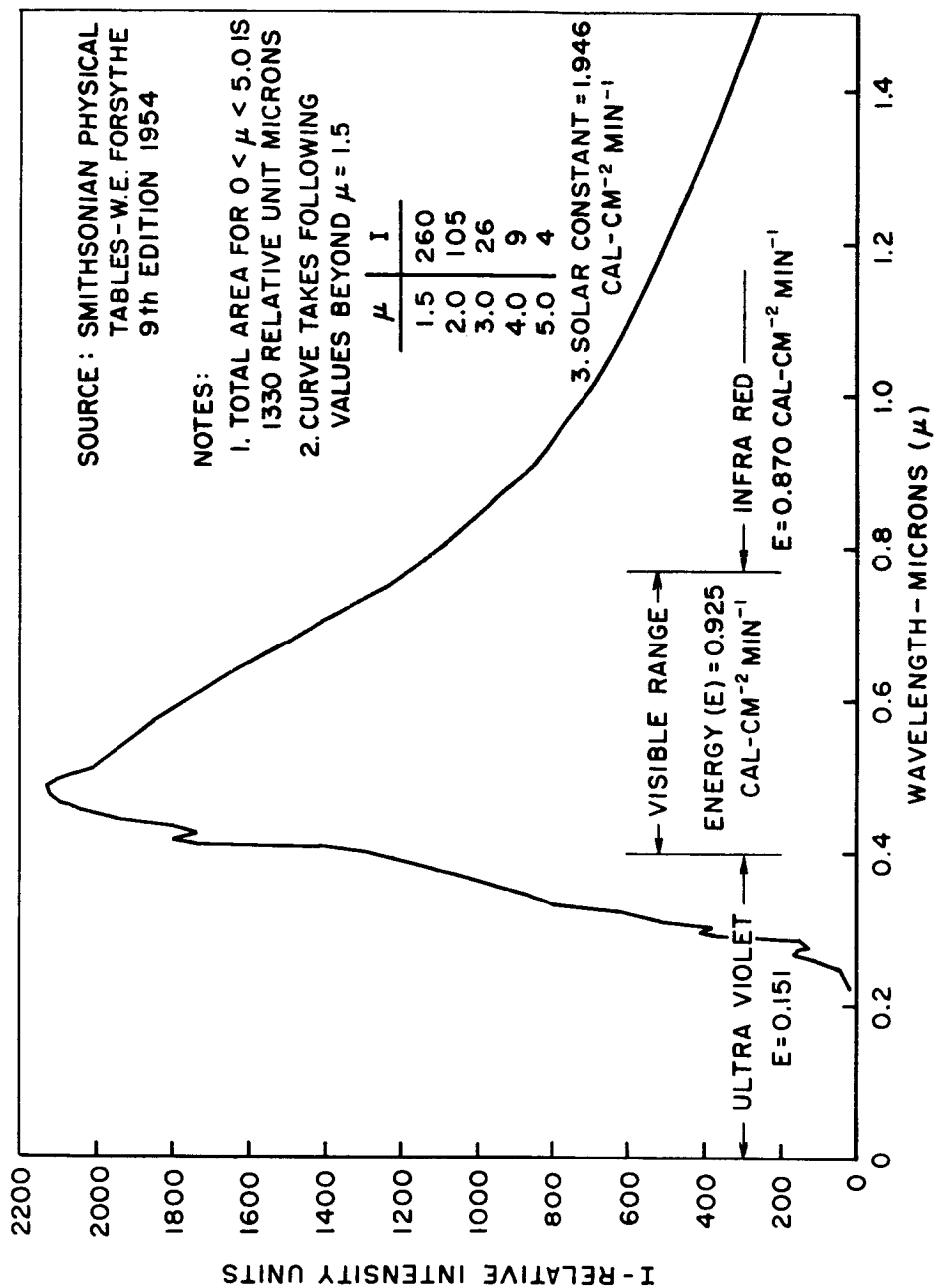
Fig. 6–4   Spectral distribution of solar radiation.

In an interplanetary voyage the energy available for heating a vehicle will vary inversely as the square of the solar distance. Thus,

$$E = 8.3 \times 10^{-4} \left(\frac{r_e}{r}\right)^2 \frac{Btu}{Sec\text{-}in.^2},$$

where

r_e = earth's mean distance from the sun

r = vehicle distance from the sun

E = energy available from the sun

Then, for Venus ($r = 108.27 \times 10^6$ Km), earth ($r = 149.68 \times 10^6$ Km) and Mars ($r = 228.06 \times 10^6$ Km) we have[27]:

$$E_{(VENUS)} = 15.85 \times 10^{-4} \ Btu\text{-}sec^{-1}\text{-}in.^{-2}$$

$$E_{(EARTH)} = 8.3 \times 10^{-4} \ Btu\text{-}sec^{-1}\text{-}in.^{-2}$$

$$E_{(MARS)} = 3.56 \times 10^{-4} \ Btu\text{-}sec^{-1}\text{-}in.^{-2}$$

D.   Planetary Atmosphere

Answers to questions involving the close pass or entry into a planetary atmosphere require knowledge of the composition and density of that atmosphere. It is very difficult to obtain quantitative measurements of this type, and estimates (particularly of composition) vary.

A good first guess of atmospheric density as a function of altitude can be made by assuming an isothermal atmosphere in hydrostatic equilibrium. This leads to the following expression for density:

$$\rho = \rho_{SL} e^{-\alpha h}$$

where:

ρ_{SL} = density at the planet's surface

h = altitude above the planet's surface

α = a constant, its value dependent upon atmospheric composition, temperature, and the planet's gravity.

$$\alpha = \frac{Mg}{RT}$$

The actual composition of planetary atmospheres is not known, but estimates are available. Gazley and others[23, 24, 25, 26] give the data summarized in Table 6-4.

II. Environmental Effects, Problems and Tests

A. Vibration, Noise, Shock, Acceleration, Altitude, Humidity

The primary (initial) effect of these disturbances is often one of the following:

a. Mechanical displacement, bending, loosening of a part or adjustment, or sympathetic vibration due to mechanical resonance;

b. Fracture of a mechanical part; and

c. Electrical arcing (moisture or lowering of pressure).

Determination of primary failures is often complicated by secondary failures. For example, a transformer broken loose by vibration may damage other parts which would otherwise be completely unaffected by the vibration. The important thing to eliminate is the primary failure.

Testing under actual or simulated conditions is usually required to weed out such troubles. Flight testing in a missile is difficult to instrument and appraise, and much too expensive for routine developmental testing of equipment. We must, there-

TABLE 6-4

PLANETARY DATA

Atmosphere [23, 24, 25, 26]

Body	Atmospheric Composition (%)	Mean Mol Weight M(gm/mol)	Mean atm. Temperature T (°K)	α (ft^{-1})	ρ_{SL} (lb/ft^3)
Moon	————	——	——	———	0
Venus	CO_2, N_2(90, 10)	40	270	4.9×10^{-5}	1.0
Earth	N_2, O_2(79, 20)	29	240	4.15×10^{-5}	0.0765
Mars	N_2, CO_2(95, 5)	30	220	1.2×10^{-5}	0.0062
Jupiter	H_2, CH_4	3	170	1.2×10^{-5}	

ASTRONOMICAL DATA [27]

Body	Radius	Mean Surface Gravity	Escape Velocity (km/sec)	Albedo	Stellar Magnitude	Mean dist from Sun (km)
Moon	0.27	0.165	2.4	0.07	-12.55	———
Venus	0.97	0.86	10.2	0.59	- 4.07	108.3×10^6
Earth	1	1.0	11.2	0.29	- 3.8	149.7×10^6
Mars	0.53	0.37	5.0	0.15	- 1.85	228.1×10^6
Jupiter	11.0	2.64	60.0	0.44	- 2.23	778.7×10^6

fore, simulate missile conditions in the laboratory. Early tests usually separate the environments, since simultaneous disturbances are difficult to produce, and failures are hard to analyze. Tests cannot be considered complete, however, until more realistic (simultaneous) environmental conditions are imposed.

The Instrumentation Laboratory makes frequent use of the following facilities for developmental testing.

Shaker (Electrodynamic)

Force limit	7000 lbs.
Frequency range	20 → 2000 cps
Inputs	sinusoidal, random, or tape
Amplitude limit	1/2" peak to peak
Weight of moving element + mounting plate	127 lbs.

Centrifuge

Arm length	32 ft.
Acceleration limit	30 g
Table	Fixed or counter-rotating as required

Altitude Chamber

Work space	7ft x 7ft x 10ft
Altitude limit	100,000 ft (approx 8 mm Hg)
Humidity	20% → 95% (35°F → 185°F)
Temperature	-100°F to + 200°F

Several simultaneously imposed environments are possible. For example, the shaker can be operated within the operating altitude chamber. A vibration exciter is also being built to mount on the centrifuge. Most difficulties caused by the booster environments under consideration can be found and

corrected with the aid of this equipment.

Acoustic noise is a problem only in the presence of an atmosphere, since the energy is transmitted to equipment via the atmosphere. This environment is produced by exciting a "loud speaker" in a specially designed chamber. AVCO makes a chamber of this type which has a volume of 2.7 ft^3 and is used by that company to test equipment at sound pressure levels in excess of 140 db (Ref. 0002 microhms).

Initial testing of guidance equipment will be directed toward development of competent designs. Thus life, reliability, and performance must be examined under appropriate environmental conditions.

B. Vacuum

Materials under continuous exposure to vacuum exhibit many peculiar properties. Tests at the Naval Research Laboratory in Washington have shown that some metals grow stronger, while others weaken in a vacuum. Ordinary glass achieves three times its normal strength. Dr. Achter of NRL attributes such behavior to surface reactions which occur in air[34]. For example, steel is expected to exhibit superior strength if a surface finish entirely impervious to air is applied.

Tests by NASA have indicated that moving metal surfaces, in a vacuum, tend to weld together by molecular adhesion. Magnesium tends to sublimate and effectively disappear.

Bearings are difficult to maintain in a vacuum because of evaporation of the lubricant. Oil evaporation tests at Airborn Instruments Laboratory[33] have been made for a large variety of commercial lubricants. The results are encouraging in that many of the lubricants tested evaporate at a slow rate. Dry lubricants are being sought by many researchers in the hopes that materials with low vapor pressure and good lubricating qualities will be found. One such material is molybdenum disulphide, which

will be discussed presently.

Thus we see that many new problems are introduced by the vacuum environment of space. Several of these problems will now be assessed.

1. Vacuum Seals

It is often possible to avoid vacuum problems by pressurizing a sealed unit. The difficulty of maintaining a seal depends upon the container material, the pressurizing gas, environment, and life requirement. Heliarc welding is recommended for seams to avoid porosity of the weld. Porosity of the container can be avoided in many ways. For example, materials such as copper, aluminum, stainless steel or glass are practically non-porous. Plating the container with tin, painting with shellac, or applying one of special preparations available for vacuum sealing will also help.

Electrical leads can be brought through ceramic or glass seals. Special glass sealing alloys are available for the purpose[35].

Covers and removable parts can be sealed in several ways. Gold o-rings are very effective. Knife-edge seals are also used, and even fiber gaskets soaked in glyptol will give a good vacuum seal. The particular method used depends upon the quality of seal required.

It is worth noting at this point that a seal must only be good enough to maintain pressurization for the desired life span of a unit. If pressurization is supplied, for example, by a high vapor pressure substance in reserve, small losses through the seals or container can be tolerated.

Moving parts extending into a vacuum may be "sealed" in several ways. By "sealed" we mean reducing leakage to a negligible amount for the application. "Wilson" and "Chevron" seals are commonly used in vacuum systems where sliding and

rotating motions of a shaft are required. The seal consists of a number of rubber washers, fitting tightly over the shaft, held in place by a compression nut. A disadvantage of this seal is that it requires frequent lubrication. Bellows are also used to good advantage in sealing reciprocating as well as rotating shafts[30]. In some cases it is sufficient to simply use close fitting parts for a seal. Here the leakage path is elongated, has small cross section, and is lubricated with vacuum grease.

2. Sublimation and Evaporation

A theoretical estimate of evaporation and sublimation rates for various materials can be made if the material's vapor pressure is known. Fig. 6-5 and Table 6-5 show the vapor pressure for a number of materials. Table 6-6 shows the theoretical evaporation and sublimation rates for many materials, based upon the following relationship derived from kinetic theory (see Chapter 7).

$$\mu = 1.8 \times 10^6 \, P \sqrt{\frac{M}{T}} \, gm/cm^2 - year,$$

where

μ = mass depletion rate for an exposed area of 1 cm^2,

P = vapor pressure of material (mm Hg),

M = molecular weight of material,

T = absolute temperature of material (^{O}K);

it has been assumed that dissociation of the molecules does not occur.

It is noted from Table 6-6 that sublimation rates for metals such as aluminum and beryllium are small, even at high temperatures. An aluminum surface, just below its melting temperature is lost at the approximate rate of 0.001 cm per year. This rate goes down by a factor of about 10 for every 100°C, therefore, at room temperature the rate would be in the order of 10^{-9} cm/year. Some metals should be avoided in applications
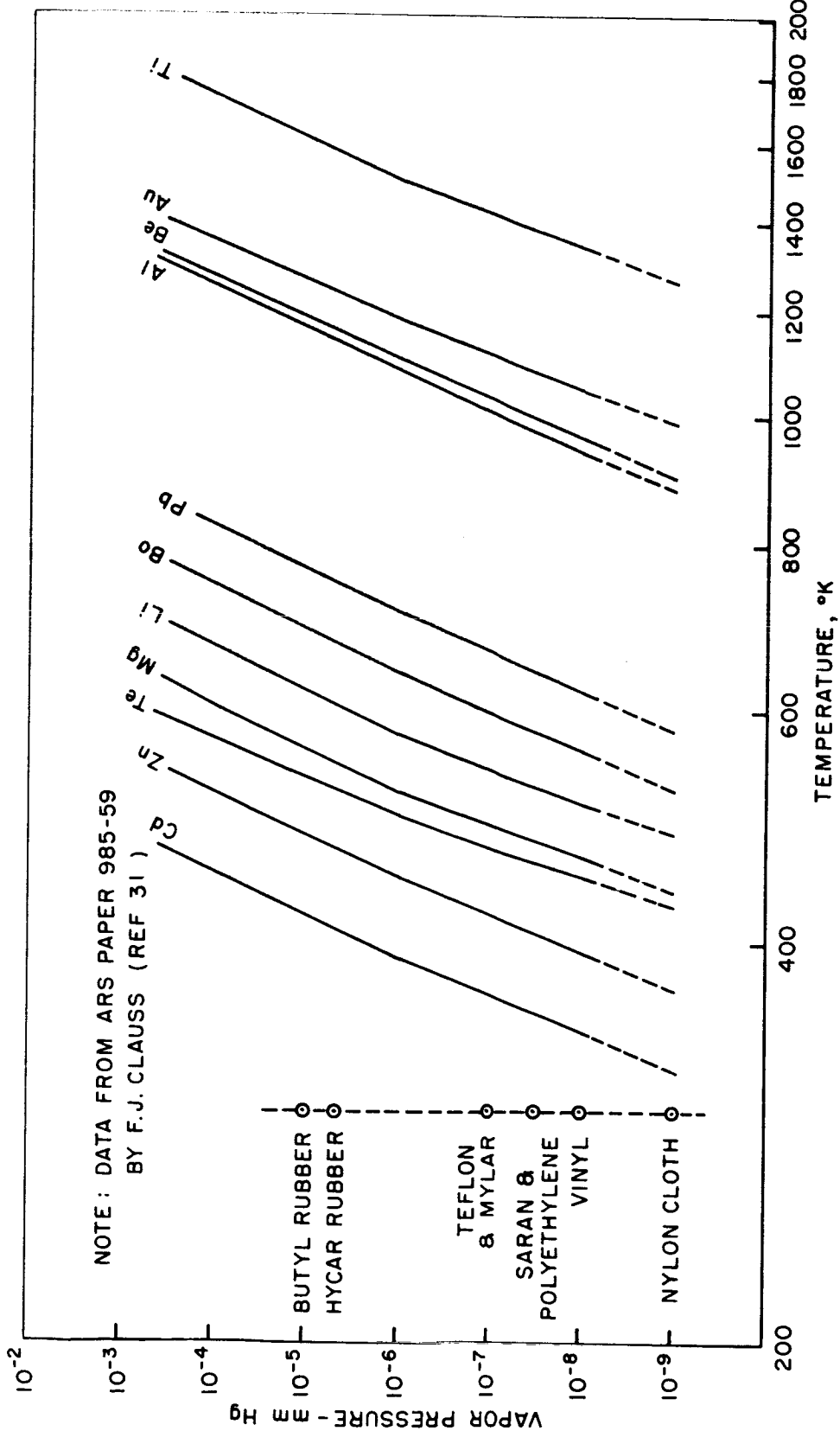
Fig. 6-5   Vapor pressure--temperature characteristics for general materials.

TABLE 6-5

VAPOR PRESSURE FOR VARIOUS MATERIALS

Material	Temperature °C	Vapor Pressure mm Hg	Source
Ice (H_2O)	-78	5.6×10^{-4}	Ref 28
Iodine (I_2)	20	0.25	Ref 28
Napthalene ($C_{10}H_8$)	20	5.6×10^{-2}	Ref 28
Camphor ($C_{10}H_{16}O$)	20	0.3	Ref 28
Mercury (Hg)	20	1.2×10^{-3}	Ref 28
Apiezon-B-DP-Oil	25	1×10^{-7}	Ref 29
Octoil	25	2×10^{-7}	Ref 29
Silicone DC 703	25	5×10^{-8}	Ref 29
Apiezon-L-Vac. Gr.	20	5×10^{-6}	Ref 29
Gallium (Liquid)	500	$< 1 \times 10^{-8}$	Ref 32
Indium (Liquid)	500	$< 1 \times 10^{-8}$	Ref 32
Tin (Liquid)	500	$< 1 \times 10^{-8}$	Ref 32
Bismuth (Liquid)	300	$< 1 \times 10^{-8}$	Ref 32
Lead (Liquid)	350	$< 1 \times 10^{-8}$	Ref 32
Ga-In-Sn (Liquid)	500	$< 1 \times 10^{-8}$	Ref 32

115

TABLE 6-6

THEORETICAL DEPLETION RATE FOR SELECTED MATERIALS

Material	Temp $^{\circ}C$	State	$\mu \left(\dfrac{gm}{cm^2 - year} \right)$
Ice (H_2O)	-78	solid	3.05×10^2
Iodine (I_2)	20	solid	4.2×10^5
Napthalene ($C_{10}H_8$)	20	solid	6.73×10^4
Camphor ($C_{10}H_{16}O$)	20	solid	4.30×10^5
Mercury Hg	20	liquid	1.79×10^3
Apiezon-B-DP-Oil	25	liquid	0.211
Apiezon -L-Vac. Gr.	20	viscous solid	10.05
Silicone DC 703 Oil	25	liquid	0.10
Butyl Rubber	25	solid	14.9
Teflon	25	solid	0.149
Vinyl	25	solid	1.49×10^{-2}
Nylon Cloth	25	solid	1.49×10^{-3}
Aluminum	650	solid	3.08×10^{-3}
Beryllium	625	solid	1.8×10^{-4}
Lead	320	solid	2.14×10^{-3}
Magnesium	200	solid	1.21×10^{-2}
Zinc	150	solid	7.15×10^{-2}
Ga-In-Sn alloy	500	liquid	6.15×10^{-3}
Magnesium	515	solid	3.16×10^4
Zinc	405	solid	5.6×10^4

where surface evaporation could create a problem. Magnesium and zinc are examples of such metals. It appears, therefore, that if materials are properly selected, the problem of surface depletion can be avoided.

3. Lubrication

The vacuum environment is responsible for lubrication difficulties because of loss of the lubricant and various surface contaminants. It is important not to lose these materials because they produce low friction, reduce wear, and prevent adhesion between contacting surfaces.

Sliding friction between metals is believed to be caused by a large number of welded junctions[37] occurring between sliding surfaces. Shearing action either breaks the welds, or shears the bearing material near the weld. A lubricant serves to separate surfaces (partially or completely) thereby reducing the area involved in welded junctions. When surfaces are completely separated by a fluid film there is no wear, and the condition is known as complete lubrication. When surfaces are separated by a thin film (measured in molecular diameters) there is wear, and the condition is known as boundary lubrication. Boundary lubrication is common where loads are pulsating or particularly high or where continuous lubrication is not possible.

Lubrication is not a property restricted to viscous materials. A material which reduces the welding efficiency at points of contact may act as a lubricant--an oxide coating, for example. A soft surface film which shears easily could also act as a lubricant.

Adhesion between surfaces is a hazard in the vacuum environment. Many examples are cited[37] which indicate that metal surfaces, if perfectly clean, will adhere to one another and in time even "grow" together. However, experiments show that very thin surface films (oxides, adsorbed gas, lubricants, etc.) are effective in preventing adhesion.
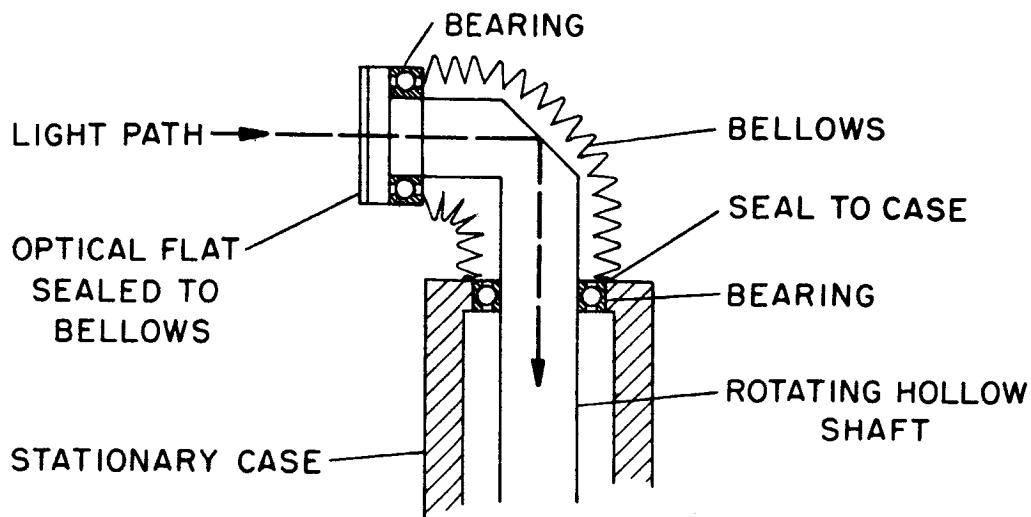
Mechanical gadgets can be classified as those which can be sealed from the vacuum, and those which cannot. Attitude-control-flywheels, gyros, and accelerometers are examples of units which can be placed in tightly sealed containers, essentially solving their lubrication problem. Thermal control blinds, iodine jet valves, and mobile star trackers are examples of units which do present lubrication problems, since moving parts may extend into the vacuum.

The star tracker presents an especially difficult problem because of the precision required of mechanical and optical elements. Among the solutions to this problem are the means of sealing the unit. Three methods are described below:
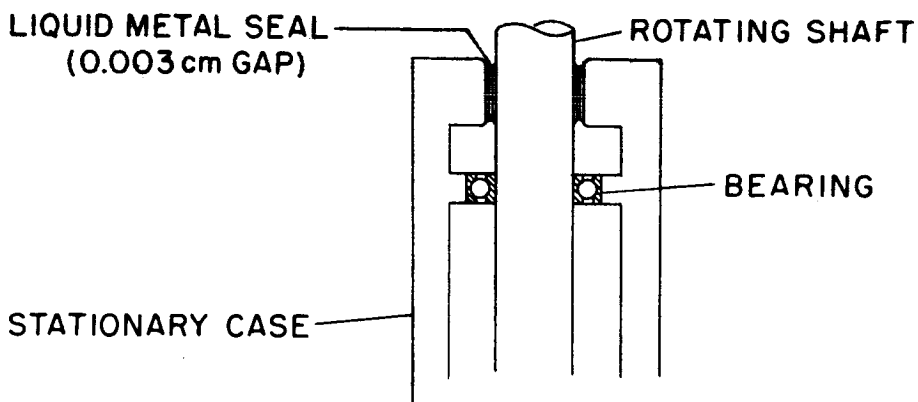
(a) Transparent Enclosure - This is a cylindrical enclosure within which the star tracker rotates. It allows sealing the unit but presents a particularly difficult optical problem.

(b) Bellows - The configuration illustrated in Fig 6-6, using a bellows, would allow sealing the unit. A possible objection to this method is that puncture, or breakage of the bellows might be catastrophic. This could be overcome, however, by the use of a special sealant which repairs leaks, a secondary enclosure affording protection from punctures, or both.

(c) Liquid Metal Seal - It is possible to seal a rotating shaft from a vacuum with a liquid, taking advantage of its surface tension (Fig. 6-6). This is accomplished by filling the clearance gap between housing and shaft with a liquid such as the eutectic alloy of Ga-In-Sn[32]. The alloy has a melting point of $10.7^{\circ}C$, and a very low vapor pressure ($< 10^{-8}$ at $500^{\circ}C$). The liquid film can withstand atmospheric pressure across a maximum theoretical gap of 10^{-3} cm. The alloy can be made to wet W, Mo, Ta, Pyrex, quartz and certain
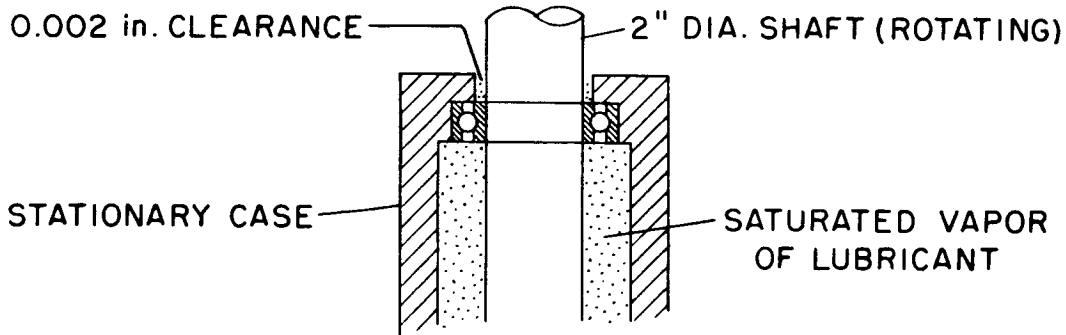
BEARING

LIGHT PATH →

BELLOWS

SEAL TO CASE

OPTICAL FLAT
SEALED TO
BELLOWS

BEARING

ROTATING HOLLOW
SHAFT

STATIONARY CASE

a. Bellows (sealed system)

LIQUID METAL SEAL
(0.003 cm GAP)

ROTATING SHAFT

BEARING

STATIONARY CASE

b. Liquid metal seal

0.002 in. CLEARANCE

2" DIA. SHAFT (ROTATING)

STATIONARY CASE

SATURATED VAPOR
OF LUBRICANT

c. Lubrication with no seal

Fig. 6-6   Lubrication methods in a vacuum.

ceramics. These materials will also withstand the corrosive action of this alloy.

However, there are disadvantages to using this alloy. It attacks many solids, and reacts with oxygen and certain vapors; it can lose its wetting bond due to decomposition at high temperature; surface tension is affected by temperature, contamination, or any chemical reaction. Thus liquid metal seals require research and development to make them practical, but the prospect of developing a good seal is attractive.

There may be solutions to the lubrication problem which do not require sealing the unit. Consideration of the theory of friction and lubrication, as well as many experimental findings, suggest several:

(a) boundary lubrication, supplied by the vapor of a lubricant at its vapor pressure;

(b) very thin surface films formed by chemical action occurring at the bearing surface (oxides, metallic soaps);

(c) solid lubricants and various bearing materials and alloys;

(d) special bearing materials and alloys; and

(e) metallic film lubricants (thin plating on a bearing surface).

Boundary Lubrication - Consider the problem of lubricating the bearing of a 2 in. shaft, one side exposed to the vacuum, with no seal installed (Fig. 6-6) in a 0.002 in. radial gap. The area around the shaft, exposed to the vacuum, is 0.08 cm^2. Accordingly, an oil with an evaporation rate of 3 gm/cm^2-year (see Sec. II, B, 2) would be lost at the rate of 0.24 gm/year. This loss can be easily supplied by reserve oil (oily-rag concept). The practical problem to be solved involves proper lubrication of the bearing by a saturated vapor at low pressure rather than the problem of complete

120

loss of lubricant. One solution might be to make surrounding surfaces warmer (periodically) than the average bearing temperature, thereby condensing oil on bearing surfaces.

Experimental evidence must be accumulated to determine if lubrication is sufficient, under these conditions, to prevent excessive wear and adhesion of contacting surfaces. Experimental work must also determine the most suitable lubricant for this type of service. For example, silicone oils might be selected because of their low vapor pressure. This could be a poor choice, however, since these oils are considered poor boundary lubricants.

Thin Surface Films formed by chemical action occurring at the bearing surface are effective in reducing friction and preventing adhesion. A particularly good lubricating film is achieved when a liquid lubricant is allowed to react with the bearing surface to form a metallic soap. This metallic soap adheres firmly to the bearing surface, is a durable compound, and has excellent lubricating properties[37]. An oxide formed on the bearing surface is also effective in preventing adhesion and in lowering friction.

Solid Lubricants - Some materials have a laminar structure and act as a lubricant because of the low friction between sliding laminations. Graphite, molybdenum disulphide, uranium and tungsten sulphide are examples (Fig. 6-6). Graphite is not a suitable lubricant in a vacuum since adsorbed moisture is believed to account for its low friction and wear. Molybdenum disulphide has the undesirable property of oxidizing easily (increasing friction). Despite these problems, solid lubricants deserve consideration for use in a vacuum. They exhibit very low friction coefficients and do not evaporate rapidly.

Special Bearing Materials and Alloys - Of the plastics which exhibit low friction, Teflon is the most outstanding. This material requires no lubricant when rubbing on itself, and adhesion is not apparent.

121

Bearing materials are often alloys containing a soft, low melting point constituent. Copper-lead alloy is an example. Shearing of welded junctions takes place in the lead and results in low friction. The same result is obtained if a soft metallic film is simply smeared on a harder surface.

Combinations of materials produce durable, low friction surfaces. The incorporation of Teflon in porous sintered copper, and porous metallic molybdenum attacked chemically to form a surface of MoS_2, are examples of combinations giving excellent results.

Metallic Film Lubricants - The desirable properties of two materials can be used to advantage by plating one on the other. For example, silver bearings exhibit high friction and are difficult to lubricate. A thin film of lead plated on the silver results in an excellent bearing, taking advantage of the desirable properties of silver (good fatigue strength and thermal conductivity) and lead (low shear strength and easily lubricated with oil). Attlee[38] used a film of barium for lubricating ball races in rotating anode X-ray tubes.

It is seen that many approaches to the problem exist concerning lubrication of bearings in a vacuum. The advisability of isolating or not isolating moving parts from a vacuum is difficult to determine. It might, at present, be expedient to seal units whenever possible, but the prospect of not requiring a vacuum seal is certainly attractive. Even with a sealed unit, the possibility of a leak or puncture exists. Consider, for example, the space sextant sealed within a bellows. A leak might result in complete loss of lubricant. However, the lubricant could be retained by employing both the bellows and the method previously described under Boundary Lubrication of an unsealed unit.

The measurement of friction and adhesion coefficients for materials is difficult. The results vary a great deal with the material's environment, past and present. Representative values

122

are available, however, some of which are shown in Table 6-7.

C. Meteoritic Material

Thus far it has not been possible to reach the velocities attributed to meteoric particles. The mechanism of penetration and damage must be inferred from laboratory tests at relatively low velocities.

Herrman of MIT uses a special "rifle", accelerating particles to about 3 km per second. Scully[40] indicates that particles have been accelerated to velocities as high as 6 km per second by some investigators. This is still a low velocity compared to meteoric values, which sometimes reach 72 km per second.

Most high velocity impact tests have been carried out at velocities below the sonic value of metallic target materials. In this range it is found that penetration and velocity can be simply related. For example, if target material and projectile are of the same material, the relationship is:

$$P/Dp = K \left(\frac{V}{C}\right)^N$$

where:

$$K = 1 \rightarrow 3$$
$$N = 0.5 \rightarrow 2$$
$$C = \text{sonic velocity of target material}$$
$$Dp = \text{pellet diameter}$$

It is suspected that when pellet velocity exceeds C of the target material, the mechanism of penetration and damage changes. Partridge[41] notes that tests of this type have been performed using paraffin pellets and targets. These tests indicate a considerable increase in damage beyond the sonic point (at least for paraffin pellets fired at a paraffin target). Other factors must also affect penetration. As previously noted,

TABLE 6-7

FRICTION AND ADHESION
CHARACTERISTICS FOR SEVERAL MATERIALS

(1) Lubricated Steel or Steel on Bearing Surface

Lubricant	Coeff. of Friction	Source
Silver Sulphate	0.054	Ref 39
Graphite	0.058	Ref 39
Molybdenum Disulphide	0.033	Ref 39
Tungsten Disulphide	0.037	Ref 39
Copper Impregnated with Teflon	0.05	Ref 37
MoS_2 on Pourous Molybdenum Base	0.07	Ref 37
Teflon	0.05	Ref 37

(2) Metallic Film Lubricants (thickness $10^{-3} \rightarrow 10^{-4}$ cm)

Lubricant	Coeff. of Friction	Source
Indium Film on Steel	0.04 → 0.08	Ref 37
Indium Film on Silver	0.07 → 0.1	Ref 37
Lead Film on Copper	0.12 → 0.18	Ref 37

(3) Misc Lubricated Surfaces[37]

Steel - On bearing alloy (lead or tin base)
Mineral oil lubricant — $\mu = 0.11$
Stearic acid lubricant — $\mu = 00.07$
Ball Bearings — $\mu = 0.001 \rightarrow 0.003$

TABLE 6-7 (cont'd)

(4) <u>Clean Metals in a Vacuum</u>[37]

 (a) Coeff. of friction of 100 and larger may be
   observed with many metals. Complete
   seizure occurs in the case of Nickel, Platinum,
   and Iron.

Metal	Adhesion			
	Clean	Paraffin Oil	Paraffin plus 1% Lauric acid	Oxide
Indium	1	0. 6	0	———
Lead	1	0. 15	0	———
Tin	1	———	0	———
Nickle	Seizure	———	———	3. 0
Platinum	Seizure	———	———	3. 0
Iron	Seizure	———	———	1. 2

125

meteoric particles are believed to be brittle, and have a density of about 0.05 gm/cm^3. It is reasonable to assume that damage by this type of projectile is different from damage by such things as lead pellets, and that extrapolation of data, particularly from the low velocity range, cannot be made with confidence.

A simple and reasonable picture of how meteoric damage occurs is adopted by Whipple[13]. He calculates penetration by equating the kinetic energy of the meteoroid to the energy required to melt a right circular cone of material from the target surface. The result (with cone apex angle selected as 60°) is:

$$P = \left(\frac{9}{\pi \rho h}\right)^{1/3} E^{1/3},$$

where: P = depth of penetration,
           ρ = density of target material,
           h = heat of fusion of target material,
           E = kinetic energy of meteoroid,

Penetration calculated in this manner will be used to appraise meteoric damage to a surface in space. Data for an aluminum surface in the earth's meteoric environment are shown in Table 6-2.

Consider an aluminum sphere traveling in an environment identical to that of the earth. Thus the data of Table 6-2 apply. Meteoric penetration will be calculated for a 50 cm diameter sphere.

Surface area   = 0.785 m^2
Assumed skin thickness   = 0.17 cm (about 1/16 in.)
Puncture probability(Table 6-2)   = 3.55 x10^{-3} per day
Particle size   = 0.0492 cm (radius) and larger

Approximately once in 280 days a particle of radius equal to or larger than 0.05 cm will puncture the skin.

The effect of increasing skin thickness can be seen by

recalculating the penetration if skin thickness is doubled.

Surface area	$= 0.785 \text{ m}^2$
Assumed skin thickness	$= 0.335$ cm (about 1/8 in.)
Puncture probability (Table 6-2)	$= 5.61 \times 10^{-4}$ per day
Particle size	$= 0.091$ cm (radius) and larger

Approximately once in 1800 days a particle will puncture the skin. For this case a 1/8 in. skin should eliminate puncture hazard on trips lasting many years.

Another method of reducing puncture hazard is suggested by Whipple[13]. This involves a thin secondary layer of surface placed a few thicknesses (of major surface) from the major surface. This "meteor bumper" should act to explode and possibly vaporize meteoric particles before they reach the major surface. It is estimated that a bumper 10% as thick as the major surface would reduce punctures by a factor of 10 → 100.

It appears that the puncture hazard can be avoided by proper selection of skin thickness, or by the use of a secondary surface. Of the two methods, double containers for vital equipment is the lightest. Both methods seem practical, however.

Surface erosion caused by frequent impact of extremely small particles is another meteoric hazard. Damage is assumed to be caused by the same mechanism as penetration. Particles of importance range over 20 visual magnitudes (Table 6-2), extending to meteoric dust. Damage will be calculated for the previously assumed sphere (50 cm diameter).

Mass of material striking surface $(\text{day}^{-1}\text{-m}^{-2})$
    (a) Per visual magnitude $= 11.3 \times 10^{-8}$ gm (Table 6-2)
    (b) Per 20 magnitudes $= 226 \times 10^{-8}$ gm
Average velocity $= 15$ km - sec.$^{-1}$ (Table 6-2)

127

Total Kinetic Energy of meteoroids per day

$$KE = \frac{1}{2}(266 \times 10^{-8})(15)^2 \times 10^{10} \times 10^{-4}$$

$$= 254 \text{ ergs per cm}^2$$

Heat of fusion of aluminum $= 3 \times 10^{10}$ ergs/cm^3

Erosion rate $= (254)(3 \times 10^{10}) = 0.85 \times 10^{-8}$ cm/day

$$= 310 \text{ A}^{\circ} \text{ per year}$$

The finest optical surfaces have irregularities of the order of 1/100 to 1/20 the wavelength of light. Let us assume that such a surface exhibits undesirable characteristics when erosion, as calculated above, amounts to 1/50 the wavelength of light. Under these assumptions it will take about two months of continuous exposure to micrometeoric dust before the effects are important. This is an encouraging result, even when considering the space sextant's optical system. Here we have a mirror subject to erosion while the tracker is in use. The tracker is in use for a total of about 40 hours during a one way trip to Mars. The remaining time is spent with the tracker in the stowed position, presumably well protected from erosion.

It should be noted that most external surfaces would not be aluminum, but ceramic, glass, oxide, or a precious metal plating. Also, the mechanism of damage is not actually known for any material. Experimental work is required despite the optimistic results obtained by calculation. Test results from satellite vehicles and space probes will help resolve the issue.

D. Radiation

Radiation damage suffered by a material is a function of the energy absorbed or deposited per unit mass of material. A unit of energy deposition commonly used is the rad, one rad being an absorbed dose of 100 ergs per gram of material. Another unit commonly used, particularly in the field of biological damage,

128

is the roentgen. The roentgen is defined as the quantity of x-ray
on gamma rays which produce one e. s. u. of electricity in 1 cc
of dry air. One r is equivalent to an absorbed dose of 83. 8 ergs
per gram of material. The mechanism by which energy is trans-
ferred to materials varies with the material, the type of radiation,
and often level of radiation. However, a discussion by Hess[47]
indicates that the point at which radiation damage becomes im-
portant can be derived from tests of materials in a reactor.
Data of this type are readily available for a large variety of
materials. Table (6-8) indicates the dosage required to cause
threshold damage (25% of damage necessary for failure) for a
number of materials.

The dosage due to radiations in space has been estimated
by Kraushaar[53]. For cosmic radiation, the estimate is cal-
culated from

$$\text{Dose} \cong 2J \ (3. 2 \times 10^{-3})(1 + kt) \ \text{Roentgens per day,}$$

where J = Omni-directional intensity of cosmic
radiation = 1. 8 cm^{-2} sec^{-1}.

k = (0. 006) for absorbing materials of low
atomic weight and (0. 018) for absorbing
materials of high atomic weight.

t = Thickness of absorber gm-cm^{-2}.

This results in a dose of about 4 Roentgen per year. Thus the
damage to various materials (Table 6-8) due to cosmic-radi-
ation seems to be insignificant. Solar flares are known to re-
sult in large increases in cosmic radiation. Kraushaar indi-
cates a dose rate of about 1000 Roentgen per day under 0. 3
gm-cm^{-2} of shielding, and about 4 Roentgen per day under
10 gm-cm^{-2} of shielding. This radiation could last from one
to ten days. Thus, most materials could be easily protected
by shielding, or by traveling during periods of low solar activity.

Kraushaar also investigates the dosage contributed by
the Van Allen belts. A vehicle launched on a Mars trajectory[53]

129

TABLE 6-8

RADIATION DAMAGE TO VARIOUS COMPONENTS

Components	Radiation Susceptible Material	Estimated Threshold Damage**(25% Damage)
Capacitor	Organics - paper or oil dielectric and Bakelite or waxed paper cover	$4.5^* \rightarrow 7.0 \times 10^6$ rads
Resistors	Plastics – Bakelite cover for resistance material	$4.5^* \rightarrow 7.0 \times 10^6$ rads
Microswitches	Plastics – Plastic case and actuator	$4.5^* \rightarrow 7.0 \times 10^6$ rads
Selsyns	Electrical insulators (organics) wire insulation, brush holder, slot liners, end punchings and casing insulation	$4.5^* \rightarrow 7.0 \times 10^6$ rads
Gaskets & Seals	Elastomers, Leather	$4.5^* \rightarrow 7.0 \times 10^6$ rads
Hoses & Couplings	Rubber and plastic hoses, plastic and fabric couplings	$4.5^* \rightarrow 7.0 \times 10^6$ rads
Fuels, Lubricants and Hydraulic Fluid	Petroleum base (paraffin hydrocarbons)	$1 \rightarrow 2.5 \times 10^8$
glass		3×10^5 (Ref. 51)
transistors		1×10^5 (Ref. 51)
lubricants		$>1 \times 10^8$ (Ref. 45)
metals		$>1 \times 10^{11}$

* $4.5 \rightarrow 7.0 \times 10^6$ rads corresponds approximately to combined radiation of 1×10^{16} thermal neutrons cm^{-2}, 1×10^{15} fast neutron cm^{-2} (above .7 mev), and 5×10^{15} gammas cm^{-2} (average energy 1.0 mev).

** Data from "Radiation Damage to Non-metallic Materials" V. P. Calkins (1954) GE-ANP Department, Cincinnati 15, Ohio.

would experience a dose of about 1. 5 Roentgens if the particles were electrons, and about 30 Roentgens (one way) if the particles were 10 → 50 Mev protons. Thus the Van Allen belts present no apparent problem. Nisbet[46] similarly shows that Van Allen radiation is not a serious hazard to transistors. He takes Van Allen data (Pioneer III), assumes it to be 100 Mev Protons and compares the number of displacements per second in a transistor (occasions when an atom is displaced from its regular position in the crystal lattice) with the number of displacements caused by a known gamma source (which resulted in serious damage to the transistor). It is estimated that the life of a transistor in the radiation belt may be of the order of 10^5 hours.

In general, then, the radiation hazard to most materials and various types of equipment is not serious. There would be some hazard if biological or photographic materials were being considered. Here, as indicated in Ref 53, moderate shielding would be necessary.

III. Environmental Test Program

A. Early Tests

Early environmental test activities must be aimed at providing design information in questionable areas. Among the most prominent inquiries are:

a. Investigation of several schemes for, and subsequent development of a method for lubricating bearings in the vacuum environment (see Section II, B, 3).

b. Investigation of methods for sealing and pressurizing certain untis. Examples of units, where sealing may be desirable, are attitude control flywheels, electronic gadgets, computer components, gyros and accelerometers.

c. Behavior of materials in the vacuum environment (see Section II, B).

131

d. Tests of iodine-jet operation. This includes the measurement of thrust, and investigations leading to the development of a satisfactory valving arrangement.

e. Tests and investigations leading to the design of thermal controls, and thermal control surfaces. This should include studies of surface characteristics in various environments, and the effect of micrometeorite erosion (see Section II, C).

f. Tests of the effect of booster environment upon various gadgets, in support of design activities.

Most of the facilities necessary for this testing program are available at the Instrumentation Laboratory. The 50 ft^3 -10^{-6} mm Hg vacuum chamber can be used for initial studies of boundary layer lubrication, iodine-jet operation, and thermal control. The laboratory's altitude chamber, shaker table, and centrifuge (see Section II, A) can be used to explore the effects of booster environments.

A particularly important facility which the laboratory does not have is a small vacuum chamber capable of extremely high vacuums. A chamber of this type is necessary, in order to make "clean surface" studies, advanced tests on seals and bearings in a vacuum, and vacuum behavior of materials studies. To illustrate this need, consider an initially clean surface placed in a vacuum of 10^{-7} mm Hg. At this pressure there still remains 3×10^9 molecules per cm^3. In about 2 minutes (at room temperature) the surface would be contaminated with a mono-layer of the molecules in the chamber. If the pressure is reduced to 10^{-9} mm Hg, the time interval before contamination would be troublesome is extended to several hours. Several systems capable of 10^{-9} mm Hg were described at the 1959 AVS symposium.[54, 55, 56, 57, 58] These systems were small glass enclosures as well as 40 ft^3 chambers.

Adequate testing of guidance equipment requires a de-

vice for testing attitude control systems. This is, ideally, a zero-friction suspension with three degrees of freedom capable of operating in a vacuum chamber. The configuration of this device is still a matter for speculation.

An outline of specific tests in various areas is being worked out on the basis of presently available environmental information and preliminary guidance equipment designs. The outline is obviously tentative since developmental testing, by its nature, must be done within a flexible program.

B. Life and Reliability

Many space missions require the operation of equipment for extended periods. A trip to Mars, for example, may require six months. A round trip could take several years. These operating and shelf-life requirements add to the difficulty of designing and testing equipment, particularly for use in the space environment. Closely related to the life of equipment is its reliability, defined as "the probability of adequate performance of a specified function or functions for a specified time under specified conditions"[61]. Note that performance data must be collected for equipment operating over its specified lifetime. Unfortunately, testing for extremely long periods of time is not always practical. We must use data collected from relatively short tests to deduce the lifetime reliability.

Analytical studies of reliability[62] show the need for virtually flawless equipment if complicated space vehicles are to succeed. Thus, testing must be aimed at always improving the equipment under test rather than trying to measure a quantity called reliability. Lusser[60] shows the virtue of this attack, and how "testing to failure" quickly results in improved equipment designs. Once the design stage is passed, other test methods may be justified. See Ref 63 for further discussion of this point.

133

REFERENCES

1. Preliminary Specifications for Inertial Guidance System of the Centaur, Convair-Astronautics Specification 55-04000. (SECRET)

2. Vigness, I., Shock and Vibration, U.S. Naval Research Lab. Electrical Manufacturing June 1959.

3. Beckwith, H.M., Vibration Data on Atlas Series A Missiles, Space Technology Labs. Rpt. GM TR-0165-00480, 1958 (CONFIDENTIAL).

4. Douglas, D.G., Vibration Report on Tital Missile A-5, Space Technology Laboratories Report GM 40.2-548, 1959 (CONFIDENTIAL)

5. Vibration Data from Thor Missiles, Space Technology Laboratories Series of Memos, GM 40.2, 1958 (CONFIDENTIAL).

6. Vibration Data from Jupiter Missiles, Space Technology Laboratories Series of Memos GM 40.2, 1957 (CONFIDENTIAL).

7. Morrow, C.T., Muchmore, R.B., Shortcomings of Present Methods of Measuring and Simulating Vibration Environments, Journal of Applied Mechanics Sept. 1955.

8. Whitney, C.A., The Structure of the High Atmosphere, IGY Satellite Report No. 8, June 1959.

9. Pioneer IV Data Alters Van Allen Theory, Aviation Week, May 11, 1959.

10. Van Allen, J.A. and Frank, L.A., Radiation Measurements to 658,300 Km with Pioneer IV, University of Iowa, 1959.

11. Simons, Jr., J.C., *Simulation of Environmental Conditions in Near Space*, ARS Paper 984-59, November 1959.

12. Beard, D.B., *Interplanetary Dust and Erosion Effects*, A.A.S. Preprint No. 58-23, August 1958.

13. Whipple, F.L., *The Meteoritic Risk to Space Vehicles*, Vistas in Astronautics, Pergamon Press, 1958.

14. *Results of Scientific Investigations made by Soviet Sputniks and Cosmic Rockets*, ARS Journal, January 1960.

15. Manning, E., Dublin, M., *Satellite Micrometeorite Measurements*, IGY Satellite Report No. 3, May 1958.

16. Hawkins, G.S., Whipple, F.L., *The Meteoric Influx*, 5th Sagamore Ordnance Materials Research Conference, 1959 Syracuse University.

17. Watson, F.G., *Between the Planets*, Harvard University Press, 1956.

18. *A Recoverable Interplanetary Space Probe*, MIT Instrumentation Laboratory Report R-235, July 1959.

19. *Papers on the Solar Constant*, Vol. 3e No. 3, 1958, Smithsonian Contributions to Astrophysics.

20. Friedman, H., *Solar X-rays and the Ionisphere*, Vistas in Astronautics, 1958.

21. Forsythe, W.E., *Smithsonian Physical Tables*, 9th Edition, 1954.

22. *Space Radiation as an Environmental Constituent*, Radiation Effects Information Center, January 1960, Battell Memorial Institute.

23. Gazley, Jr., C., *Deceleration and Heating of a Body Entering a Planetary Atmosphere from Space*, Vistas In Astronautics, 1958.

24. Chapman, R., *An Approximate Analytical Method for Studying Entry into Planetary Atmospheres*, NACA TN 4276 (1958).

25. Kuiper, G.P., *The Atmospheres of the Earth and Planets*, University of Chic. Press, 1949

60WWRN 5337

26. Struve, O., The Atmospheres of Jupiter and Saturn, Sky and Telescope, August 1954.

27. Russell, Dugan, Steward, Astronomy - Vol I, Ginn and Co. 1945.

28. Handbook of Chemistry and Physics, Chem. Rubber Publishing Co., 38th Edition.

29. Yarwood, J., High Vacuum Techniques, 3rd Edition, 1956.

30. Guthrie, A., Wakerling, R., Vacuum Equipment and Techniques, McGraw-Hill, 1949.

31. Clauss, F. J., Surface Behavior in Near Space, ARS Paper No. 985-59 (1959).

32. Utilization of the Surface Tension of Liquid Metals in Making High Vacuum Seals, AVS Symposium, 1957.

33. Lubrication Problems in Space Vehicles, AAS Annual Meeting, December 1958.

34. Achter, M. R., The Effect of Atmosphere on Creep and Fatigue at Elevated Temperature, 5th Sagamore Ordnance Materials Research Conference, Syracuse University, 1958.

35. Keenan, M. W., Selection of Alloy Tubing for Glass Sealing, Electronic Design, October 14, 1959.

36. Hamilton, J., Lewis, J., Denny, J., Physical Chemistry of Gallium-Indium Alloys, University of Utah.

37. The Friction and Lubrication of Solids, Bowden and Tabor, 1954.

38. Attlee, Wilson, Filmer, Journal of Applied Physics, 1940.

39. Mechanical Engineers Handbook, L. S. Marks 5th edition.

40. Scully, C. N., Effects of Meteorites on Materials and Simulation Testing, 5th Sagamore Ordnance Materials Research Conference, Syracuse University, 1959.

41. Partridge, W. S., High Velocity Impact, 5th Sagamore Ordnance Materials Research Conference, Syracuse University, 1958.

60WWRN - 5337

42.   Petterson, H., Cosmic Spherules and Meteoritic Dust,
       Scientific American, February 1960.

43.   Micrometeorites, High Velocity Impact Studies, and
       Problems of Space Travel Relating to Particle Impact,
       JPL/CIT Astronautics Information Literature Search #143
       October 1959.

44.   Calkins, V. P., Radiation Damage to Non-metallic
       Materials, GE-ANP Department, Cincinnati, Ohio, 1954.

45.   Bolt, R. O., Carroll, J. G., Wright, J. R., Radiation
       Resistant Lubricants - Their Development and Status,
       California Research Corp. Richmond, California, 1954.

46.   Nisbet, T. R., How Radiation Affects Electronic Equip-
       ment, Electronic Equipment Engineering, May 1959.

47.   Hess, R. E., Badertscher, R. F., Space Radiation as an
       Environmental Constituent, REIC-19, Bottelle Memorial
       Institute, January 1960.

48.   Schmidt, E., Radiation Effects on Metals. [*]

49.   Dvorak, H. R., Radiation Effects on Non-Metals. [*]

50.   Pollard, E. C., Davidson, W. L., Applied Nuclear
       Physics, 2nd Edition, 1951.

51.   Harwood, J. J., Effects of Radiation on Materials,
       1st Edition, 1958.

52.   Lapp, R. E., Andrews, H. L., Nuclear Radiation Physics,
       2nd Edition, 1954.

53.   A Recoverable Interplanetary Space Probe, MIT Instru-
       mentation Laboratory Report R-235, 1959.

54.   Farkass, I., Vanderschmidt, G. F., The Production
       of Ultra-high Vacuum in Metal System larger than 1000
       Liters, National Research Corporation, Cambridge,
       Massachusetts. [**]

---

[*] Materials in Space Environment Proceedings of 5th Sagamore
Ordnance Materials Research Conference, Syracuse University,
1959.

[**] Reference 54 will appear in the Proceedings of the 6th National
Vacuum Symposium (1959) sponsored by the American Vacuum
Society.

55. Simons, J. C., _An Ultra-high Vacuum Chamber for Space Simulation_, National Research Corporation, Cambridge, Massachusetts.[*]

56. Behrndt, K. H., _A Demountable Ultra-high Vacuum Glass System and its Components_, International Business Machines, Federal System Division, Kingston, New York.[*]

57. Klopfer, E., _Properties of A Small Titanium-Ion-Pump_, Allegemline Deutsche Phillips Industries, Aachen, Germany.[*]

58. Ames, I., Christensen, R. L., _Some Studies of Getter-Ion Pumped Vacuum Systems_, International Business Machines, Poughkeepsie, New York.[*]

59. Ullman, J. R., _A Large Metal System Permitting Low Base Pressures_, University of California Radiation Laboratory, Livermore, California, (1957 AVC Symposium).

60. Lusser, R., _Testing to Specified Limits versus Testing to Failure_, Redstone Arsenal, Huntsville, Alabama, 1956.

61. Greene, K., _What is Reliability_, Electronic Equipment Engineering, January 1960.

62. Pieruschka, E., _Mathematical Foundations of Reliability Theory_, Redstone Arsenal, Huntsville, Alabama, 1958.

63. Campbell, C. C., _Atlas Reliability Program Yields Improved Components_, Aero Space Engineering, December 1959.

64. Lusser, R., _A Study of Methods for Achieving Reliability of Guided Missiles_, Redstone Arsenal, Huntsville, Alabama, 1950.

65. Krohn, C. A., _Reliability Analysis Techniques_, Proceedings of the IRE, February 1960.

---

[*]References 55, 56, 57, and 58 will appear in the Proceedings of the 6th National Vacuum Symposium (1959) sponsored by the American Vacuum Society.

CHAPTER 7

SUBLIMATING-SOLID TORQUING JET

by

Kenneth Nordtvedt

March 1960

141

TABLE OF CONTENTS

LIST OF ILLUSTRATIONS

CHAPTER 7

SUBLIMATING-SOLID TORQUING JET

Introduction

For a space vehicle to perform some of its vital functions spatial attitude must be controlled. The space vehicle navigation and attitude control system under study performs changes in vehicle orientation by the rotation of mobility flywheels. The need for incorporating torquing jets in the attitude control system is not for immediate change of orientation of the vehicle. Rather, the jets perform the following auxiliary but necessary functions.

Over extended periods of time the spacecraft will acquire a total net angular momentum from such sources as micrometeorites, gravitational torques, and torques resulting from thrust misalignment of the main rockets. Now all of this angular momentum can be absorbed by the flywheels, leaving the orientation of the vehicle in inertial space fixed in any desired orientation. However, we must keep the angular velocity of the flywheels at a minimum for the following important reasons. First, wheels must never saturate their angular velocity capacity. Second, we want to minimize the energy requirements needed to operate the flywheels. And finally, we want to minimize the turning of the flywheels in order to maximize their operating life and reliability. So the purpose of the torquing jets will be to remove the angular momentum from the mobility flywheels. *

-----

* Refer to Chapter 3 for a detailed discussion of the integration of the torquing jets with the rest of the attitude control system.

There are several types of controlled torquing systems which could be considered---gravitational torques, aerodynamic and solar pressure torques, * and jets of one type or another.

Gravitational torques can easily be ruled out because the magnitudes of these torques in interplanetary space are minute. For example, consider a simple dumbbell in the gravitational field of a celestial body with mass M and at a distance R. (A dumbbell shape is the optimum shape of a body utilizing gravitational torques.) The equation for the oscillation of the dumbbell about its equilibrium orientation of alignment with the radial direction is

$$\ddot{\theta} + \frac{2\gamma M}{R^3}\theta = 0,$$

where γ is the gravitational constant. This gives us a characteristic frequency of

$$\omega = \sqrt{\frac{2\gamma M}{R^3}} .$$

Taking the conditions of deep space where the sun's gravitational field predominates, this frequency becomes of the order of one cycle per year which is much too long for our consideration.

There are two principle types of pressures being applied to the vehicle in interplanetary space. The electromagnetic radiation from the sun exerts a pressure on a reflecting surface of $2E/c$ dynes/cm^2 where E is the energy flux in ergs/cm^2-sec, and c is the velocity of light. The aerodynamic pressure of a vehicle moving with velocity v through a gas of density ρ is $1/2\ \rho v^2$. Consider a space vehicle in deep space at the earth's distance from the sun. Then we have the following approximate values for the constants.

Solar energy flux	$E \approx 1.3 \times 10$ ergs/cm^2-sec,
Density of gas (assuming 1000 particles per cm^3 and all particles protons)	$\rho \approx 10^{-21}$ gm/cm^3,
Velocity of vehicle with respect to the gas assuming gas at rest in solar system.	$v \approx 3 \times 10^6$ cm/sec.

*M. I. T. Instrumentation Lab report R-235 discusses the solar vane method of angular momentum trimming.

This results in a solar radiation pressure of $P_s = 8 \times 10^{-5}$ dynes/cm^2 and an aerodynamic pressure of $P_a = 5 \times 10^{-9}$ dynes/cm^2. So we see that of external pressures, solar radiation pressure is the dominant one. The solar vane concept originally proposed in Ref. 2 is limited by the necessity of protruding reflecting vanes. This requires an integrated design of the solar vanes into the total spacecraft which greatly inhibits the flexibility of our guidance system.
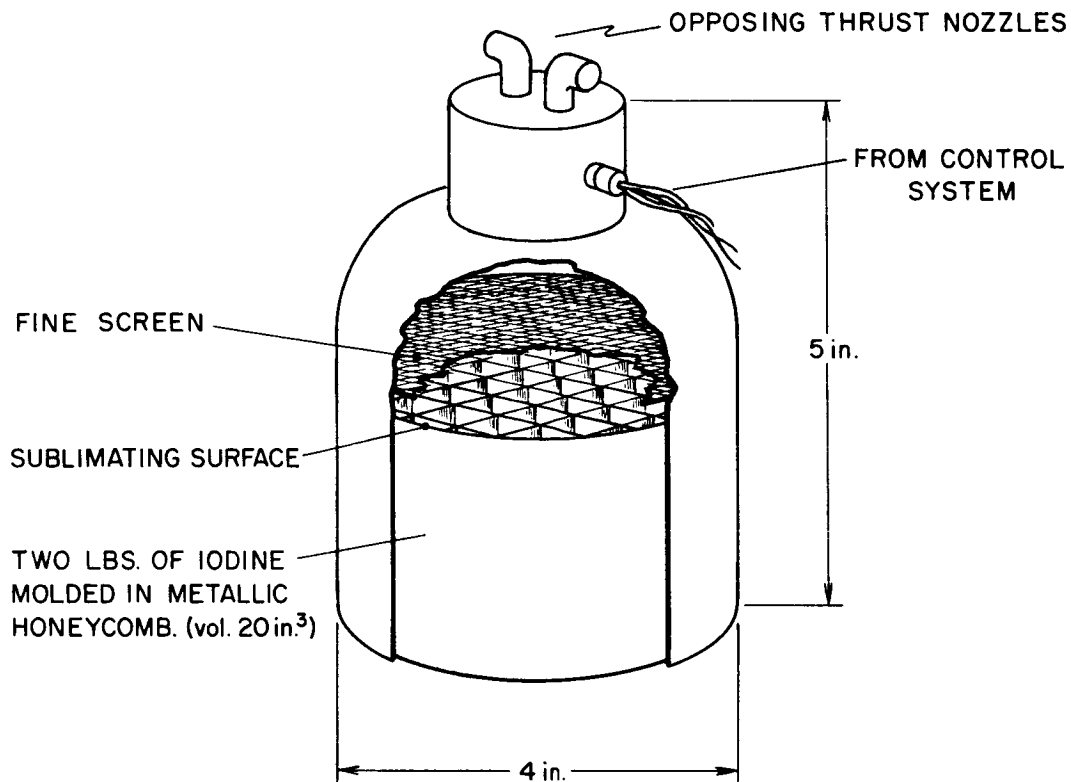
The most versatile of the possible systems uses torquing jets. The possible types of jets are chemical propellant rockets, non-reacting gases stored at high pressure, a liquid which is vaporized by use of vehicle energy, or a sublimating-solid which will generate the propulsive vapors. It is the purpose of this chapter to show the feasibility of the sublimating-solid system and why it is favored over the other competing jet systems.

I. The Sublimating-Solid Jet

The fact that several solid materials possess an appreciable vapor pressure at the typical space vehicle temperatures contemplated makes the sublimating-solid jet possible. And as we know, the rate at which a material will vaporize is proportional to its vapor pressure. If a solid is placed in a chamber which has an outlet into the vacuum, thrust can be developed by the escape of the sublimated vapors through the outlet. Proper orientation of the outlet results in the desired trimming torques.

The sublimating-solid torquing jet system is shown in detail in Fig. 7-1. The solid iodine* is imbedded thermally in the vehicle in order to maintain it at the vehicle temperature. The solid iodine is molded in a metallic honeycomb for two reasons. First, the metallic honeycomb aids heat conduction to the sublimating surface. This prevents the temperature of the

---

* The solid iodine is used in this report for illustration. It is one of several solids which are under consideration. See Section V of this chapter.

OPPOSING THRUST NOZZLES

FROM CONTROL SYSTEM

5 in.

FINE SCREEN

SUBLIMATING SURFACE

TWO LBS. OF IODINE MOLDED IN METALLIC HONEYCOMB. (vol. 20 in.^{3})

4 in.

OVERALL DIMENSIONS 4"x 4"x 5"

(NOTE: This is one geometry; the shape of the device can be changed to conform to most any configuration. However the total system volume of 80 in.^{3} will probably be relatively constant.)

Fig. 7-1 Detailed view of the sublimating-solid jet.

sublimating surface from dropping appreciably during operation. Also, the metallic honeycomb structurally strengthens the relatively weak solid iodine.

A fine screen is included in the chamber to prevent any crumbled pieces of solid from reaching and clogging the valves.

On command from the control system, the appropriate valve is opened and the sublimated vapor escapes through one of the nozzles producing the desired thrust. The chamber pressure falls until the rate of sublimation balances the rate of vapor flow out the nozzle. Upon ending the thrust period, the valve is closed, the chamber pressure rises to the vapor pressure of the solid, and sublimation ceases.

Let us summarize the more significant performance parameters, before discussing in detail their theory and derivation. To illustrate the magnitudes involved in the system, we couple it to a typical vehicle. Consider a vehicle with the following dimensions pictured in Fig. 7-2.
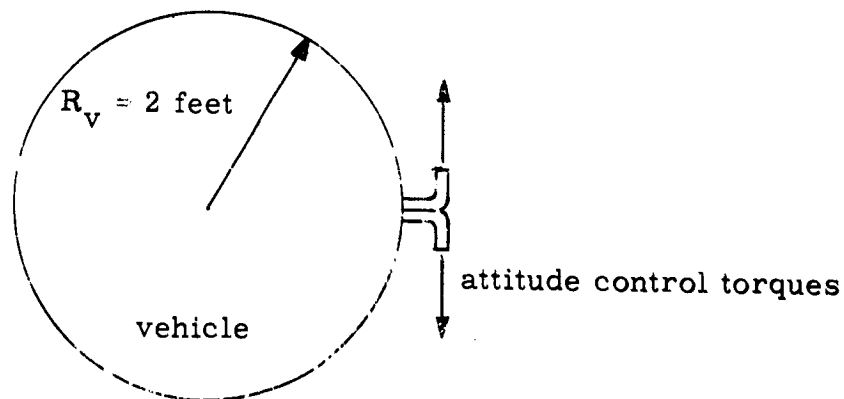
Fig. 7-2 Vehicle-jet configuration.

Mass	$M_v = 1000$ pounds
Shape	Roughly spherical
Radius	$R_v = 2$ feet
Moment of Inertia	$I_v = 48$ slug-ft^2
Vehicle Temperature Range	$T = 53^{\circ}F$ to $92^{\circ}F$

We mount the thrust jets so they have a maximum lever arm of 2 feet.

Sublimating-Solid	iodine
Nozzle Throat Area	1 cm^2
Weight of Iodine	2 pounds
Weight of valves	1 pound
Weight of casing	1 pound
Total Weight	4 pounds

Below is tabulated the performance of the system at the two extreme temperatures assumed for the vehicle.

	$53^{\circ}F$	$93^{\circ}F$
Thrust	72 dynes	420 dynes
Torque	4300 dyne-cm	25000 dyne-cm
Time required to remove .1/sec* from the vehicle assumed on previous page	6.2 minutes	1.1 minutes
Heat flow to sublimating iodine	22 calories/min	110 cal/min
Total Angular Velocity Change Capacity For Two Pounds of Iodine	1 radian/sec	

* .1°/sec is a typical angular velocity removal magnitude. See Chapter 4 for a discussion of this.

II. Derivation of the Sublimation and Flow Rates

We are interested in deriving the formula for the equilibrium thrust and vapor flow rate when the jet is operating. As seen in the diagram, this equilibrium rate is obtained by equating the rate of sublimation of solid into vapor to the rate of vapor flow out the nozzle.
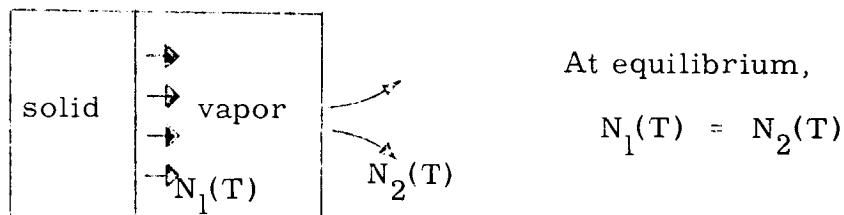

At equilibrium,

$$N_1(T) = N_2(T)$$

Fig. 7-3 Steady state condition of system.

Our nozzles will be non-expansive. This sacrifice in specific impulse is made to minimize the recombination problem of the vapors. This will be discussed later in Section III, B of this chapter.

All of our flow rate calculations will be made on a kinetic theory approach. This viewpoint is strictly valid when the nozzle diameter is much smaller than the mean free path of the vapor molecules. We are in the borderline region where the nozzle diameter is of the same order of magnitude as the molecular mean free path. The slight resulting errors introduced are not serious, and indeed this view gives a more accurate picture of the flow than the isentropic flow equations normally used for nozzle flow.

The mean free path of the gas molecules is obtained by

$\lambda \approx 1/4n\sigma$ where n is the number of molecules/cm^3

σ is the cross section of the molecules

Now $n = P/kT = 3 \times 10^{15}$ molecules/cm^3 at .1 mm of pressure

300°K temperature

$\sigma = 5 \times 10^{-16}$ cm^2 for the iodine molecule, I_2,

Then $\lambda = 0.16$ cm, which is compared to 1 cm for the nozzle diameter.

Consider a gas of molecular weight M and temperature T. $n(v)$ is the Boltzmann speed distribution of the molecules at temperature T. Consider the infinitesimal volume element pictured in Fig. 7-4:
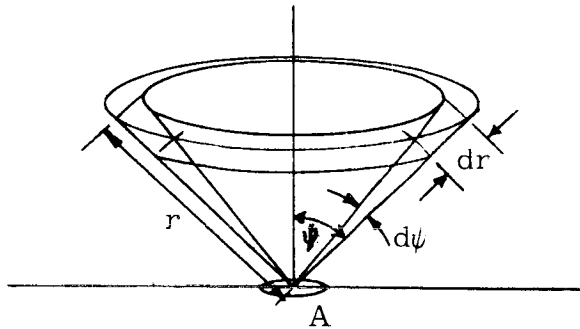
$$dV = 2\pi r^2 \, dr \, \sin \psi \, d\psi.$$

Fig. 7-4   Volume element.

Now consider a surface element at the origin of the coordinate system. The number of molecules impinging on that surface element per unit time of velocity v and originating in our volume element is

$$dN = \frac{A \cos \psi \, n(v) \, dV}{4\pi r^2}.$$

Integrating over all volume elements and molecular speeds we get the total impingement rate.

$$N = \int_0^\infty \int_0^v \int_0^{\pi/2} A \, n(v) \, 2\pi r^2 \, dv \, \sin \psi \, d\psi \frac{\cos \psi}{4\pi r^2} \, dr = \frac{A}{4} \int_0^\infty v \, n(v) \, dv.$$

Boltzmann's distribution is $n(v) = (\frac{8M^3}{\pi R^5 T^5})^{1/2} P v^2 e^{-\frac{Mv^2}{2RT}}$,

so $N = A \sqrt{\frac{M}{2\pi RT}} P$; where P is the gas pressure, R is the gas constant. Now if $P = P_v$, the vapor pressure of the solid, this

152
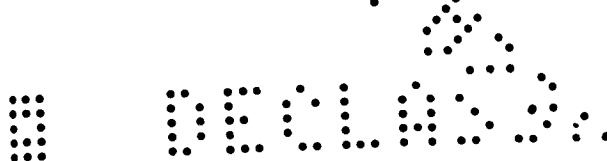
rate of impingement of the vapor onto the surface is just balanced by the rate of sublimation of the solid into vapor. Therefore by setting $P = P_v$, we can call the rate N_o the sublimation rate of the solid into a vacuum.

$$N_o = A_s \sqrt{\frac{M}{2\pi RT}} \, P_v(T) \, ,$$

A_s = area of sublimating solid. However, if the chamber is at a pressure P rather than being a vacuum, the net rate of sublimation is

$$N_1(T) = A_s \sqrt{\frac{M}{2\pi RT}} \, (P_v(T) - P).$$

If the chamber is at pressure P and if the nozzle outlet to the vacuum has area A_h, the rate at which the vapor flows out the nozzle is given by the rate of impingement of the molecules on an area A_h in our kinetic theory approximation. This rate is then given by

$$N_2(T) = A_h \sqrt{\frac{M}{2\pi RT}} \, P.$$

Our equilibrium condition is with $N_1(T) = N_2(T)$, so

$$A_s \sqrt{\frac{M}{2\pi RT}} \, (P_v(T) - P) = A_h \sqrt{\frac{M}{2\pi RT}} \, P \quad \text{or}$$

$$N_1(T) = N_2(T) = \sqrt{\frac{M}{2\pi RT}} \, P_v(T) \, \frac{A_h A_s}{A_h + A_s} \, .$$

A measure of the thrust of the jet is obtained by kinetic theory, assuming no expansion and cooling of the gas in the nozzle. Each molecule which escapes from the chamber has an axial component of momentum, $mv \cos \psi$, so the total thrust is

$$F = \int_0^\infty \int_0^v \int_0^{\pi/2} mv \cos \psi \, n(v) \, \frac{2\pi r^2 dr}{4\pi r^2} \sin \psi \, d\psi \, A_h \cos \psi \, dv;$$

$$F = 1/2 \, P \, A_h = \frac{1}{2} \frac{A_h A_s}{A_h + A_s} P_v(T).$$

The rate of heat consumption during the sublimation is $H_s(T) \, N_2(T)$, where $H_s(T)$ is the heat of sublimation of the solid. Clayperon's thermodynamic equation for the heat of vaporization is used:[*]

$$H_s(T) = \frac{RT^2}{M} \, \frac{d \ln P_v(T)}{dT} \, .$$

From this we get the rate of heat absorption

$$H = \sqrt{\frac{R}{2\pi M}} \; T^{3/2} \, P_v(T) \; \frac{d \ln P_v(T)}{dT} \; \frac{A_s A_h}{A_s + A_h} \, .$$

We couple this system to a vehicle of moment of inertia I_v with the jet operating through a lever arm of length R_v . Then the following table summarizes all of the parameters of the system.

Thrust $F = \dfrac{1}{2} \dfrac{A_h A_s}{A_h + A_s} P_v(T)$

Torque $\tau = \dfrac{1}{2} R_v \dfrac{A_h A_s}{A_h + A_s} P_v(T)$

Required amount of sublimating solid to give total angular velocity correction ω

$$M = \frac{2 I_v \omega}{R_v} \sqrt{\frac{M}{2\pi RT}}$$

Time required for angular velocity correction $\Delta \omega$

$$t = \frac{2 I_v \Delta \omega}{\dfrac{A_h A_s}{A_h + A_s} P_v(T)}$$

Rate of heat absorption

$$H = \sqrt{\frac{R}{2\pi M}} \; \frac{A_s A_h}{A_s + A_h} \; T^{3/2} \, P_v(T) \; \frac{d \ln P_v(T)}{dT}$$

----

[*]Chemical Principles, Noyes and Sherill, 2nd Edition, Page 213.

The vapor pressure and rate of change of vapor pressure with temperature for iodine is given in Fig. 7-5 for reference. The above formulas were used to give the magnitudes quoted in Section II. We assumed that the sublimating solid area was much larger than the nozzle area, so

$$\frac{A_s A_h}{A_s + A_h}$$

reduces to A_h.

III. Design Considerations

A. Heat Conduction to Sublimating-Solid Surface

The heat flow from the vehicle into the sublimating-solid surface is a parameter which must be considered in our design. Heat conductive paths must be designed so that the required heat can flow from the immediate surroundings of the sublimating-solid without an appreciable temperature gradient during maximum sublimation rates and consequently maximum heat absorption rates.

During any given operation removing $.1^{\circ}$/second angular velocity from the vehicle we will require a total of 120 calories heat for sublimation. If we have about one pound of aluminum surrounding the solid, 120 calories represents the heat capacity of that aluminum when heated $1.3^{\circ}C$. So, indeed, we have no problem in finding sufficient thermal energy in the immediate vicinity of the sublimating-solid. The problem is conducting up to 110 calories/minute into the solid which will be required when the total 120 calories are delivered in 1.1 minutes at the higher vehicle temperature.

Using the well known heat conductivity equation
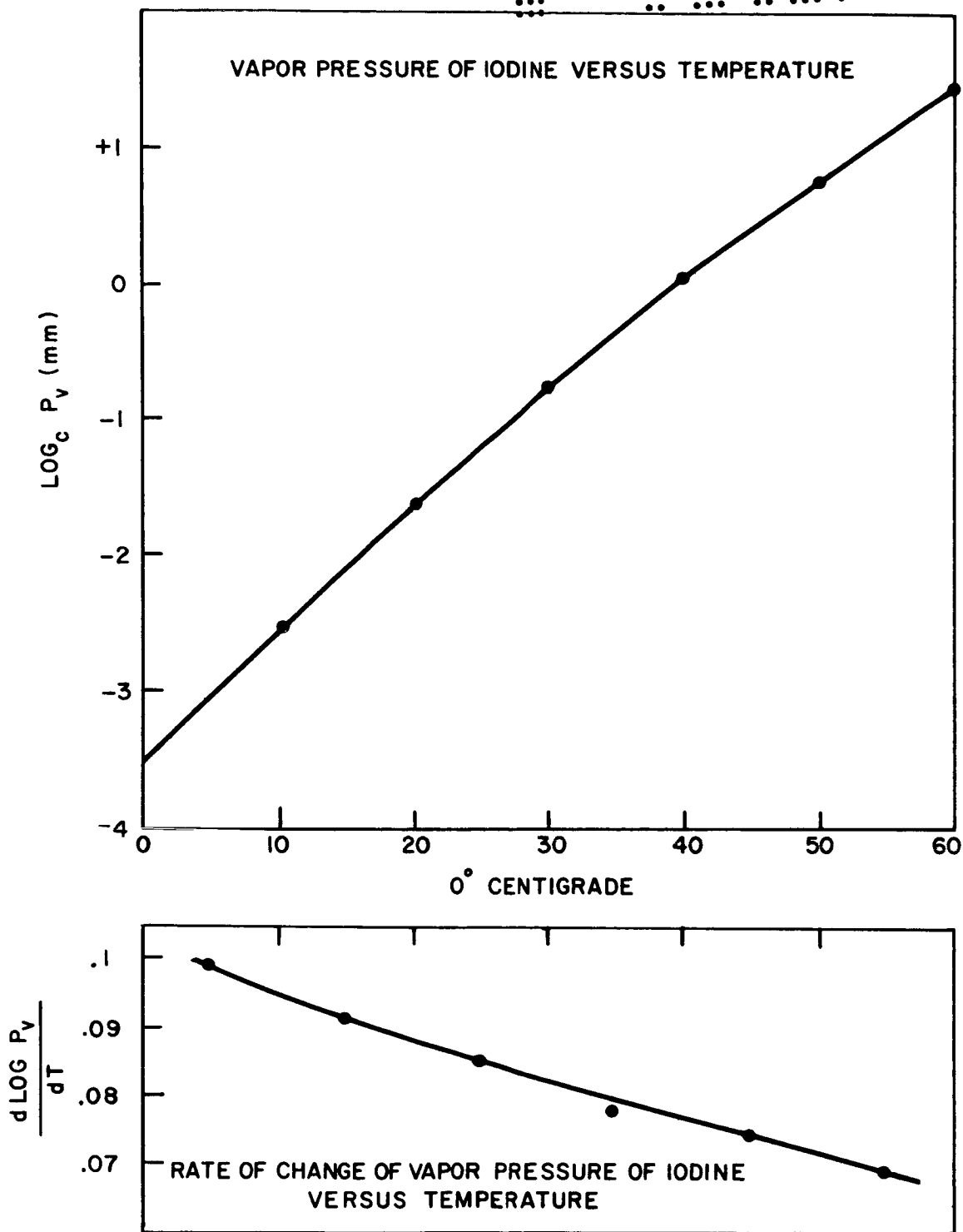
$$H = \sigma \, A/d \, \Delta T;$$

VAPOR PRESSURE OF IODINE VERSUS TEMPERATURE

RATE OF CHANGE OF VAPOR PRESSURE OF IODINE VERSUS TEMPERATURE

Fig. 7-5   Vapor pressure properties of Iodine.

156

A   =   cross section of heat conduction path,

d   =   length of heat conduction path,

σ =   heat conductivity (for solid iodine

           σ = .06 calories/cm-$^{\circ}$C-minute),

ΔT =   temperature drop along length;

and desiring to keep ΔT $\lesssim 5^{\circ}$C, we then note that our geometry must give an A/d ratio of about 400 cm. Clearly we cannot get A/d = 400 cm if the two pounds of iodine are molded in one solid cube. In that case A = 30 cm^2 and d = 2 cm, so A/d = 15 cm, which is much too small. However, a simple honeycomb of heat conductive metal such as aluminum molded in the iodine will satisfactorily serve as heat conducting paths.
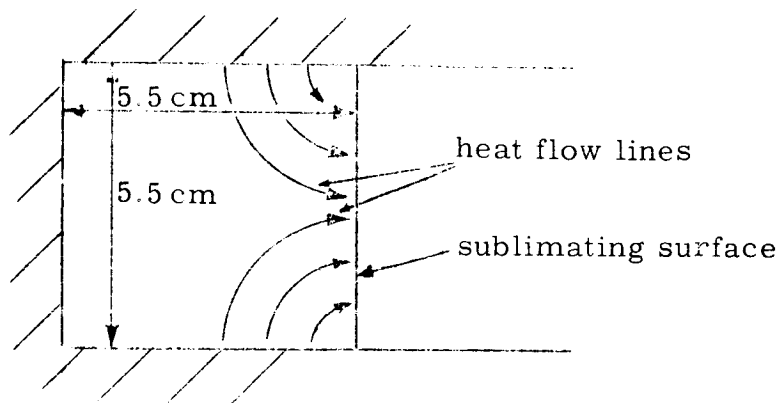
Fig. 7-6 Geometry of heat flow.

In the diagram, Fig. 7-7, we see that A = 90 cm^2 but d is only about .2 cm, so A/d = 450 cm, which is sufficient for our purposes. This design will permit 110 calories/minute heat transfer rate from the immediate surroundings to the surface of the sublimating-solid with less than a 5°C temperature drop.
This discussion is not intended to fix the above configuration as the best one, but only to show that some similar configuration
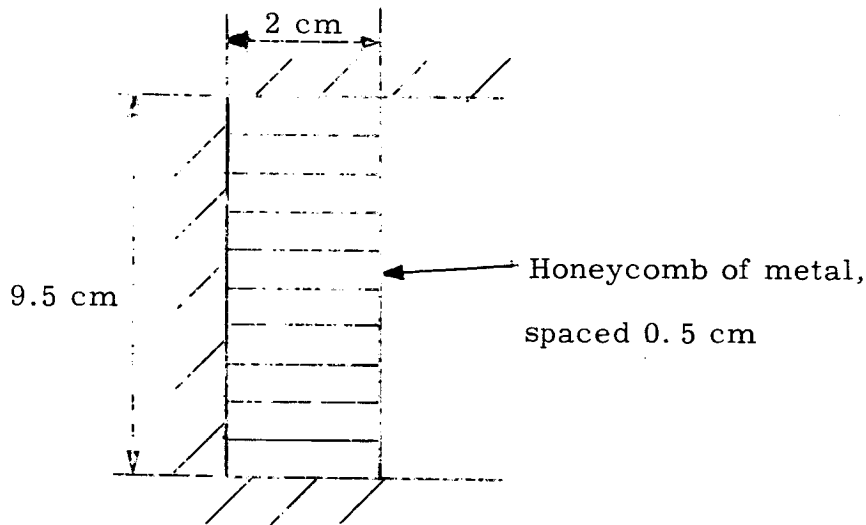
could meet the design requirement.

Fig. 7-7   Heat flow with addition of honeycomb.

B.   Recombination of Jet Gases

As propellant gases expand and consequently cool in the nozzle of a rocket, recombination and condensation of the gases can take place.   This is especially true when the gases have not been greatly superheated.   In general this recombination or condensation has two effects on the specific impulse of the rocket. The heat released in the recombination tends to increase the available kinetic energy of the gases, and therefore increases the specific impulse of the propellant.   However, the recombination also increases the mean molecular weight of the exhaust gas particles, and therefore tends to decrease the specific impulse of the propellant.

For most chemical rockets the liberated heat effect dominates and the specific impulse increases slightly.   However, for propellants such as steam or iodine vapor, the crucial reaction is the physical change of state from vapor to liquid or solid.

In these cases the condensation drastically reduces the specific impulse of the propellant. The condensation of steam has plagued researchers working on small steam attitude control jets. A very pertinent question is, will this same problem effect the performance of the sublimating-solid system?

Consideration of this problem has led us to use a non-expanding nozzle which should minimize the possibility of the vapor recondensing on the nozzle as it cools. If this does not prove sufficient, the addition of a very low-power heating coil in the nozzle will prevent any accumulation of the vapor on the nozzle. This system is aided by the very low pressures and mass flows through the nozzle. During operation the mass flow will range from .2 to 1 gram of vapor per minute. Although it remains to be checked by the testing of some prototype devices, it appears that this system will not have a serious recombination problem.

IV. The Possible Sublimating-Solids

In choosing the sublimating-solid for the system the following factors must be considered.

1. Reasonable vapor pressure at vehicle temperatures (about 10^{-3} mm to about 1 mm).

2. Non-toxicity, to facilitate human handling, designing, and pre-flight preparation.

3. Inertness to chemical change, to corrosiveness, or reaction with the other materials it comes in contact with.

4. A melting point appreciably above the expected extreme high temperature of the vehicle.

5. Resistence to crumbling over long periods of time in an environment of occasional vibrations.

Possible solids which we have found are listed below.

POSSIBLE SUBLIMATING SOLIDS

TABLE 7-1

Solid	Formula	Molecular Weight	Melt. Pt. $^{\circ}$C	Vap. Press at 20°C. mm	Spec. Grav.
d Camphor	$C_{10}H_{16}O$	152	178	.3	1.53
Iodine	I_2	253	113	.25	4.93
1245 Tetra-methylbenzene	$C_{10}H_{14}$	134	80	.10	1.60
Antimony Chloride	$Sb\ Cl_3$	228	73	.10	3.14
Napthalene (moth balls)	$C_{10}H_8$	128	80	.05*	1.58
Selenium Tetrachloride	$Se\ Cl_4$	221	170	10^{-2}*	3.8
Di hydro-decaborane	$B_{10}H_{14}$	122	99	10^{-2}*	0.94
Aluminum bromide	$Al\ Br_3$	267	97.5	$10^{-2}-10^{-3}$*	3.01
Gallium Chloride	$Ga\ Cl_3$	176	77	$10^{-2}-10^{-3}$*	2.47
Antimony Iodide	$Sb\ I_3$	503	164	$10^{-2}-10^{-3}$*	4.77
Aluminum Chloride	$Al\ Cl_3$	133	192	$10^{-3}-10^{-4}$*	2.44

*These values are only approximate. They were obtained by extrapolation of existing tables found in Handbook of Chemistry and Physics.

We have great flexibility in selecting the particular solid. The fixed performance quantity is the thrust of the jets. Because this is proportional to the product of pressure and hole area, we can use any sublimating-solid over a wide range of vapor pressures just by varying the opening size. Of course any solid must fulfill the other criteria.

Regardless of the choice of solid we must plan on the possibility of the solid crumbling. This has led to the following considerations. The solid might be solidified with steel wool or some other reinforcement, such as a honeycomb material which would serve the duel purpose of conducting heat. Otherwise a fine screen could be inserted in the chamber between the solid and the hole to the vacuum. This would prevent the clogging of the nozzle or possible loss of unsublimated solid material.

For this report we assume the use of iodine as our sublimating material. At this point we know more about the physical and chemical properties of iodine and it appears to be very satisfactory on all accounts. However, any future experimental program must include a thorough inspection of the other candidates too. The final choice of solid will rest on the experimental tests.

V. A Brief Discussion of Competitive Systems

A. The Stored Gas System

A very common system is one in which a gas is stored in a tank at very high pressures. On command this gas is released through a nozzle without chemical reaction or heating.

We consider a sperical tank of nitrogen gas. At vehicle temperature of about $300^{\circ}K$, the specific impulse of the gas expanded in a reasonable nozzle is about 75 seconds. In order to perform the same total angular velocity corrections as the iodine system discussed in this chapter we would need .3 pound of nitrogen gas. This, alone, is a saving of weight. But then

consider that in order to confine this gas to a reasonable size
(5 inch diameter tank) requires a gas pressure of 2000 p. s. i.
Such a tank weighs about 1 pound. The valves for this system
must be several magnitudes stronger than the ones for the low
pressure sublimating-solid system. Allowing 2 pounds for the
valves of this system brings the total weight up close to the
weight of the sublimating-solid system.

The saving of less than 1 pound is not justified when we
consider that it will be difficult to duplicate the reliability of the
low pressure sublimating system in the high pressure components
because of small orifices, etc. In extended interplanetary missions
reliability is of utmost concern. It is on these grounds that we
were led to the consideration of the low pressure sublimating
system.

B. The Steam-Jet System

Consider a steam-jet system in which water in the liquid
form is carried as propellant. We vaporize the water with
electrical heaters using the steam as the propellant gas.
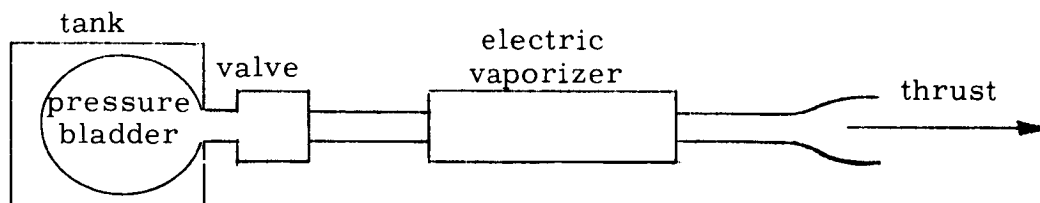
Fig. 7-8   Steam-jet system.

COWKRN · 5337

If we produce 500°K steam we acquire a specific impulse of about 127 seconds in a reasonable nozzle. To obtain the same total angular velocity correction capacity as the sublimating-solid system discussed in this chapter would require .2 pound of water. Each .1°/sec correction would consume about .5 watt-hour of electrical energy in the vaporizer (assuming .33 efficiency of the electrical heater). If we consider the weight of the tank, the pressure bladder, the valves, the electrical vaporizer, and the nozzle, we have a total system weight which is comparable to the sublimating-solid system.

This system has the disadvantage of being more complex and probably less reliable than our proposed sublimating system. Whereas these alternative systems appear to be feasible and in some cases might have a very small advantage in weight, their reliability does not appear to be comparable with that which could be obtained by the very low pressure sublimating-solid system. In order to obtain this superior reliability, these systems would need an overdesign calling for weights probably above that of our proposed system.

So even though the sublimating iodine system compares very unfavorably in specific impulse of the propellant (12 seconds for solid-sublimating iodine), it is favored upon examination of the systems taken as a whole. For these small systems we are considering the auxiliary equipment is as heavy or heavier than the propellant.

VI. Proposed Early Experimental Program

Several models of the proposed sublimating-solid system should be made and tested. In particular, the following questions must be answered by an experimental program.

1. The mass flow and thrust values as a function of temperature must be checked against the theory.

2.   The toxicity, reactive, corrosive, and crumbling properties of the various sublimating-solids should be determined. Safeguards against the clogging of the valves must be tested, such as the fine screens as discussed in Section II.

3.   If the thrust levels are as calculated, then no further investigation is necessary, but methods of combating recombination by slight heating of the nozzles might be necessary.

To measure the performance of this low pressure sublimating-solid system requires a vacuum chamber. The 4 foot diameter chamber at the MIT Instrumentation Laboratory easily meets this need.

The thrust of the device will be measured by mounting the system on a torsion pendulum and measuring the angular deflection.

The mass flow can be obtained by directly measuring the weight of the system before and after a run of a known length of time.

The above measurements will be made with the sublimating-solid at a known, regulated temperature.

Suppose we have two 100-dyne thrusts applied to a torsion bar apparatus sketched below.
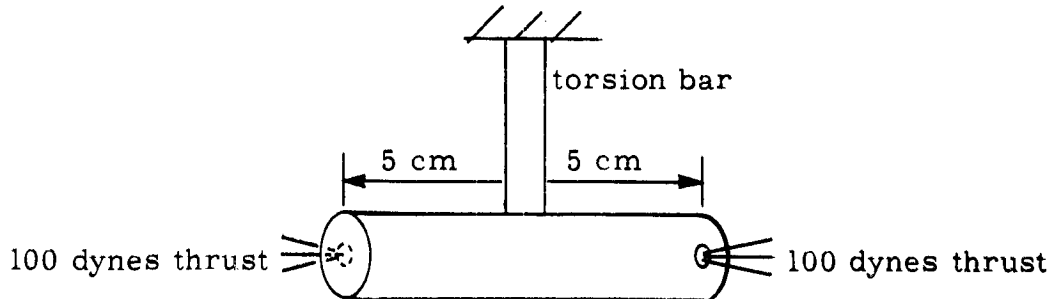
Fig. 7-9   Torsion bar apparatus.

With a lever arm of 5 centimeters, the torque is

$$\tau = 1000 \text{ dyne-cm.}$$

If we designed the torsion bar to twist through 3° under this torque, the twist could be accurately measured by a variety of methods, such as counter-turning the top of the torsion bar to compensate for this torque, or directly measuring the angular twist with optics.

$\sigma = \dfrac{\pi M r^4}{2l} =$ the torsion constant, where $r =$ radius of torsion bar,

$l =$ length of torsion bar,

$M =$ rigidity modulus of bar;

now

$\sigma \psi = 1000 \text{ dyne-cm}$ and $\psi = 1/20$ radian.

Therefore $\sigma = 2 \times 10^4 \text{ dyne-cm.}$

This can be obtained with a steel bar of 50 cm length and .6 millimeter diameter.

In practice, we would accurately determine σ by directly measuring the period of a torsion pendulum with a known moment of inertia attached to the end of the torsion bar. Then we simply have

$\sigma = I \omega^2$, where I is the known moment of inertia,

and ω is the measured frequency.

These tests will be run over a temperature range covering the entire potential vehicle temperature range, and should lead to a working design which can be integrated with the rest of the guidance system.

CHAPTER 8

PROPOSED ADVANCED DEVELOPMENT
PROGRAM, SCHEDULES, AND REQUIRED FUNDING

by

Milton B. Trageser

POWARN 5337

CHAPTER 8

PROPOSED ADVANCED DEVELOPMENT
PROGRAM, SCHEDULES, AND REQUIRED FUNDING

A letter has been prepared which outlines the necessary advanced development program, the schedules, and the required funding to bring the major guidance elements suggested in this report to a status where they can be considered for system integration in spacecraft as early as 1963. This letter is addressed to W. E. Giberson, Chief of Guidance Development, Jet Propulsion Laboratory, dated 18 March 1960, and is from M. B. Trageser, Group Leader, Instrumentation Laboratory. It is reproduced as part of this study report under separate cover from the technical material, according to the custom of the Laboratory concerning program, schedule, and funding information. This document is referenced as the R-273 Supplement.

60W/WRN - 5337

Unclassified Title

R-273

INTERPLANETARY NAVIGATION
SYSTEM STUDY

April, 1960

by

J. H. Laning, Jr.   J. M. Dahlen

R. Battin   R. J. Magee

P. Bowditch   K. Nordtvedt

M. B. Trageser   R. A. Scholten

R. L. Alonso   H. H. Seward

W. E. Toth

Unclassified Title

R-273

SUPPLEMENT

INTERPLANETARY NAVIGATION

SYSTEM STUDY

April, 1960

by

J. H. Laning, Jr.	J. M. Dahlen
R. Battin	R. J. Magee
P. Bowditch	K. Nordtvedt
M. B. Trageser	R. A. Scholten
R. L. Alonso	H. H. Seward

W. E. Toth

DECLASSIFIED

Supplement

Unclassified Title

R-273

INTERPLANETARY NAVIGATION SYSTEM STUDY

by

J. H. Laning, Jr.	J. M. Dahlen
R. Battin	R. J. Magee
P. Bowditch	K. Nordtvedt
M. B. Trageser	R. A. Scholten
R. L. Alonso	H. H. Seward

W. E. Toth

April, 1960

INSTRUMENTATION LABORATORY
MASSACHUSETTS INSTITUTE OF TECHNOLOGY
CAMBRIDGE 39, MASSACHUSETTS

Approved by: *Roger B Woodbury*
Associate Director

DECLASSIFIED

ACKNOWLEDGEMENT

TABLE OF CONTENTS

Supplement (separately bound)

Blank
p. 4

CHAPTER 8

PROPOSED ADVANCED DEVELOPMENT
PROGRAM, SCHEDULES, AND REQUIRED FUNDING

INTRODUCTION

The attached letter outlines the necessary advanced development program, shcedules, and the required funding to bring the major guidance elements suggested in the study presented in the first volume to a status where they can be considered for system integration in space craft as early as 1963. The program, schedule, and funding information is presented as part of this study report under separate cover from the technical material according to the custom of the Laboratory.

18 March 1960

Jet Propulsion Laboratory
California Institute of Technology
4800 Oak Grove Drive
Pasadena 3, California

Attention: W. E. Giberson, Chief
              Guidance Development

Dear Gene:

This letter attempts to outline the advanced development program for interplanetary navigation and control which we discussed in our telephone conversation of March 7, 1960. I believe that it contains the information you requested. It should be understood that this is a budgetary planning estimate rather than a proposal, since it has not been presented to the M. I. T. administration.

The M. I. T. Instrumentation Laboratory is interested in undertaking an advanced development program in interplanetary navigation and control. The program outlined below is designed to participate in the development of guidance and control equipment for use in space craft which are injected into space by Centaur vehicles starting in 1964.

Before outlining the program, it is necessary to develop the criteria on which the program is based. First, it can be anticipated that interplanetary space craft within the domain of Centaur payloads and within the time period under consideration will probably conduct their missions by using one or a combination of the following operations: 1) the atmospheric injection of an aerodynamic vehicle on a trajectory of some specified maximum acceleration for landing on the planet; 2) the injection of

the space craft into satellite orbit about the planet, more or less accurately; 3) the accurately guided passage of the space craft near the planet, perhaps for effective reconnaissance; 4) the accurately guided passage of the space craft near the planet with its later return to the earth or its vicinity for the landing of a re-covery capsule or for the communication of large quantities of stored data at short range.

Preliminary analysis indicates that many probable guidance and control requirements for the above operations can very likely be met by a guidance and control system which would weigh signi-ficantly less than 100 pounds and require less than 2 cubic feet. The systems could be packaged in guidance and control canisters which could be used as parts of complete space craft for instru-menting various missions through the several operations mentioned above. These systems would be similar except with respect to the program and the data in the non-erasable storage of the digi-tal computer.

The development program for the realization of such a system or for the perfection of the components and techniques from which it can be quickly synthesized can be resolved into the following overlapping phases: Phase I - Feasibility Study; Phase II - Preliminary Design; Phase III - Breadboard; Phase IV - **Prototype; and Phase V - Fabrication, Programming, and Test** of Flight Hardware. Each of these phases involves integrated effort in the following categories: Category I - Theoretical Work, Orbits and Navigation; Category II - Analysis of Hardware and Its Operation as Part of Space Craft; Category III - Digital Com-puter Development; Category IV - Other Component Developments, i.e., space sextant, flywheels, gyros, electronic circuits, etc.; Category V - System Engineering, i.e., making the components work together; Category VI - Long Life, Reliability, and Environ-ment Tests.

        We would like to participate in the JPL interplanetary space
craft program through significant activity in the above development
program. It is not reasonable at this time, however, to attempt
to outline the program Phases I through V because of the present
uncertainties in space craft missions, configurations, and opera-
tion. But it is reasonable to undertake Phases I through the middle
of Phase IV with a very general guide from you on these questions.
In so doing, we would intend to supplement your activities rather
than parallel them by establishing good liaison between JPL and MIT
counterparts and avoiding redundancy.

        Now, assuming that our program would allow activities in
Categories I through VI above, I would like to outline the program,
schedules, and budgetary estimates. I will further assume that it
is in the intent of the program Phases I through the middle of Phase
IV to lay a good foundation in interplanetary navigation and control
rather than concentrate on a specific piece of flight hardware; how-
ever, we would hope that future circumstances would permit our
strong participation in Phase V also.

        Now, I will consider each category above and identify the
activity within this category according to phase. I will associate
anticipated dates and required funding with the phases.

CATEGORY I - THEORETICAL WORK - ORBITS AND NAVIGATION

        Phase I - Feasibility Study - Period to End of NASA Study
                  Nearly complete.

        Phase II - Preliminary Design - April 1, 1960 to August 15,
                  1960. Work nearly complete for round trip and
                  planetary impact operations. Planetary satellite
                  and near passage operations should be organized
                  into a consistent presentation. The compatibility
                  of the several operations with the single guidance
                  approach, instrument accuracies, and operation
                  speeds will be firmly established.

Phase III - <u>Breadboard - July 1, 1960 to June 30, 1961</u>
Navigation mathematics will be formulated in detail and tested using several sets of assumed specifications for each of the several operations. This will involve a considerable extension of the Phase II work. The optimum method for obtaining and using navigational information and the amount of computation and stored data of one sort or another will be established.

Phase IV - <u>Prototype - January 1, 1961 to June 30, 1962</u>
That part of the navigation problem to be solved aboard the space craft will be programmed for the type of computer under consideration. This will result in a good specification of the storage and computation ability for the prototype computer and will indicate load on the data link to earth resulting from navigational requirements. This work also includes developing methods for simple handling of small effects in the navigation, such as the aberration of light.

Required funding for this category is as follows:

April 1, 1960 - June 30, 1960	$ 25,000
July 1, 1960 - June 30, 1961	145,000
July 1, 1961 - June 30, 1962	150,000
Total	$ 320,000

CATEGORY II - ANALYSIS OF HARDWARE AND ITS OPERATION AS PART OF SPACE CRAFT

Phase I - <u>Feasibility Study</u> - Complete except for continued examination of new schemes as they occur throughout program.

9

Phase II - <u>Preliminary Design - April 1, 1960 to August 15, 1960</u>

This involves a variety of problems including dynamics of controlling attitude of space craft having large difference in moments of inertia, speeds required of equipment for various operations, etc.

Phase III - <u>Breadboard - July 1, 1960 to March 31, 1961</u>

Components for various space craft sizes and operations will be scaled to evolve the characteristics desired in the prototype components. The selection of specific parameters for equipment will be made.

Phase IV - <u>Prototype - April 1, 1961 to June 30, 1962</u>

All analytical work required to develop manner in which the selected prototype components will operate several assumed space craft will be worked out. Methods of simulation will be studied.

Required funding for this category is as follows:

April 1, 1960 - June 30, 1960	$ 10,000
July 1, 1960 - June 30, 1961	60,000
July 1, 1961 - June 30, 1962	80,000
Total	$ 150,000

CATEGORY III - DIGITAL COMPUTER DEVELOPMENT

Phase I - Feasibility Study - Already complete. Feasibility of storage method and circuits have been experimentally demonstrated.

Phase II - <u>Preliminary Design - April 1, 1960 to August 15, 1960</u>

This includes additional logical design work tailored toward space craft computers. Also a computer presently under construction (Model

1A) on another Instrumentation Laboratory program will be completed. This computer is a breadboard for basic circuit development and it has very simple logic and a 256-word storage of 12 bits each. This effort is common to a computer development program for space craft or for missiles. The funding estimates given below do not cover this breadboard effort.

Phase III - <u>Breadboard - April 1, 1960 to March 31, 1961</u>

It can be reasonably assumed that the large effort and funding required for this phase will be supplied by another laboratory program to develop the computer for an application other than space craft. Our missile programs are expected to carry out the following steps which are in some respects common to those required for the development of space craft computers as well as missile computers.

Computer 1B is physically distinct from 1A described above but is essentially the same computer with extra logic added for input-output (counters, interrupt circuitry, possible punched paper type input). This computer could control a flywheel or some other simple accessory in addition to and simultaneously with some principal routine such as a self-checking program.

Computer 1C is essentially the same as 1B but is packaged appropriately for missile flight.

Computer 1D is the same as 1C but will be used for missile flight or sled test as well as other environmental tests.

Computer 2A has a 2000-word 18 bit rope storage and has simple logic. The objective of

11

this, computer is the perfection and testing of large memories.

Computer 2B is a breadboard model having large-scale logic and is designed to operate with the rope storage from 2A.

It is possible for the space craft computer development program to handsomely capitalize on the work described above which it does not fund but which is substantial. To do so requires a small effort alongside of but close to the main development program. This effort would consider problems and conduct experiments related to those problems which are special to the application of this general type of computer to space craft. These problems include input-output methods, logical design for long term reliability, the appropriate logical design for solving space craft problems rather than missile problems, and special design problems related to the environment.

The missile and space craft efforts must be closely coupled and it is expected that the above breadboard designs will be influenced by space craft computer criteria. With this influence, the above described missile motivated experimental breadboards should be nearly as meaningful to space craft computer development as to missile computer development. It is equally important for this space craft computer effort to exist close to the efforts in the other space craft categories in order to establish a real and practical set of specifications.

Phase IV - <u>Prototype - April 1, 1961 to June 30, 1962</u>

It is presently expected that a flyable prototype computer tailored to the missile application will enter its design phase during early November, 1960. This computer will not be influenced by space craft criteria in any way; and it is expected that it will not be fit for use in space craft although many of the design and technical problems are similar. Under the present schedule this design effort lasts for five months; the construction phase begins in early January, 1961, and also requires five months; finally laboratory and environmental tests start in early June, 1961, and run for five months.

The realization of the space craft flyable prototype is an effort of the same kind and magnitude as that required for the missile computer. A reasonable program for the space craft computer prototype would follow, phase by phase, the respective work on the missile computer with roughly the same personnel. So the design phase would **begin early in April, 1961,** and the effort would cover the same span of one year required for the missile effort until the conclusion of the laboratory and environmental tests before June 30, 1962.

The required funding for this category is of course strongly affected by the anticipated military computer development program. The estimate given below assumes that strong advantage in the breadboard phase. It does, however, include all the costs associated with the realization of the prototype. This estimate is in the neighborhood of half what it would be if there were no military program supporting the same general type of computer.

13

April 1, 1960 - June 30, 1960	$ 30,000
July 1, 1960 - June 30, 1961	140,000
July 1, 1961 - June 30, 1962	260,000
Total	$ 430,000

CATEGORY IV - OTHER COMPONENT DEVELOPMENTS

Phase I - Feasibility Study - Complete except for continued examination of new schemes as they occur throughout the program.

Phase II - Preliminary Design - April 1, 1960 to August 15, 1960

The preliminary design of most major components has been covered in R-235, in our current NASA study, and by the Laboratory's extensive experience in long operating life gyroscopes and electromechanical precision instruments. A breadboard effort should be started on these based on our current preliminary design. Concurrently further preliminary design effort should more thoroughly explore the characteristics desired of the instruments expecially with respect to any new requirements generated by the work in Phase II of Category I.

Phase III - Breadboard - April 1, 1960 to August 31, 1961

It is expected that most of the components (space sextant, flywheels, gyros, accelerometers, clock, electronic circuits to operate each, etc.) will undergo three breadboard efforts before they are ready to enter the prototype stage. Describing this evolution for the space sextant will illustrate the process.

The first breadboard effort will be started at the beginning of the breadboard phase. This effort will evolve several relatively crude pieces

of hardware. One of these pieces will be a sun tracker, another will be a star tracker, and a third will be a working precision drive of the correct general dimensions. These will be separately used to conduct sun, star, and moon tracking experiments designed to define the difficult engineering problems and to check out the breadboard electronics.

After experience with the first breadboard effort, a design of a complete space sextant will begin. This design will incorporate the experience gained through the first design and the information generated in Phase II of Categories I and V and in Phase III of Category III with respect to input-output and the method of operation with the computer. This will be a well-designed working model with breadboarded electronics. It will be used on a precision mounting to test its accuracy and operation. It will probably be operated together with one of the Phase III computers.

Three to five units will be constructed from the third breadboard design. This design has the objectives of ironing out the wrinkles discovered by using the earlier design and of providing several units for meaningful life and environmental tests. This design will combine the experience of the second design with the information generated by Phase III in Categories I, II, III, V, and VI. While life and environmental tests are in progress, the instrument will enter its prototype design stage.

Phase IV - Prototype - July 1, 1961 to June 30, 1962

The prototype design will differ from the third breadboard with respect to mechanical and

electronic packaging, fixes for any deficiencies detected in the test program conducted with the third breadboard design, and any necessary changes resulting from new information generated in other component work or the later phases of work in other categories.

I believe it is apparent that a similar pattern would be required for the proper development of flywheels or other components.

Required funding for this category is as follows:

April 1, 1960 - July 1, 1960	$ 75,000
July 1, 1960 - July , 1961	310,000
July 1, 1961 - July 1, 1962	360,000
Total	$745,000

CATEGORY V - SYSTEM ENGINEERING

Phase I - Feasibility Study - Complete in R-235 and current NASA Study

Phase II - Preliminary Design - April 1, 1960 to August 15, 1960

This effort can be resolved into two parts. The first part supplements the Phase II efforts in Categories I and II. This part involves the fitting together of the theoretical work, the hardware analyses, and the ideas on the likely nature of the computer and other components into a specific and consistent pattern.

The second part of this effort is very significant but is nearly microscopic. Using an early logical design from Phase III of Category III and using the studies in Categories II and IV, various subrountines to control components will be programmed. This work will lead to the establishment of the

16

general criteria for chosing the desired logical designs, computer speed, input-output, and storage for a computer which will effectively control a space craft.

Phase III - <u>Breadboard - August 15, 1960 to June 30, 1961</u>

The two parts of the preliminary design effort described above are brought together and expanded. This effort includes the preparation of many more equipment subroutines, measurement routines which use these subroutines, and several overall operation schedules. This work depends on the information generated in all of the other categories for its ground rules. Further, it depends on cooperation and exchange of information with JPL to enable the proper trade off between computations and decisions to be made within the space craft versus those to be made on the earth with communicated data.

The above effort is necessary to specify the correct parameters for the space craft computer.

A second breadboard effort in this category supports the above with simulation and experimental work. Many of the subroutines, etc., can be simulated on our computing facilities to establish their logical correctness, time requirements, etc., power requirements for the computer and components, etc. Experimentally, some of the equipment subroutines will be used with the components and computers of Phase III.

Phase IV - <u>Prototype - July 1, 1961 to June 30, 1962</u>

An assumed specific operation will be analyzed and programmed consistently with the prototype

work in other categories. The methods of system checking by computer simulation, special fixture simulation and tests of dynamics and operation, and preflight checkout procedures will be under study.

By July 1, 1962, this effort should reveal that the computer, components, theoretical work, and hardware analyses together will solve a typical precision interplanetary guidance problem.

Further, this effort will result in a well-integrated prototype guidance and control system. It is expected that by July 1, 1962, one system suitably packaged for space craft operation will be assembled and checked out using the prototype computer and components.

Required funding for this category is as follows:

April 1, 1960 - June 30, 1960	$ 25,000
July 1, 1960 - June 30, 1961	175,000
July 1, 1961 - June 30, 1962	550,000
Total	$750,000

CATEGORY VI -- LONG LIFE, RELIABILITY, AND ENVIRON-
MENTAL PROBLEMS

Phase I - Feasibility Study - Complete in R-235 and current NASA study

Phase II - Preliminary Design - April 1, 1960 to August 15, 1960

This effort includes the design of a specific test program to be used on the Phase III hardware.

Several experimental problems will be started. One involves some simple experiments in vapor pressure lubrication of component bearings. A second involves shaker tests on static

unpreloaded flywheel bearings with subsequent
life tests. A third experiment involves the con-
tinuous operation of one of the Phase III computers
with error checking.

Phase III - <u>Breadboard - July 1, 1960 to December 31, 1961</u>
Various shaker, centrifuge, vacuum, life, and
other tests will be run on the Phase III computers
and components. Study of new developments in
space environmental knowledge will continue.
The rigorous test program for the prototype
phase will be designed. An experimental environ-
mental program will be continued.

Phase IV - <u>Prototype - July 1, 1961 to June 30, 1962</u>
A careful test program will be undertaken on the
prototype components and system in an effort to
estimate the life expectancy and the reliability
of each one singly and in combination.

Required funding for this category is as follows:

April 1, 1960 - July 1, 1960	$ 20,000
July 1, 1960 - July 1, 1961	90,000
July 1, 1961 - July 1, 1962	90,000
Total	**$ 200,000**

The total required funding for this interplanetary space
craft guidance and control advanced development program is as
follows:

April 1, 1960 - July 1, 1960	$ 185,000
July 1, 1960 - July 1, 1961	920,000
July 1, 1961 - July 1, 1962	1,490,000
Total	$ 2,595,000

I sincerely hope that we can get together on this activity.

Very truly yours,

Massachusetts Institute of Technology
Instrumentation Laboratory

Milton B. Trageser
Group Leader

MBT/rf

cc: E. Cortright - NASA
      J. Scull - NASA